DEPARTMENT OF PHYSICS,
UNIVERSITY OF JYVÄSKYLÄ
RESEARCH REPORT No. 9/2009

ALPHA-DECAY FINE STRUCTURE IN EVEN-EVEN NUCLEI

BY

SAMI PELTONEN

Academic Dissertation
for the Degree of
Doctor of Philosophy

Jyväskylä, Finland
August 2009

DEPARTMENT OF PHYSICS
UNIVERSITY OF JYVÄSKYLÄ
RESEARCH REPORT No. 9/2009

ALPHA-DECAY FINE STRUCTURE IN EVEN-EVEN NUCLEI

BY
SAMI PELTONEN

Academic Dissertation
for the Degree of
Doctor of Philosophy

To be presented, by permission of the
Faculty of Mathematics and Natural Sciences
of the University of Jyväskylä,
for public examination in Auditorium FYS-1 of the
University of Jyväskylä on August 5, 2009
at 12 o'clock noon

Jyväskylä, Finland
August 2009

Preface

This thesis is based on the work done at the Department of Physics, University of Jyväskylä during the years 2005-2009. During that period occasional visits to the National Institute of Physics and Nuclear Engineering Bucharest, Romania, were paid.

This work has been supported by the Academy of Finland under the Finnish Centre of Excellence Programme, and by the Ellen and Artturi Nyyssönen Foundation. In addition, my visits to Bucharest were supported by the Center of Excellency IDRANAP of the National Institute of Physics and Nuclear Engineering Bucharest - Romania and the Contract IDEI-119 of the Ministry of Education and Research of Romania.

I wish to thank my supervisors, professor Doru Delion from Romania, and professor Jouni Suhonen. The guidance by both professors has been invaluable.

I also wish to thank the staff of the Department of Physics, JYFL. They are friendly, extremely efficient and flexible. With them the bureaucracy of the university becomes bearable. I am also grateful to my friends in the Department, both the former colleagues and the students. The atmosphere in the Department has been great throughout the years, and these people have contributed to that. Special thanks go to Veli Maaranen, Markus Kortelainen, Juha Merikoski, Heikki Penttilä, to everyone I had lunch with during workdays, and to all my students in the Propedeutic course in spring 2009. Also special thanks go to Leena Leino for target group proofreading.

I wish to thank the staff of the APO teaching studies in the Jyväskylä University, and my fellow students there, for new perspectives, stimulating experience and some wisdom for life.

Thanks to my tabletop- and RPG-gaming friends. Gaming has been important part of my life through my years at the University. It has given me joy, and energy needed in the academic work. My gaming friends made that possible.

And last but not least I wish to thank my families, the one in Virrat where I grew up, and my spouse Heini Kyllönen. Thanks to my parents and all my brothers, sisters and relatives, and to my spouse Heini, for their support.

Finally to anyone who reads our articles or this thesis and learns anything from them I am grateful, for making all this work meaningful.

In Jyväskylä 22th of July 2009
Sami Peltonen

List of publications

This thesis is based on the work contained within the following publications:

I **Systematics of the α-decay to vibrational 2^+ states**
S. Peltonen, D. S. Delion and J. Suhonen,
Phys. Rev. C **71**, 044315 (2005).

II **Systematics of the α-decay to rotational states**
D. S. Delion, S. Peltonen and J. Suhonen,
Phys. Rev. C **73**, 014315 (2006).

III **Folding description of the fine structure of α decay to 2^+ vibrational and transitional states**
S. Peltonen, D. S. Delion and J. Suhonen,
Phys. Rev. C **75**, 054301 (2007).

IV **α-decay spectroscopy of deformed nuclei reexamined**
S. Peltonen, D. S. Delion and J. Suhonen,
Phys. Rev. C **78**, 034608 (2008).

The author wrote the Introduction part of the thesis, except for 8 lines borrowed from article I, in page 19. The author perfomed all the computing in all the included articles, except the G-matrix was computed by Prof. J. Suhonen. The author made all the pictures in articles III and IV, all pictures except number 2 in article I, and pictures 6-8 in article II. Rest of the pictures were made by Prof. D. Delion. The author gathered all the input data from articles and databases except the 2+ energy data used in the first article. The author wrote all the codes for the result analysis, and performed the result analysis under the supervision of Prof. D. Delion. The author participated in writing all the articles and was corresponding author for one or two of the latest articles. For most part the research included in this thesis was done in close collaboration between the author and Prof. D. Delion. Prof. J. Suhonen made large contribution in the QRPA-part of the first article, and contributed in the writing of all the articles.

Abstract

The aim of this work has been to study the systematics of α-decay fine structure in those cases, where the daughter nucleus is doubly even and has a 2^+ state as the lowest excited state. Restriction to these decays is a practical one, as doubly even nuclei have a simpler excitation level structure than other nuclei. Also the lowest 2^+ state corresponds to either a one phonon excitation or the first rotational state, and that helps us to keep our microscopic and macroscopic models simple.

We have concentrated on the main features reproducible with simple models, trying to find fundamental connections, thumb-rules and order-of-magnitude estimates instead of complex fit formulas to reproduce exactly all given numbers. This trend is reflected by our choice of units. We deal mostly with logarithmic units of time and intensity ratios, because the time scales and intensity scales vary hugely over the nuclide chart.

This kind of systematic analysis about α-decay fine structure did not exist previously, even though there were lots of measured data. Although the general impression about α-decay at the time this work was started was, that everything important about this decay mode was already known from the 1950's-1960's, the fine structure and even the preformation part of ground-state-to-ground-state α-decay is still worth investigating even at a rather basic level.

This work is divided into macroscopic and microscopic approach. The first is a collective model using coupled channels formalism and double folding integration over the matter density in both the α-particle and daughter nucleus to create an effective potential for the alpha particle to escape from. The second is a microscopic quasi-particle model where both the daughter and parent nucleus are constructed from an inert core and some active nucleons that occupy some single-particle levels. Here the probability to decay to a certain final configuration is calculated as an overlap integral between the starting configuration and the final configuration.

The macroscopic part is further divided to a rotational case and a vibrational case. Rotational nuclei exhibit clearly more collective characteristics than vibrational ones, so this was the first and more straightforward application of the model. Later, with some modifications, we have successfully implemented a similar model also for the vibrational cases.

Contents

Chapter 1

History

1.1 From discovery of radioactivity to alpha-decay fine structure

This section is based on the book "The History of Early Nuclear Physics" [1] and an article by I. Perlman and J. O. Rasmussen [2].

History of the research of radioactivity begins with two accidental discoveries. On November 8th 1895, professor Wilhelm Röntgen was experimenting with a discharge tube, when he noticed that a luminescent screen, left accidentally at the table, was scintillating. This is how X-rays were first found. On March 1896, Henri Becquerel was studying phosphorescent materials under the hypothesis that phosphorescent emanations could include X-rays. However his experiment did not get enough sunlight because of the weather. He did develop the photographic plates anyway and thus discovered that uranium salts emit some kind of radiation that blacken photographic plates through black paper. In his later papers he called his finding "uranic radiations" [3, 4]. Rutherford, in 1899 in his first paper, announced that uranic radiations consist of at least two types of radiation labeling them as α-radiation and β-radiation, for convenience [5].

After an experiment in which Mme Curie showed that alpha rays differed from Röntgen rays in that they became degraded in energy in traversing matter, she suggested in 1900 that alpha rays were heavy projected particles [6]. This conclusion was first reinforced by the work of Strutt (1901) and Crookes (1902) in ionization produced in gases, and finally clearly demonstrated by Rutherford in 1903, by measurements of deflection of alpha rays in magnetic and electrostatic fields [7–9]. Strutt had concluded in his work in 1901 that α-rays might be positively charged fast bodies [7]. Charge-to-mass ratios of alpha rays were measured with magnetic deflection, and identified with "canal rays" found in 1886 by Goldstein. Canal rays are positive particles emerging through holes in the cathode in a special gas discharge tube, accelerated by high voltage. From the measured charge-to-mass ratios Mme Curie suggested (1903) that the mass

of α-particles is of the same order of magnitude as the one of the hydrogen atom [10]. Rutherford commented that "if the α-particle consists of any known matter, this result indicates that it consists either of projected helium or hydrogen" [11]. The helium hypothesis was verified by Soddy and Ramsay by getting the spectral lines of helium from the gas produced by a radium compound [12].

Further deflection experiments (particularly those of MacKenzie [13]) showed that a mixture of alpha emitters produced a mixture of homogeneous alpha groups, each with different velocity. Mme Curie [6] had demonstrated that alpha particles from a thin polonium source had a definite range. Bragg [14] extended this work firmly establishing the concept of range as a distinguishing feature of each alpha emitter. The relation between the range (or velocity) of the alpha group and the half-life for emission was noted by Rutherford already in 1907 [15]. Later Geiger and Nuttall (1911) [16] and (1912) [17] examined this relationship systematically and were able to show that the logarithm of the decay constant changed linearly with the logarithm of range.

Rutherford [18] introduced the concept of atomic nucleus as the center of mass and positive charge of the atom in 1911. This was due to his α-ray scattering experiments, that showed that gold foil can reflect α-rays that were known to be relatively massive fast particles. Based on Rutherford's idea of a compact nucleus and all kinds of other measured facts, Bohr created his famous atomic model which he published in three parts in 1913 [19].

The understanding of α-decay grew with the invention on quantum mechanics: In 1928, Gamow [20] and Condon and Gurney [21] independently showed that the wave nature of matter permits the alpha-particle to penetrate the region of potential energy higher than its kinetic energy. This solved the question of how an alpha particle could leave a heavy nucleus but not be free to enter. They obtained excellent quantitative agreement for the dependence of the decay constant upon the decay energy, explaining the principal feature of the Geiger-Nuttall relation.

The fine structure of α-ray spectra was found by Salomon Rosenblum in 1929 [22]. This was possible because he had access to the new magnet of L'Académie des Sciences de Paris, construction of which finished in 1928. This new equipment gave more than 60 times greater resolution than what had been possible with previous equipment. The first explanation of this fine structure, and actually a correct one came from Gamow in 1930 in his letter to "Nature" [23]. He correctly deduced that the different observed spectral lines correspond to α-decay from one energy state of parent nucleus to several energy states of the daughter nucleus. This interpretation was proven by Rutherford and Bowden in 1932 [24]. They measured the emitted γ-rays from the decays of states that were populated in the α-decay.

1.2 Alpha decay in the last decades

Alpha decay was studied extensively up to 1950's-1960's. After that there has been very little going on in the field of α-decay theory until recently. The field fell out of fashion when most of the things that could be measured or calculated with the equipment of that period had already been done.

Measurements of the α-decay have been going on from that time, and the amount of accumulated data (see for example [25]), with advances in nuclear theory and computing power, allow us today to make new discoveries in the field.

Points of interest in alpha-decay fine structure in last decades include fine structure involving excited 0^+ states in vibrational-like Pb nuclei (see for example [26,27] and the references therein). Also all the so called super heavy elements are alpha emitters, making alpha decay a crucial tool to everyone working with their production.

Chapter 2

Basics

2.1 Alpha-decay half-life

Alpha decay is a process, where a radioactive nucleus emits an α- particle as shown in Fig.2.1. This α-particle is a ^{4}He-nucleus, consisting of 4 nucleons: 2 protons and 2 neutrons, a combination that is unusually strongly bound together. In this process the α-decaying emitter nucleus, called the parent nucleus, loses 4 nucleons to the α-particle and converts to another nucleus, called daughter nucleus.

Only certain nuclei have the ability to α-decay. This depends on the energetics of the decay. The mass of a nucleus depends on two things: the mass of the nucleons that it is made of, and the strength of their binding together. The more bound the nuclei are, the less the nucleus weights. Basically, the α-decay can proceed when the sum of the masses of the α-particle and the decay daughter is less than the mass of the parent nucleus.

The mechanism of α-decay is simple: The α-particle tunnels out of the parent nucleus through the Coulomb barrier of the daughter-α system according to the laws of quantum mechanics. Quantitative quantum mechanical treatment of the tunneling process explains the connection between the energy released in the decay (called Q-value) and α-decay half-life. This is the famous Geiger-Nuttal law.

Geiger-Nuttal law states that the logarithm of the α-decay half-life (τ) is roughly proportional to the proton number of the daughter nucleus (Z_D) and inverse square root of the Q-value:

$$\ln \tau = a_1 \frac{Z_D}{\sqrt{Q}} + a_2, \tag{2.1}$$

where a_1 and a_2 are constants.

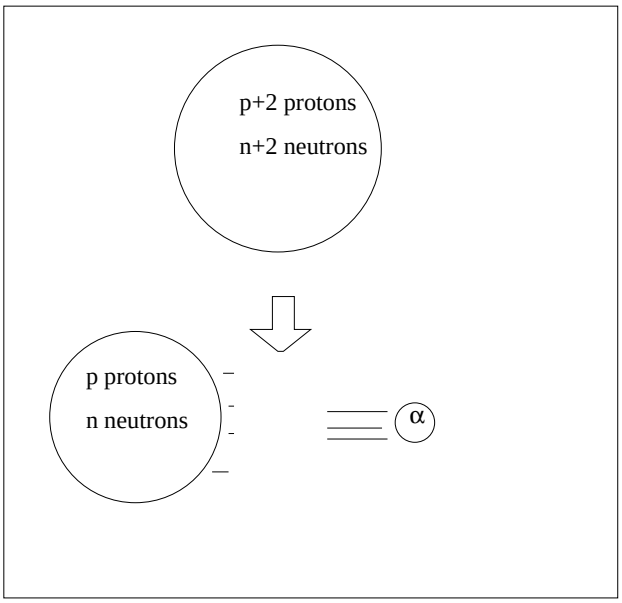

Figure 2.1: Alpha decay: The parent nucleus shoots out an α-particle and becomes the daughter nucleus in the process.

2.2 Alpha-decay fine structure

A nucleus can dwell in different energy states. Most nuclei are usually in their lowest energy state called the ground state. The other possible energy states are called excited states. Energy states are labeled by their spin angular momentum and parity, which gives the inversion symmetry of the wave function in question (+ means symmetric, - antisymmetric). In doubly even nuclei (with even numbers of neutrons and protons) the ground state is a 0^+ state, having spin 0 and parity +.

Collective excited states are usually modeled as rotational or vibrational. Examples of rotational and vibrational spectra are shown in Fig.2.2. If one assumes that a nucleus is like a tiny blob of liquid, with some symmetric shape like ellipsoid, and that it can rotate, then quantum mechanics dictates that the allowed energy levels for this rotation follow a certain pattern, called a rotation series or rotation band. On the other hand if one assumes that instead of rotation the blob can vibrate, one arrives at a different kind of pattern for the energy levels, called a vibration series. When a nucleus is in an excited state, it usually de-excites fast by emitting the energy out as one or more γ-rays. A γ-ray is just a high-energy photon and it can penetrate matter and be harmful to living cells. The lowest rotation series in rotational doubly even nuclei, called

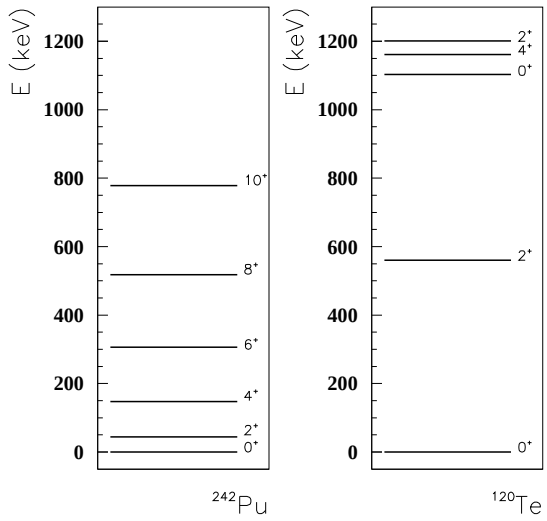

Figure 2.2: Examples of rotation series (^{242}Pu) and vibration series (^{120}Tc). Only the lowest levels are shown.

the ground state band, starts from the 0^+ ground state and continues with even angular momenta $2^+, 4^+, 6^+, ...$ Many heavy nuclei have several nice rotation series, one example being ^{242}Pu. A vibration series at its simplest has as first state the 0^+ ground state and a 2^+ and then follows a triplet $0^+, 2^+, 4^+$. Simplest quantum mechanical approximation to a vibrating nucleus, the so-called harmonic approximation, predicts that this triplet should be degenerate and exist at excitation energy that is double that of the first 2^+ state. In reality anharmonicities of the vibrations spread the triplet out. A representative example of a vibrational triplet can be seen for example in ^{120}Tc. In heavier nuclei like the ones typically involved in the α-decay, the experimental level scheme does not show a clear vibrational triplet. In this work we are not interested in vibrational triplets however, because their energy is high and therefore the branches of the α-decay involving states of the triplet are so small that it is not possible to measure them directly.

In reality collective nuclei have quite complicated level structures possibly involving several vibrational and rotational series, but usually for doubly even nuclei the lowest exited state is a 2^+ that is either part of a rotational or a vibrational series, and a 4^+ state belonging to the same series is also found nearby. From the energetics of these excited states a nucleus can be categorized

as either rotational or vibrational, and this (along with a possible 6^+ state higher up) is enough for our purposes. The division between rotational-like and vibrational-like nuclei is useful, as it tells us about the nature of collectivity of the nucleons in a given nucleus. Rotational nuclei are very collective but vibrational nuclei are less so. This is seen in the energies of exited states and the γ-ray intensity of their decay. For this reason the rotational nuclei are usually modeled by macroscopic models where nuclear matter rotates as a liquid drop, and the vibrational nuclei are modeled by microscopic models, where the nucleus is assumed to be built up from individual nucleons.

Most of the α-decays in the nuclei studied in this work start from the ground state of the parent nucleus. The reason for this is that α-decay is usually much slower than γ-ray emission, so that even if the parent nucleus happens to be in an excited state it usually de-excites by emitting γ-rays before the α-decay takes place. Exceptions to this can occur if the excited state of the parent is exceptionally long lived (a so called isomeric state where the normal γ-ray emission is hindered by the absence of suitable final states), or if the α-decay is particularly fast, in microsecond range. These exceptional cases have not been studied here, because they would significantly complicate our α-decay modeling.

There are two principles of priority in the α-decay, energetics and similarity of states. The more energetic the α-particle is, the easier it is for it to tunnel out of the nuclear potential well, because at higher energies the potential wall is much thinner. This is the main reason why the α-branching to 4^+ state in vibrational nuclei is so low that it cannot be measured directly. Also most of the α-decays tend to populate that state in the daughter nucleus which is the most similar to the initial state of the parent nucleus. Similarity here means spin, parity and deformation. Most α-decays in doubly even nuclei end up in the ground state of the daughter nucleus, because it is both energetically most favorable and the most similar to the ground state of the parent nucleus. Even here there are exceptions. In some lead nuclei, for example, there exist several low-lying energy states that have the same spin and parity as the ground state but correspond to different quadrupole deformations. There the favored state is the one with a shape similar to the one of the ground state of the parent nucleus. In odd mass nuclei ground states differ much more from each other than in doubly even nuclei: usually α-decay favors the lowest of the energy states that have the same spin and parity as the ground state of the parent nucleus. Here the studies have been limited to doubly even (or even-even) nuclei, because their configurations are the simplest to model.

Fine structure of α-decay results from the fact that even though α-decay to one particular state is favored, decays to other states also occur. This is depicted schematically in Fig.2.3. The aim of the present work was to chart how much of the α-decay goes to the ground state and how much to each of the few lowest excited states in the discussed nuclei. Alpha-decay fine structure may also result from α-decays from several excited states of a short-lived α emitting nucleus or from α-decays from long-lived so called isomeric states in α emitting nucleus.

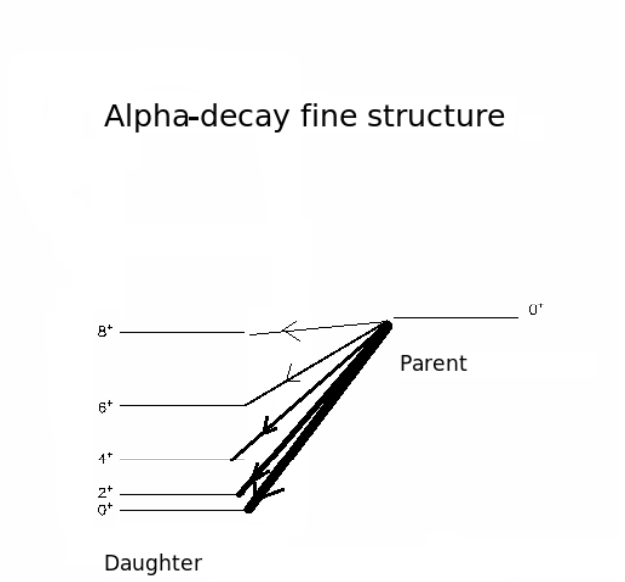

Figure 2.3: Alpha-decay fine structure. As the parent nucleus shoots out an α-particle, it becomes daughter nucleus in one of its excited states or in its ground state. Thickness of the lines showing the decay transitions indicates the relative intensities of the decay channels.

This form of α-decay fine structure is beyond the scope of the present study.

The shape of an α-emitter affects the α-decay fine structure, but the shape of the nucleus is actually something that cannot be seen directly. In our calculations we use the information about nuclear shapes that comes from a global model [33] that is able to reasonably well explain some collective characteristics of all measured nuclei. However it is worth pointing out that it is possible that our calculations are more sensitive to nuclear shape variations than the method [33] used to model them.

2.3 Definitions

Microscopic model. Nuclear model, where the nuclear many-body problem is solved by starting from the nucleon-nucleon two-body (and possibly three-body) interaction. Collective properties are only accessible through integration over the properties of individual nucleons.

Macroscopic model. Nuclear model, where nucleons are not treated as

individual particles but as a chunk of mass with only collective properties, like density, collective shape and charge distribution.

Parent nucleus and daughter nucleus. In the α-decay the so-called parent nucleus changes to the so-called daughter nucleus. Daughter nucleus has a mass number 4 less than the parent, and a charge number 2 less than the parent. Usually in the literature α-decay is identified by only one nucleus, mostly the daughter.

Static approximation. Calculation of, for example, the α-decay in such a way that the decaying nucleus is assumed not to be affected by the decay in the time the decay takes place. This means that during the tunneling the effects of the moving α-particle on the mass and charge density of the rest of the nucleus are not taken into account. This simplifies the calculation very much, but the approximation must be justified by estimating the magnitudes of the neglected effects - if they are small the approximation is valid.

Q-value is the kinetic energy released in an α-decay, obtained easily experimentally by measuring the energy of the α-particle. It includes the correction for nuclear recoil. It is not corrected for the electron screening effect.

Alpha-decay intensity Γ_J. The number of α-decays during a time period to a given nuclear state (excited or ground state) identified with spin J. Usually normalized to the total number of α-decays from the same parent nucleus happening in the same time period, and given as a persentage.

Intensity units I_2 *and* I_4. Intensity units are calculated in the following way: First divide the number of measured α-decays to the 0^+ ground state by the number of measured α-decays to the relevant exited state, lowest 2^+ excited state for I_2 or lowest 4^+ excited state for I_4. Then take 10-based logarithm of the result.

$$I_J = \log_{10} \frac{\Gamma_0}{\Gamma_J} \tag{2.2}$$

This definition usually gives positive numbers smaller than 10.

Hindrance factor HF. The α-decay happens in two stages, namely via preformation of the α-particle in the decaying nucleus and the subsequent barrier penetration. In some simplest models the preformation is called the knocking frequency. Basically the hindrance factor is the α-decay half-life corrected for barrier penetration, leaving only the preformation part. There are several technical definitions for HF, for example the Nuclear

Data Sheets uses spin-independent equations of Preston [28]. Our definition of HF is based on Coulomb functions in the following manner:

$$\begin{aligned} \mathrm{HF} &\equiv \frac{\Gamma_0}{\Gamma_J}\frac{P_J}{P_0}, \\ P_J &\equiv \frac{2\kappa_J R}{G_J^2(\kappa_J R)}, \\ \kappa_J &= \sqrt{\frac{2\mu(E-E_J)}{\hbar^2}}, \end{aligned} \tag{2.3}$$

where Γ_J is the α-decay intensity to the state J^+, P_J is called penetrability, $G_J(\kappa_J R)$ is the irregular Coulomb function, E is total α-decay energy (Q-value) and E_J is the excitation energy of the first J^+ state. The HF is practically independent of the radius R, for which we have used the touching radius $R = 1.2(A_D^{1/3} + A_\alpha^{1/3})$, D denoting the daughter nucleus. As HFs are model dependent, we recommend the use of intensity ratios Γ_0/Γ_J or logarithms of those (2.2) instead, as those are measurable quantities.

BCS theory. The Bardeen-Cooper-Schrieffer theory is the theory of superconductivity developed by John Bardeen, Leon N Cooper and John R. Schrieffer in 1957. It was adopted for nucleon pairing by Bohr and Mottelson a year later [29]. Attractive short-range interaction between nucleons may produce a superconducting-like state in nuclei. The BCS theory focuses on the consequences of an attractive two-body interaction between any fermions in any many-fermion system. In the BCS ground state fermions form pairs that behave like bosons.

M3Y nucleon-nucleon interaction. Fit of the interactions between nucleons having a form of a sum of three Yukawa-type terms

$$Y(x) = \frac{e^{-x}}{x} \tag{2.4}$$

based on elastic scattering data. [30]

Universal parametrization. Parametrization of the Woods- Saxon potential we used in [31]. This parametrization is suitable for generating proton and neutron single-particle spectra, especially for nuclei around Pb region [32]

Branching. When nuclear decay proceeds via two or more different routes, those routes are called branches. The term branching also refers to the relative intensities of those branches, i.e. "Alpha-decay branching to 4^+ state is less than 0.01%" means that less than 1 out of 10000 alpha decays goes through 4^+ state.

Soft core and hard core approximations. The hard core approximation in our work means that the α-particle does not exist inside the nuclear core. This corresponds to high and steep potential barrier felt by the α-particle at small radius inside the nucleus. This leads to a narrow effective potential well for the α-particle. The hard core approximation works best for vibrational-like nuclei and for rotational nuclei with masses up to the Pb region, having 130 or less neutrons. The soft core approximation permits the α-particle to exist deeper inside the nucleus. In this case the potential felt by the α-particle is wider and shallower inside the nucleus. This approximation works best for rotational nuclei, typically heavier than lead, having more than 130 neutrons.

Quasiparticle model. The quasiparticle model extends the particle-hole picture of a magic proton and/or neutron nucleus to a quasiparticle picture of an open-shell nucleus. The quasiparticle picture leads to smeared Fermi surfaces for protons and/or neutrons and thus lends the quasiparticle partly a particle, partly a hole character. This, in turn, leads to the loss of good particle number, unless an additional particle-number projection is applied.

Deformation parameters β_2 and β_4. Deformation parameters tell about the shape of a nucleus. The shape of a nucleus is not something that can be seen directly, but it is deduced from exitation energy spectrum or electrical transition probabilities using some model dependent assumptions. Deformation parameter β_2 (quadrupole deformation) represents how elongated (prolate, like american football) or flattened (oblate, like pancake) the nucleus is. β_3 (octupole deformation) tells how egg-shaped the nucleus is. Hexadecapole deformation β_4 tells how closely the shape of a nucleus corresponds to a four-leaved clover. Technically these deformation parameters come from the expansion of the nuclear surface as

$$r(\theta, \phi) = R_0(1 + \sum_{l=1}^{\infty} \sum_{m=-l}^{l} \beta_{lm} Y_l^m) \ , \tag{2.5}$$

where R_0 depends on deformation in such a way that the volume inside the nuclear surface is conserved when going from a spherical to a deformed nucleus. The Y_l^m are the spherical harmonics and, when only axially symmetric cases ($m = 0$) are considered, the notation β_l is used for β_{l0}. For the values of β_l we adopted in this work the ones of Ref. [33].

Spectroscopic factor. In [34] we use two definitions for spectroscopic factor. The microscopic spectroscopic factor is

$$S_{\mathrm{micr}} = \int_0^{\infty} |\mathcal{F}(\mathbf{R})|^{\mathbf{2}} \mathbf{dR} \ , \tag{2.6}$$

where $\mathcal{F}$ is a so-called preformation amplitude. For definition of the preformation amplitude see equation (3.8) in [34]. Our so-called phenomenological spectroscopic factor is simply defined by

$$S = \frac{T_{\mathrm{comp}}}{T_{\mathrm{exp}}} \ , \tag{2.7}$$

where T_{comp} is the computed α-decay half-life and T_{exp} is the measured α-decay half-life.

Phonon. Quantum of vibrational energy.

Model space. In microscopic nuclear calculations the model space consists of those energy levels that actively partake in the calculation. This means that only the single-particle levels of the model space can be occupied by nucleons, quasiparticles, etc. The size of the model space must be determined on case-by-case basis, too small space rendering inaccurate results, too large space consuming a lot of the CPU time.

Parameter. A parameter is a numeric variable of the model that can be adjusted to improve the computed results. A free parameter can be adjusted separately for each nucleus, or globally for several nuclei. The more free parameters a model contains the better it can fit the measured data regardless of their physical motivation. We restrict ourselves to a minimal set of free parameters in order to test the validity of our models.

Chapter 3

Macroscopic model

3.1 Effective potential

Our macroscopic model is based on the double folding model previously used in binary fission calculations. The idea is to model the daughter nucleus as a homogeneous Fermi-like mass and charge distribution with symmetric shape, and the α-particle as a homogeneous spherical Gaussian mass and charge distribution. We integrate the nucleon-nucleon plus Coulomb interaction over both bodies to find an effective potential the α-particle feels in the decay. The shape of the daughter nucleus we obtain from the compilation of quadrupole and hexadecapole deformations of nuclei by Möller and Nix [33]. The resulting effective potential is usually taken to be of the Woods-Saxon shape. The problem with the Woods-Saxon potential well is that it generates many energetically very favorable decay resonances that do not correspond to measured decay energies. Thus it seems more logical that the potential well must be quite shallow compared to the Woods-Saxon potential well, so that the measured α-decay energies correspond to the lowest resonances (in our case nodeless resonances) in the well. This motivated us to use a pocket-like potential without modifying the outer barrier part. In practice we smoothly fit a parabola inside the barrier by matching the curves and their derivatives. This simulates the effect of Pauli principle, especially the fact that the α-particle is formed in the surface region of the parent nucleus. Microscopic calculations [35] support this idea.

The α-decay intensity ratios of vibrational and light transitional nuclei are best reproduced using narrow potential pocket, in other words a hard-core approximation (an example given in Fig. 3.1). This is due to the fact that these nuclei have only few particles or holes outside closed major shells so that single-particle energy levels with most of their wave functions at small radius are already tightly occupied. These nuclei are found in the Pb region or below it in the nuclear chart, so that their structure is influenced by large shell gaps and relatively small major shells as compared to the Uranium region.

For heavy rotational nuclei above the Pb region, the α-decay intensity ratios are best reproduced by a wide and shallow pocket, in other words a soft-core

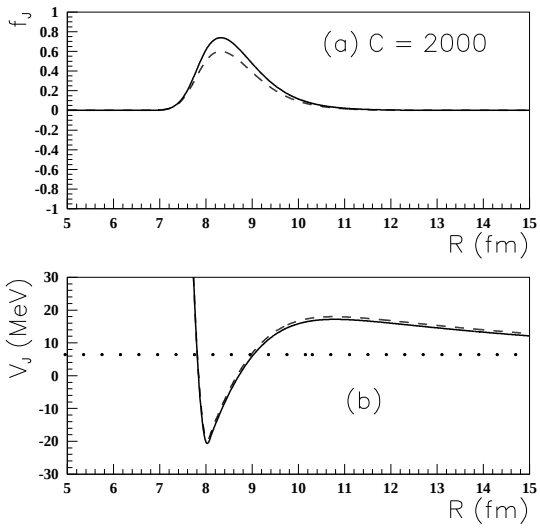

Figure 3.1: (a) The components of the wave function Ψ (3.2) for $J = 0$ (solid line) and $J = 2$ (dashed line) for the α-decay to ^{216}Po calculated using hard core approximation. (b) Components of the diagonal terms $U_J(R)$ (3.3) of the potential (3.1) for $J = 0$ (solid line) and $J = 2$ (dashed line).

approximation (example of a heavy transitional nucleus is displayed in Fig. 3.2). Many of these nuclei are located in mid-shell of a large major shell, and therefore the α-particle can also be formed deeper inside the nucleus, as there are plenty of such single-particle energy levels available, that have their wave functions confined close to the nuclear center.

The effective potential can be divided into a spherical (V_0) and a deformed component (V_d) as follows

$$\begin{aligned} V(\mathbf{R}, \Omega_D) &= V_0(R) + V_d(\mathbf{R}, \Omega_D) \\ &= V_0(R) + \sum_{\lambda>0} V_\lambda(R) \mathcal{Y}_\lambda(\Omega, \Omega_D) \ . \end{aligned} \tag{3.1}$$

Here the angular part of the wave function $\mathcal{Y}_\lambda$ depends on wether we are using rotational [38] or vibrational [37] model. The wave function is

$$\Psi(\mathbf{R}, \alpha_2) = \frac{1}{R} \sum_{J=0,2} f_J(R) \mathcal{Z}_J(\Omega, \alpha_2) \ , \tag{3.2}$$

where $\mathcal{Z}_J$ also depends on wether we are using rotational [38] or vibrational [37] model. See the mentioned references for details.

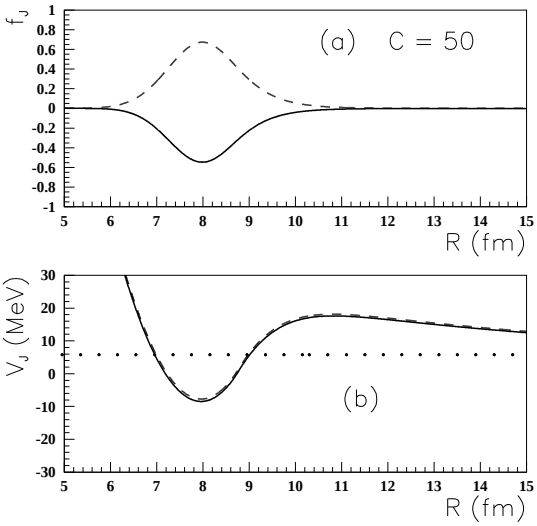

Figure 3.2: (a) The components of the wave function Ψ (3.2) for $J = 0$ (solid line) and $J = 2$ (dashed line) for the α-decay to ^{220}Rn calculated using soft core approximation. (b) Components of the diagonal terms $U_J(R)$ (3.3) of the potential (3.1) for $J = 0$ (solid line) and $J = 2$ (dashed line).

In Figures 3.1 (a) and 3.2 (a) we plotted the radial components of the wave function for J=0 (solid line) and J=2 (dashes) corresponding to the pocket-like repulsions. In Figures 3.1 (b) and 3.2 (b) we give the radial dependencies of the diagonal terms of the channel coupling matrix analogously to the curves in (a). The diagonal part of the channel coupling matrix corresponds to the α-daughter potential plus the centrifugal barrier, i.e.

$$U_J(R) = \langle \mathcal{Y}_J | \overline{V}(R) | \mathcal{Y}_J \rangle + \frac{\hbar^2 J(J+1)}{2\mu R^2} \ . \tag{3.3}$$

Here again the form of the first term of (3.3) depends on wether we are using rotational [38] or vibrational [37] model.

Only the spherical component is important in transitions between the 0^+ ground states, but deformed components strongly affect transitions to the excited 2^+ and 4^+ states. Actually there is a correlation between I_2:s (2.2) and β_2 deformations (2.5), and between I_4:s (2.2) and β_4 deformations (2.5). This is one of the main results in Ref. [38]. The correlation is clear for both the calculated and experimental data, but the experimental data for I_4:s is even more strongly correlated than our calculated results. One straightforward explanation for this is that the β_4 deformation parameters are in reality larger and change more from

one nucleus to the next than estimated in Ref. [33]. The I_2:s and I_4:s are also strongly affected by major shell gaps, as are deformation parameters β_2 and β_4.

3.2 Computational procedure

Application of our model has the following steps: 1) We compute the attractive part of the effective potential of the daughter nucleus felt by the α-particle using the M3Y nucleon-nucleon interaction. The result of this step is a potential well with a Woods-Saxon shape. 2) We compute the repulsion by fitting a parabola at the inner barrier wall of the Woods- Saxon potential and solve the Schrödinger equation to find the first resonance. 3) We normalize the total decay width and the wave functions. 4) We extract the intensities, resonant energy and α-decay half-life.

For a given nucleus the practical computation with our code is done in the following way. We first choose the form of the potential pocket and the resonance that best describes the nuclear decay. As discussed in section 3.1 the fine structure of the vibrational nuclei can be obtained by using a hard core, that means a narrow potential pocket. The fine structure of the heavy rotational nuclei is better reproduced by a soft core, meaning a wider, shallower potential pocket. In both cases there are two nodeless resonances to choose from. For example in our paper [37] concerning vibrational and transitional nuclei, we use for most nuclei the first resonance and the narrow potential pocket, but for the heaviest transitional nuclei we use the second resonance and the shallow potential pocket. We fit the depth of the potential pocket to produce the correct Q-value. In our earlier papers [37, 38] we also fitted the interaction strength (including both nucleon-nucleon interaction and Coulomb force) to reproduce the measured α-decay half-life. In our new approach we keep the two-body interaction fixed and use the bare M3Y interaction based on scattering experiments [30]. Furthermore we calculate the spectroscopic factor (2.7) from the difference of calculated and measured half lives. Our phenomenological spectroscopic factor $S_{\rm phen}$ (2.7) is less than one because the potential we use is based on scattering experiments. For this reason the preformation part of the α-decay is not taken into account in the potential. This is identical to assuming pre-existing α-particle inside the nucleus.

In our publications we found that our simple model produces a connection between the fine-structure intensities and deformation parameters. As a byproduct we extracted a law that gives predictions for spectroscopic factors (2.7). We interpret our results for the spectroscopic factors as evidence of α-clustering. In principle it is possible to use the α-decay fine-structure data to improve the quality of the nuclear deformation parameters for a suitable set of nuclei.

Chapter 4

Microscopic model

The idea behind our microscopic model [31] was to expand the scope of the previous work [40]. In [40] a model was developed that combined a microscopic nuclear-structure calculation with a way to extract α-decay probabilities from the resulting nuclear wave functions. This approach had been applied to model α-decays of three nuclei.

The work in [31] faced many challenges. In the beginning we realized that a systematic analysis of a large number of nuclei over a vast area of the nuclide chart sets quite difficult demands on nuclear-structure calculations. First of all, the model space must be large enough to allow for all our nuclei a sufficient number of excited configurations. Also it was quite difficult to find a minimal set of parameters that would adequately describe all the considered nuclei.

One big difference between this work and our macroscopic work is that here we are not interested in the barrier penetration. We just assume that the barrier is penetrated in a standard way, and concentrate on producing a microscopic hindrance factor, by definition the effect left when barrier penetration has been subtracted away. In hindsight I see the following problem in our calculation [31]. The Rasmussen's early spherical integration model of penetration [39] is one commonly used definition of hindrance factor. It is spin-independent as is Preston's definition used in Nuclear Data sheets [28]. Our own simple enough definition of hindrance factor as a ratio of two irregular Coulomb functions in Eqs. (2.3) does not completely agree with these definitions.

The microscopic model is built from several calculation steps. First we need a set of single-particle energies and wave functions to define our valence space. These we obtain from a Woods-Saxon mean field calculation. In the chosen valence space we perform a BCS calculation to define our quasiparticles that occupy those levels. As the next step we add the residual interaction of the nucleons by performing a quasiparticle random-phase approximation (QRPA) calculation. For this we have to choose the form of the residual interaction. We have used the G-matrix interaction based on the Bonn one-boson-exchange potential. With that the nuclear-structure part of the calculation is finished. Finally we use the resulting wave functions to extract any decay rates we are

interested in.

In our work we tried to reproduce electromagentic transition probabilities B(E2)s, between the 0^+ ground states and the first excited 2^+ states. We wanted also to reproduce the α-decay hindrance factors simultaneously. We adopted bare nucleonic charges for simplicity, as we had no independent data to fix the values of effective charges. In this way we could affix the parameters of our model. The results show that the B(E2)s are nicely reproduced. Unfortunately the contrast between the B(E2)s and the α-decay hindrance factors was hard to achieve, since for nuclei where the B(E2)s are measured, there are almost no measurements of the α-decay fine-structure hindrance factors.

As parameters in our calculation we had R_1 the ratio of isovector strength to isoscalar strenght, and the proton neutron asymmetry ratio R_2. These are defined in the following way. Let us denote the interaction strength between two protons by V_π, the interaction strength between two neutrons by V_ν and the interaction strength between proton and neutron by $V_{\pi\nu}$. Then

$$R_1 \equiv \frac{V_\pi + V_\nu - 2V_{\pi\nu}}{V_\pi + V_\nu + 2V_{\pi\nu}} , \tag{4.1}$$

$$R_2 \equiv \frac{V_\pi - V_\nu}{V_\pi + V_\nu} . \tag{4.2}$$

Usually the isovector component is taken as small, but we did the calculations with the whole range of these ratios ($-1 < R_i < +1$), where normal isoscalar interaction corresponds to $R_{1,2} = 0$. The results were almost equally good (or bad) for a wide range of these parameters, but the best result was obtained for $R_1 = 0$ and $R_2 = -0.75$. The large absolute value of R_2 corresponds to (unrealistically) large enhancement of the effective neutron-neutron interaction.

This formalism was able to explain the main trends seen in the systematics of experimental data, namely the universal decrease of the B(E2) value and the increase of the HF with increasing energy E_{2^+} along any neutron chain. Moreover, the specific character of each isotope chain, concerning the slope of the HF versus E_{2^+}, could be explained by concrete nuclear structure details. We proposed an empirical linear dependence between the logarithm of the hindrance factor and the lowest energy E_{2^+}. This dependence was confirmed by our QRPA calculations.

The results of our calculations could explain the gross features of the α-decay data. The limitation of our model stems from the inability of the traditional shell model to produce large enough differences between the ground-state wave functions of different nuclei.

Possible ways to improve these calculations include a larger model space, introducing excitation levels in the continuum above the bound states of the nucleus and introducing 3- or 4-particle interactions.

Bibliography

[1] M. Mladjenović, The History of Early Nuclear Physics (1896-1931), World Scientific, Singapore 1992.

[2] I. Perlman and J. O. Rasmussen, Alpha Radioactivity, Handbuch der Physik Vol XLII, p. 109-204, Springer-Verlag, Berlin 1957.

[3] H. Becquerel, C. R. Acad. Sci. Paris **122**, 689 (1896).

[4] H. Becquerel, C. R. Acad. Sci. Paris **122**, 855 (1896).

[5] E. Rutherford, Phil. Mag. **47**, 109 (1899).

[6] M. Curie, C. R. Acad. Sci. Paris **130**, 76 (1900).

[7] R. J. Strutt, Phil. Trans. Roy. Soc. Lond., Ser. A **196**, 507 (1901).

[8] W. Crookes, Proc. Roy. Soc. Lond., Ser. A **69**, 413 (1902).

[9] E. Rutherford, Phys. Z. **4**, 235 (1903); *ibid* Phil. Mag. **5**, 177 (1903).

[10] Mme Curie, Thesis, p. 186.

[11] E. Rutherford, Radio-activity, Cambridge University Press, p. 125 (1904).

[12] W. Ramsay and F. Soddy, Proc. Roy. Soc. **72**, 204 (1903).

[13] D. R. MacKenzie, Phil. Mag. **10**, 538 (1905).

[14] W. H. Bragg, Phil. Mag. **8**, 719 (1904); *ibid* **10**, 600 (1905); *ibid* **11**, 617 (1906); W. H. Bragg and R. Kleeman, Phil. Mag. **8**, 726 (1904); *ibid* **10**, 318 (1905).

[15] E. Rutherford, Phil. Mag. **13**, 110 (1907).

[16] H. Geiger and J. M. Nuttall, Phil. Mag. **22**, 613 (1911).

[17] H. Geiger and J. M. Nuttall, Phil. Mag. **23**, 439 (1912).

[18] E. Rutherford, Phil. Mag. **21**, 669 (1911).

[19] N. Bohr, Phil. Mag. **26**, 1 (1913); *ibid* **26**, 476 (1913); *ibid* **26**, 857 (1913).

[20] G. Gamow, Z. Phys. **51**, 204 (1928).

[21] R. W. Gurney and E. U. Condon, Phys. Rev. **33**, 127 (1929).

[22] S. Rosenblum, C. R. Acad. Sci. Paris **188**, 1401 (1929); *ibid* J. Phys. **1**, 438 (1930).

[23] G. Gamow, Nature **126**, 387 (1930).

[24] E. Rutherford and B. V. Bowden, Proc. Roy. Soc. A **136**, 407 (1932).

[25] Y. A. Akovali, Nucl. Data Sheets **84**, 1 (1998).

[26] D. S. Delion, A. Florescu, M. Huyse, J. Wauters, P. Van Duppen, ISOLDE Collaboration, A. Insolia and R. J. Liotta, Phys. Rev. Lett. **74**, 3939 (1995).

[27] D. S. Delion, A. Florescu, M. Huyse, J. Wauters, P. Van Duppen, ISOLDE Collaboration, A. Insolia and R. J. Liotta, Phys. Rev. C **54**, 1169 (1996).

[28] M. A. Preston, Phys. Rev. **71**, 865 (1947).

[29] A. Bohr, B. R. Mottelson and D. Pines, Phys. Rev. **110**, 936 (1958).

[30] G. Bertsch, J. Borysowicz, H. McManus and W.G. Love, Nucl. Phys. A **284**, 399 (1977).

[31] S. Peltonen, D. S. Delion and J. Suhonen, Phys. Rev. C **71**, 044315 (2005).

[32] J. Dudek, Z. Szymanski and T. Werner, Phys. Rev. C **23**, 920 (1981).

[33] P. Möller, J. R. Nix, W. D. Myers and W. J. Swiatecki, At. Data Nucl. Data Tables **59**, 185 (1995).

[34] S. Peltonen, D. S. Delion and J. Suhonen, Phys. Rev. C **78**, 034608 (2008).

[35] D. S. Delion, A. Săndulescu and W. Greiner, Phys. Rev. C **69**, 044318 (2004).

[36] F. Cârstoiu and R.J. Lombard, Ann. Phys. (N.Y.) **217**, 279 (1992).

[37] S. Peltonen, D. S. Delion and J. Suhonen, Phys. Rev. C **75**, 054301 (2007)

[38] D. S. Delion, S. Peltonen and J. Suhonen, Phys. Rev. C **73**, 014315 (2006)

[39] J. Rasmussen, Phys. Rev. **113**, 1593 (1959).

[40] D. S. Delion and J. Suhonen, Phys. Rev. C **64**, 064302 (2001).

Paper II

Systematics of the α-decay to vibrational 2^+ states
S. Peltonen, D. S. Delion and J. Suhonen,
Phys. Rev. C **71**, 044315 (2005).

PHYSICAL REVIEW C **71**, 044315 (2005)

Systematics of the α decay to vibrational 2^+ states

S. Peltonen,[1] D. S. Delion,[2] and J. Suhonen[1]
[1]*Department of Physics, University of Jyväskylä, POB 35, FIN-40351, Jyväskylä, Finland*
[2]*National Institute of Physics and Nuclear Engineering, Bucharest-Măgurele, POB MG-6, Romania*
(Received 14 January 2004; revised manuscript received 3 June 2004; published 27 April 2005)

We give a systematic analysis of α decays to low-lying 2^+ states in even-even nuclei. Collective excitations are considered within the spherical quasiparticle random-phase approximation. We use realistic G-matrix elements of the Bonn interaction as a residual two-body force. The only free parameters are the ratio between the isovector and isoscalar strengths and proton-neutron asymmetry. The formalism can reproduce the main experimental trends versus the excitation energy for both the $B(E2)$ values and the α-decay hindrance factors. We reproduced most of the available data by using one common parametrization. It turns out that the fine structure of the α decay is more sensitive than electromagnetic transitions as a tool for investigating nuclear interaction. With the adopted parametrization, we predict $B(E2)$ values and α-decay hindrance factors in even-even nuclei.

DOI: 10.1103/PhysRevC.71.044315 PACS number(s): 21.60.Jz, 23.60.+e, 27.70.+q, 27.80.+w

I. INTRODUCTION

The importance of the interplay between the Coulomb barrier and Q value on α decay was one of the most important discoveries in the early days of nuclear physics [1]. It explained the exponential dependence of half-lives upon the energy of the emitted particle (Q value). The proposed physical picture was very simple though it contradicted the classical intuition, namely, a preformed α particle inside the nucleus penetrates quantum mechanically the surrounding Coulomb barrier.

Later on, the preformation probability of the α cluster inside the nucleus was introduced within the R-matrix theory [2]. This approach takes into account nuclear structure details, because the cluster is built from two protons and two neutrons moving in some mean field and interacting with each other via two-body residual forces [3]. The so-called preformation amplitude is defined as the overlap of the initial wave function and the product between the daughter and α-particle wave functions. For transitions between ground states, it is a coherent superposition of many single-particle configurations, including states in continuum. Therefore, the decay width is not very sensitive to the nuclear mean field parameters. A systematic analysis of decay widths in even- and odd-mass actinide nuclei was performed in Ref. [4] by using the pairing approach for preformation amplitudes and spherical penetration factors. The most recent calculation, including super-heavy nuclei, within a similar model was performed in Ref. [5].

The situation changes for transitions to excited states. It turns out that the decay width is very sensitive to the structure of the wave function in the daughter nucleus. The fine structure in spectra of emitted α particles cannot be explained by only different Q values, due to the excitation energy of the daughter nucleus. It is known for a long time that the experimental hindrance factors (HF), extracting the exponential dependence upon the Coulomb barrier, are not constant [6]. The first calculations of α decay in rotational nuclei by using the coupled channels method were performed in Ref. [7]. Reference [8] estimated HF's in rotational nuclei by using the Fröman approach [9] for the barrier penetration but a simple phenomenological ansatz for the preformation factor. The first attempts to calculate HF's in vibrational nuclei within the quasiparticle random-phase approximation (QRPA) were performed in Refs. [10–12]. Later, Ref. [13] gave an explanation for the connection between the HF of the first excited 0^+ state and the neutron number for Pb isotopes. The calculation was performed in terms of proton-neutron pairing vibrations within the spherical RPA formalism using two major shells above the Fermi surface.

Only relatively recent experimental papers suggested that the α-decay fine structure could be a powerful tool for investigating nuclear structure details. In the last decade, this new kind of α-decay spectroscopy was mainly used to investigate 0^+ and 2^+ excited states in the Pb region by the ISOLDE collaboration [14–20] and more recently by the Liverpool-Jyväskylä-Helsinki collaboration [21]. There is also an increasing interest in α-decay experiments searching for fine structure in the U region [22]. Moreover, in the related field of proton emission, two papers [23,24] have shown that the influence of surface vibrations on the emission process is very important.

The aim of this article is to perform a systematic analysis of the α-decay fine structure for the lowest 2^+ states in even-even nuclei with moderate quadrupole deformations. Moreover, it will be clearly shown that the α-decay fine structure is a more sensitive probe of the 2^+-state wave function than is the electromagnetic transition deexiting this state. We use the formalism developed in our previous works [25,26]. In Sec. II, we give the necessary theoretical details. In Sec. III, we investigate the HF together with electromagnetic transitions for vibrational and transitional even-even nuclei. Here some theoretical predictions are also given. Conclusions are drawn in the last section.

II. THEORETICAL BACKGROUND

The microscopic description of the α decay to vibrational states within the QRPA formalism was given in Ref. [26]. In this section, we summarize the main theoretical details necessary to compute the decay width.

Let us consider an α-decay process

$$B \rightarrow A(k) + \alpha, \tag{2.1}$$

where $k = 0$ denotes the ground state (g.s.) and $k > 0$ some excited state in the daughter nucleus. We will describe low-lying collective states in terms of particle-hole excitations within the spherical QRPA. Indeed, Ref. [27] showed that the influence of the deformation on α decay is mainly given by the penetration through the Coulomb barrier.

The excited states are described by a phonon operator acting on the daughter ground state, taken as a core

$$|A(k)\rangle = \Gamma^{\dagger}_{\lambda\mu}(k)|A\rangle. \tag{2.2}$$

The QRPA phonon is defined, as usual, by

$$\Gamma^{\dagger}_{\lambda\mu}(k) = \sum_{\tau}\sum_{j_1\leqslant j_2}\big[X^{(k)}_{\lambda}(\tau j_1 j_2)A^{\dagger}_{\lambda\mu}(\tau j_1 j_2) - Y^{(k)}_{\lambda}(\tau j_1 j_2)A_{\lambda-\mu}(\tau j_1 j_2)(-)^{\lambda-\mu}\big], \tag{2.3}$$

where $A^{\dagger}_{\lambda\mu}(\tau j_1 j_2)$ denotes the quasiparticle creation operator of the pair $(\tau j_1 j_2)$, with $\tau = \pi$ for protons and $\tau = \nu$ for neutrons. Here j is a short-hand notation for spherical quantum numbers, i.e., single-particle energy ϵ, angular momentum l, and total spin j. We will consider quadrupole phonon operators with $\lambda = 2$ to describe low-lying 2^+ collective excitations.

The amplitude of the decay process (2.1), called α-particle preformation amplitude, is given as an overlap integral over the internal coordinates of the daughter nucleus and the emitted cluster [3], i.e.,

$$F^{(k)}_{\lambda\mu}(\mathbf{R}) \equiv \langle A|(-)^{\lambda-\mu}\Gamma_{\lambda-\mu}(k)\Psi_{\alpha}|B\rangle = \int d\xi_A d\xi_{\alpha}\big[\Psi^{(k)}_{A}(\xi_A)\big]^{*}\Psi^{*}_{\alpha}(\xi_{\alpha})\Psi_{B}(\xi_B), \tag{2.4}$$

where ξ denotes the internal coordinates and $\mathbf{R}$ the center-of-mass coordinate of the α-daughter system. The preformation amplitude squared is the probability of having an α-decaying configuration inside the initial state. The above integral depends only upon the relative radius between the daughter nucleus and the emitted cluster.

We neglect the core-cluster antisymmetrization, because we estimate the overlap for distances beyond the geometrical nuclear radius, where the Pauli principle becomes less important [28]. For $k = 0$, one uses the ground state in the daughter nucleus instead of a QRPA excitation.

The most important ingredient of our calculation is the single-particle mean field, generating proton and neutron eigenstates. The single-particle wave functions are given in the harmonic oscillator (ho) representation as follows

$$\psi_{\tau\epsilon ljm}(\mathbf{r}, s) \equiv \langle \mathbf{r}, s|a^{\dagger}_{\tau\epsilon ljm}|0\rangle = \sum_{n} c_n(\tau\epsilon lj)\mathcal{R}_{nl}(\beta r^2)\big[i^l Y_l(\hat{r})\otimes\chi_{\frac{1}{2}}(s)\big]_{jm}. \tag{2.5}$$

Here $a^{\dagger}_{\tau\epsilon ljm}$ denotes the single-particle creation operator. The expansion coefficients $c_n(\tau\epsilon lj)$ are provided by the diagonalization procedure in the spherical ho basis $\mathcal{R}_{nl}(\beta r^2)$. They depend upon the standard ho parameter, defined as

$$\beta = f\frac{M_N\omega}{\hbar}, \tag{2.6}$$

where M_N is the nucleonic mass and $\hbar\omega = 41A^{-1/3}$. As shown in Refs. [5,29] the spectroscopic properties, connected with the bound spectrum, practically do not depend upon the value of the size parameter f. Moreover, Ref. [30] pointed out that the error in expanding the radial wave function in terms of the harmonic oscillator basis remains practically a constant in the interval $f \in [0.5, 1.2]$.

The radial part of the preformation amplitude for transitions to excited states is given by the following superposition

$$F^{(k)}_{\lambda}(R) = \sum_{N_{\alpha}} W^{(k)}(N_{\alpha}\lambda)\mathcal{R}_{N_{\alpha}\lambda}(4\beta R^2), \tag{2.7}$$

where the $W^{(k)}$ coefficient is given in App. A of Ref. [26]. The preformation amplitude, connecting the ground states of the two nuclei, is obtained in a similar way with $k = 0$, where the $W^{(0)}$ coefficient is defined in the same appendix. We stress the fact that the radial ho wave function $\mathcal{R}_{NL}(4\beta R^2)$ depends on four times the single-particle parameter β, due to the Talmi-Moshinsky transformation from absolute to relative and center-of-mass coordinates.

The most important ingredients entering the W coefficients in the above relations and expressing the nuclear structure details are the expansion coefficients of the mother in terms of the daughter wave function. For transitions to excited states, they are given by

$$|B\rangle = \frac{1}{2}\Bigg\{\sum_{j_1=j_2}\sum_{j_3\leqslant j_4}B(\pi j_1 j_2;\nu j_3 j_4)(a^{\dagger}_{\pi j_1}\otimes a^{\dagger}_{\pi j_2})_0\hat{\lambda} \times[(a^{\dagger}_{\nu j_3}\otimes a^{\dagger}_{\nu j_4})_{\lambda}\otimes\Gamma^{\dagger}_{\lambda}(k)]_0|A\rangle + \sum_{j_1=j_2}\sum_{j_3\leqslant j_4}B(\nu j_1 j_2;\pi j_3 j_4)(a^{\dagger}_{\nu j_1}\otimes a^{\dagger}_{\nu j_2})_0\hat{\lambda} \times[(a^{\dagger}_{\pi j_3}\otimes a^{\dagger}_{\pi j_4})_{\lambda}\otimes\Gamma^{\dagger}_{\lambda}(k)]_0|A\rangle\Bigg\}, \tag{2.8}$$

where $\hat{\lambda} = \sqrt{2\lambda+1}$. By expressing the particle operators in terms of quasiparticle operators, one obtains the following results

$$\begin{aligned} B(\pi j_1 j_2;\nu j_3 j_4) &= B^{(0)}(\pi j_1 j_2)B^{(k)}(\nu j_3 j_4),\\ B(\nu j_1 j_2;\pi j_3 j_4) &= B^{(0)}(\nu j_1 j_2)B^{(k)}(\pi j_3 j_4), \end{aligned} \tag{2.9}$$

where the two terms are given, respectively, by

$$\begin{aligned} B^{(0)}(\tau j_1 j_2) &= \delta_{j_1 j_2}\frac{\hat{j}_1}{2}u_{\tau j_1}v_{\tau j_1},\\ B^{(k)}(\tau j_3 j_4) &= \frac{1}{\sqrt{1+\delta_{j_3 j_4}}}\big[u_{\tau j_3}u_{\tau j_4}Y^{(k)}_{\lambda}(\tau j_3 j_4) - v_{\tau j_3}v_{\tau j_4}X^{(k)}_{\lambda}(\tau j_3 j_4)\big]. \end{aligned} \tag{2.10}$$

Here u, v denote BCS and X, Y QRPA amplitudes. In particular, for a g.s. to g.s. transition, one obtains the expansion given in Ref. [27].

The decay width is derived from the continuity equation and it is proportional to the asymptotic value of the radial wave function amplitude squared. The matching condition between the preformation amplitude and the outgoing Coulomb wave, for some radius R inside the Coulomb potential, gives the expression

$$\Gamma_\lambda^{(k)} = \hbar v \lim_{r\to\infty} \left|g_\lambda^{(k)}(r)\right|^2 = \left\{\frac{2\kappa R}{[G_\lambda(\kappa R)]^2}\right\}\left\{\frac{R\hbar^2}{2\mu}\left[F_\lambda^{(k)}(R)\right]^2\right\} \equiv \mathcal{P}_\lambda(E,R)\mathcal{F}_\lambda^{(k)}(R), \tag{2.11}$$

where v is the center-of-mass velocity, κ the momentum of the emitted α particle and R the center-of-mass radius. Note that the meaning of the letter Γ is different from the definition of the QRPA phonon (2.3). This quantity is a product of two functions, the penetrability $\mathcal{P}_\lambda$ and preformation probability $\mathcal{F}_\lambda$ (the so-called reduced width squared), which strongly depend upon the radius R. However, the final result $\Gamma_\lambda^{(k)}$ should be a constant in a region of several fm around the geometrical touching point. This is an important accuracy test for our calculations, and it was analyzed in detail in Ref. [26].

The HF of the first collective 2^+ state we estimate as the ratio between the corresponding "strengths" of the preformation factors, i.e.,

$$\mathrm{HF} = \frac{\left\langle R\left[F_0^{(0)}(R)\right]^2\right\rangle}{\left\langle R\left[F_2^{(1)}(R)\right]^2\right\rangle}, \tag{2.12}$$

where by brackets we denote the mean values, considered over the interval $R \geqslant R_c$, beyond the touching radius

$$R_c = 1.2\left(A_\alpha^{1/3} + A_A^{1/3}\right), \tag{2.13}$$

including the last two maxima of preformation amplitudes. We showed in Ref. [26] that the ratio of averaged quantities in (2.12) practically does not depend upon the matching radius. This definition is consistent with the experimental estimate given by

$$\mathrm{HF}_{\mathrm{exp}} = \frac{\Gamma_{\mathrm{exp}}^{(0)}}{\Gamma_{\mathrm{exp}}^{(1)}}\frac{\mathcal{P}_2(E-E_{2^+},R)}{\mathcal{P}_0(E,R)}, \tag{2.14}$$

where $\Gamma^{(k)}$, with $k=0$, denotes the decay width corresponding to a transition between ground states, and $k=1$ denotes the width associated with decay transition to the first 2^+ eigenstate. According to Rasmussen [6], the hindrance factor contains the pentration through a barrier with a sharp internal potential. As we will show later, the comparison between the two estimates gives a difference of less than a factor of 2, i.e., within the experimental error. Anyway, we prefer the estimate given by (2.14) because it depends only upon the well-defined irregular function $G_l(\kappa R)$, generated by the external Coulomb repulsion, and does not contain any arbitary internal potential.

The effect of the deformation, given by the Fröman matrix [9] for the penetration part, was recently investigated in Ref. [5], where it was shown that for $|\beta_2| \leqslant 0.2$ the effect of the barrier deformation is less than a factor of 2. Thus, the use of a deformed penetration for both transitions will give similar corrections and will not affect their ratio. This approach was used in Ref. [8] to investigate transitions to rotational states.

We also computed another useful quantity, namely, the spectroscopic factor, defined as

$$S_\alpha^{(k)} = \int_0^\infty \left|RF_\lambda^{(k)}(R)\right|^2 dR. \tag{2.15}$$

It gives the order of magnitude of the α-particle probability inside the nucleus.

Concerning the electromagnetic quadrupole transition, we used the standard relation for the reduced matrix element, namely,

$$\langle 0||T_2||k\rangle = \sum_\tau \sum_{j_1\leqslant j_2} \xi_{\tau j_1 j_2}\left[X_\lambda^{(k)}(\tau j_1 j_2) + Y_\lambda^{(k)}(\tau j_1 j_2)\right],$$
$$\xi_{\tau j_1 j_2} = \frac{e_\tau}{\sqrt{1+\delta_{j_1 j_2}}}\langle \tau j_1||r^2 Y_2||\tau j_2\rangle\left(u_{\tau j_1}v_{\tau j_2} + v_{\tau j_1}u_{\tau j_2}\right), \tag{2.16}$$

where e_τ denotes the effective charge and Y_2 the quadrupole spherical function.

III. $B(E2)$ AND HF SYSTEMATICS ALONG ISOTOPE CHAINS

A. Analysis of the experimental data

We will analyze α decays to low-lying 2^+ states in even-even nuclei with moderate quadrupole deformations, $|\beta_2| \leqslant 0.2$, i.e., in the so-called vibrational and transitional nuclei. At the same time, we will connect this strong interacting process with electromagnetic transitions in the daughter nucleus.

Concerning $B(E2)$ values, there are many available data, e.g., those in Ref. [31]. In Fig. 1 we plotted them as a function of the excitation energy for those even-even nuclei where

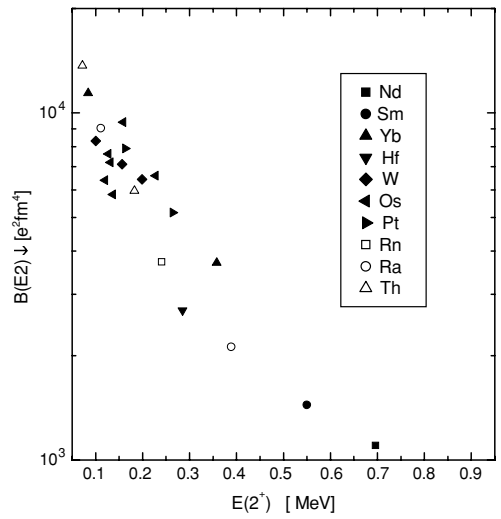

FIG. 1. Experimental $B(E2)$ values versus E_{2^+}.

TABLE I. Experimental hindrance factors [33] according to Rasmussen [6] and Eq. (2.14) (last two columns). The first columns give the three regions and the states in the abscissa of Fig. 2. The next columns give the charge and atomic numbers, energy of the 2^+ state [33], and quadrupole deformation [34]. Experimental errors for excitation energies and HF's are also given.

Region	i	Z	N	A	E_{2^+} (keV)	β_2	$HF_{\rm exp}^{\rm (Ras)}$	$HF_{\rm exp}$
(A)	1	76	96	172	228.0 ± 0.2	0.190	38 ± 19	21.287
	2	76	98	174	158.7 ± 0.3	0.226	3.3 ± 1.6	1.828
	3	78	98	176	263 ± 1	0.171	$152 \pm ??$	85.688
	4	78	100	178	170.7 ± 0.7	0.254	$31.3 \pm ??$	14.043
	5	78	102	180	$153 \pm ??$	0.265	47 ± 10	26.571
(B)	6	84	110	194	319 ± 10	0.026	110 ± 40	66.379
	7	84	112	196	463 ± 1	0.136	180 ± 60	173.541
	8	84	120	204	684.342 ± 0.010	0.009	1.25 ± 0.11	0.706
	9	84	122	206	703 ± 3	−0.018	6.9 ± 0.4	3.947
	10	84	124	208	686.528 ± 0.020	−0.018	1.43 ± 0.15	0.830
(C)	11	84	130	214	609.31 ± 0.06	−0.008	4.8 ± 0.8	2.774
	12	84	132	216	549.73 ± 0.05	0.020	3.2 ± 0.5	1.775
	13	84	134	218	511 ± 2	0.039	$1.9 \pm ??$	1.052
	14	86	130	216	461.9 ± 0.2	0.008	2.6 ± 0.8	1.565
	15	86	132	218	324.22 ± 0.05	0.040	1.45 ± 0.04	0.852
	16	86	134	220	240.986 ± 0.006	0.111	1.08 ± 0.01	0.622
	17	86	136	222	186.211 ± 0.013	0.137	0.96 ± 0.01	0.546
	18	88	130	218	389.2 ± 0.2	0.020	2.0 ± 0.7	1.219
	19	88	132	220	178.37 ± 0.09	0.103	0.96 ± 0.07	0.572
	20	88	134	222	111.12 ± 0.02	0.130	1.08 ± 0.02	0.650
	21	88	136	224	84.373 ± 0.003	0.164	0.90 ± 0.03	0.536
	22	90	132	222	$183.3 \pm ??$	0.111	1.4 ± 0.5	0.830
	23	90	134	224	93 ± 4	0.164	1.00 ± 0.07	0.579

α-decay half-lives to the ground state are measured. One can observe a universal systematic decreasing behavior versus the excitation energy, almost independent of the considered chain. This quantity is not very sensitive to other nuclear structure details, because of the collective character of the 2^+ state. Indeed, Ref. [32], showed that one has the following empirical relation between the $B(E2)$ value and E_{2^+} energy

$$B(E2) = \frac{cZ^2}{A^{2/3}E_{2^+}}, \tag{3.1}$$

where Z is the charge and A the mass number of the nucleus.

The situation is quite different concerning the α decay. At present, the amount of available HF data is limited; see, e.g. Ref. [33]. They are given in Table I. The last two columns given the experimental HF's, estimated according to the Rasmussen procedure $\mathrm{HF}_{\rm exp}^{\rm (Ras)}$ [6] and by using Eq. (2.14) $\mathrm{HF}_{\rm exp}$, respectively. One can see that they differ by a factor less than 2. Anyway, we prefer to use the simple definition (2.14), which is free of any potential parameter. We plotted the logarithm of the $\mathrm{HF}_{\rm exp}$ in Fig. 2 by a solid line, connecting experimental points along a given neutron chain. In the same figure, experimental values of the 2^+ energy are given by dashes. The labels on the abscissa correspond to the numbers in the first column of Table I. We divided the figure into three regions,

$$\begin{aligned} &\text{(A)}: Z < 82, \quad N < 126, \\ &\text{(B)}: Z > 82, \quad N < 126, \\ &\text{(C)}: Z > 82, \quad N > 126. \end{aligned} \tag{3.2}$$

First of all, one notices an opposite tendency compared to $B(E2)$ data, namely, a general decreasing trend by decreasing the excitation energy in the daughter nucleus. This is given by the solid lines along each isotope chain. It turns out that

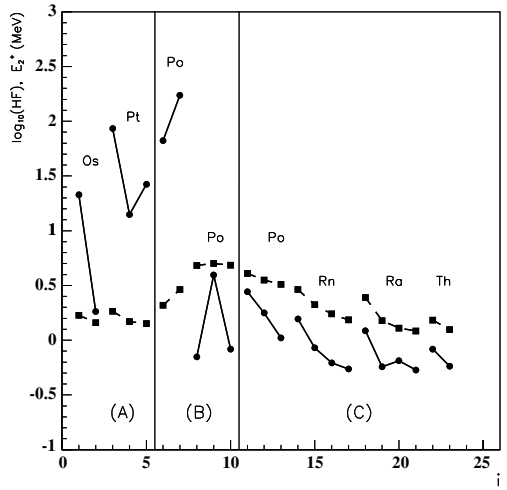

FIG. 2. Experimental hindrance factors (solid lines) and E_{2^+} (dashed lines) versus the state number in Table I.

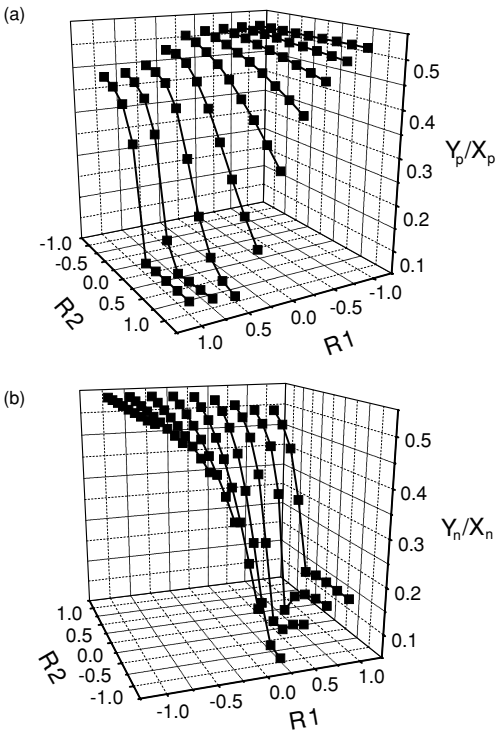

FIG. 3. The proton and neutron ratio of summed QRPA amplitudes squared Y_τ^2/X_τ^2, where (a) $\tau = \pi$ and (b) $\tau = \nu$, versus the ratios R_1 and R_2. The decay process is ^{220}Ra $\rightarrow$ ^{216}Rn.

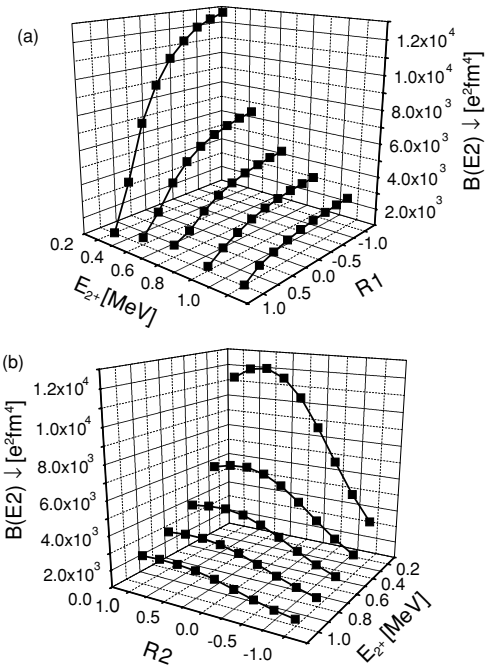

FIG. 4. $B(E2)$ values as a function of (a) E_{2^+}, R_1 for $R_2 = 0$ and (b) E_{2^+}, R_2 for $R_1 = 0$. The decay process is ^{220}Ra $\rightarrow$ ^{216}Rn.

the HF's in all the regions, apart from nuclei close to magic numbers, satisfy the following empirical rule

$$\log_{10}(\mathrm{HF}) = a E_{2^+} + b, \tag{3.3}$$

with a common coefficient for each of the regions. As a general rule, the slope of this dependence for region (A) is larger than for (C), i.e., $a_{(\mathrm{A})} > a_{(\mathrm{C})}$. The situation in region (B), describing Po isotopes as daughter nuclei, is more complex. Here one has a phase transition along Po isotopes, from large HF's, for neutron-deficient isotopes, to small ones. Unfortunately the available experimental values do not describe the full chain of Po isotopes. It seems that the left side of the region (B) has a behavior similar to that of (A), while the right one resembles the behavior of region (C).

This behavior is less universal than the trend of electromagnetic transitions. Thus, according to the available experimental material, one concludes that the α-decay fine structure is more sensitive to concrete nuclear structure details than the corresponding electromagnetic transition. This makes the study of the α decay to excited states a useful tool for investigating the properties of collective states.

B. Analysis of the QRPA features

In our analysis we will try to explain the above discussed experimental features within our QRPA formalism for collective 2^+ excitations. We used the universal parametrization of the Woods-Saxon potential, which is suitable for generating proton and neutron single-particle spectra, especially for nuclei around Pb region [35]. In the Woods-Saxon diagonalization procedure, we considered $N = 18$ major shells. In our calculation, we considered only 20 proton and 18–19 neutron *sp* states around the corresponding Fermi surfaces. Therefore, to simplify the calculations, we considered a smaller number of configurations than the value necessary to reproduce the absolute width [5]. Our analysis showed that indeed the ratio of decay widths for transitions to excited and ground state, i.e. HF, is sensitive only to spherical single-particle orbitals around the Fermi level. Moreover, HF is insensitive to the size used for parameter f because both preformation factors are changed in the same way. We used a standard value for this parameter, namely $f = 1$.

In Ref. [26] we used a modified surface δ residual interaction by decoupling strength parameters for different multipolarities. In our present analysis, we use realistic G-matrix elements generated by starting from the Bonn one-boson-exhange potential [36]. The quasiparticles are generated by the monopole part of the two-body interaction. The pairing strengths have been adjusted separately for protons and neutrons to reproduce experimental gap values. We considered

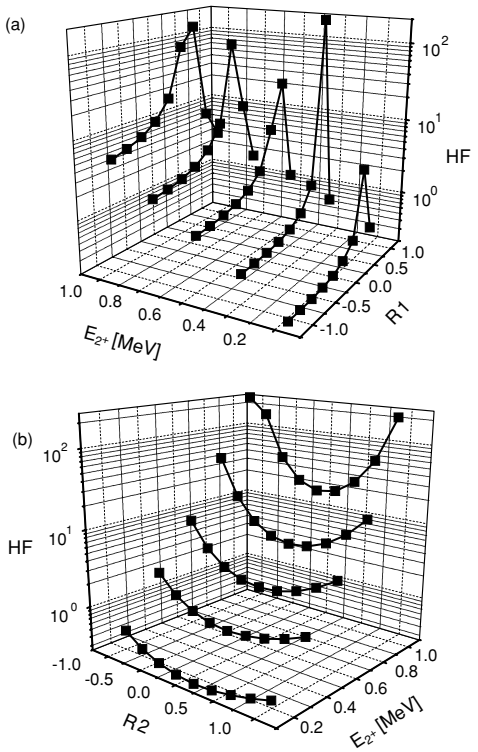

FIG. 5. Hindrance factor as a function of (a) E_{2^+}, R_1 for $R_2 = 0$ and (b) E_{2^+}, R_2 for $R_1 = 0$. The decay process is ^{220}Ra $\rightarrow$ ^{216}Rn.

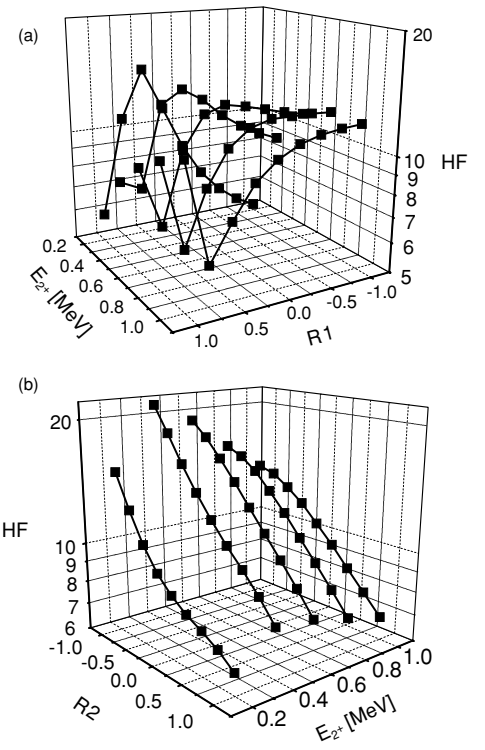

FIG. 6. Same as Fig. 5, but for the decay process ^{180}Hg $\rightarrow$ ^{176}Pt.

in our calculations only superfluid nuclei, i.e., for both mother and daughter nuclei, Z and N are not magic numbers.

To investigate the quadrupole-quadrupole part we used three parameters, namely the proton-proton V_π, neutron-neutron V_ν, and proton-neutron strengths $V_{\pi\nu}$. This allows us to schematically rewrite the residual interaction in the form

$$-V_\pi Q_\pi Q_\pi^\dagger - V_\nu Q_\nu Q_\nu^\dagger - V_{\pi\nu}\left[Q_\pi Q_\nu^\dagger + Q_\nu Q_\pi^\dagger\right] = -V_+ Q_+ Q_+^\dagger - V_- Q_- Q_-^\dagger - V_\pm\left[Q_+ Q_-^\dagger + Q_- Q_+^\dagger\right], \tag{3.4}$$

in terms of isoscalar Q_+ and isovector quadrupole components Q_-, defined as

$$Q_+ = Q_\pi + Q_\nu, \quad Q_- = Q_\pi - Q_\nu. \tag{3.5}$$

The corresponding strengths can be written as

$$V_+ = \frac{V_\pi + V_\nu + 2V_{\pi\nu}}{4}, \quad V_- = \frac{V_\pi + V_\nu - 2V_{\pi\nu}}{4}, \quad V_\pm = \frac{V_\pi - V_\nu}{4}. \tag{3.6}$$

Our analysis depends on only two parameters, namely, the following ratios

$$R_1 \equiv V_-/V_+ = \frac{V_\pi + V_\nu - 2V_{\pi\nu}}{V_\pi + V_\nu + 2V_{\pi\nu}}, \quad R_2 \equiv \frac{2V_\pm}{V_+ + V_-} = \frac{V_\pi - V_\nu}{V_\pi + V_\nu}, \tag{3.7}$$

because, after fixing them, we adjust V_+ to obtain the experimental value of the energy E_{2^+}. In what follows, we call ratio R_2 the proton-neutron asymmetry.

The QRPA amplitudes X, Y in Eq. (2.3) contain the information about the nuclear structure in the HF and $B(E2)$ values. These are the key ingredients connecting the two kinds of transition. Thus, we will characterize the "collectivity" of the first excited state, with $k = 1$, by the following proton and neutron ratios

$$Y_\tau^2 / X_\tau^2 \equiv \sum_{j_1 \leqslant j_2} Y_{\tau j_1 j_2}^2(1) \Big/ \sum_{j_1 \leqslant j_2} X_{\tau j_1 j_2}^2(1), \quad \tau = \pi, \nu. \tag{3.8}$$

The behavior of these ratios is strongly dependent upon the values of R_1 and R_2. This is shown in Fig. 3 for protons/neutrons for the decay process ^{220}Ra $\rightarrow$ ^{216}Rn.

TABLE II. Experimental and predicted HF's (in the last two columns) for α emitters below Pb. First four columns give the charge, mass number, quadrupole deformation [34] and E_{2^+} [31] in the daughter nucleus. The sixth and seventh columns give experimental $B(E2)$ values [31] and theoretical predictions. The interaction parameters are $R_1 = 0$, $R_2 = -0.75$. The fifth column gives the corresponding values of the strength V_+, according to Eqs. (3.6) and (3.7).

Z	A	β_2	E_{2^+}	V_+	$B(E2)_{\rm exp}$	$B(E2)$	$\rm HF_{exp}$	HF
60	144	0.149	0.696	0.722	$1.10\ 10^3$	$5.16\ 10^2$	–	$1.32\ 10^0$
62	146	0.155	0.747	0.709	–	$4.66\ 10^2$	–	$2.64\ 10^0$
62	148	0.161	0.550	0.671	$1.44\ 10^3$	$9.69\ 10^2$	–	$1.11\ 10^0$
64	148	0.156	0.784	0.716	–	$5.94\ 10^2$	–	$1.73\ 10^0$
64	150	0.161	0.638	0.657	–	$8.13\ 10^2$	–	$2.00\ 10^0$
66	150	0.153	0.804	0.706	–	$6.40\ 10^2$	–	$1.48\ 10^0$
68	152	−0.018	0.808	0.724	–	$8.31\ 10^2$	–	$1.22\ 10^0$
68	154	0.143	0.561	0.675	–	$1.58\ 10^3$	–	$6.35\ 10^{-1}$
70	154	−0.008	0.821	0.702	–	$5.85\ 10^2$	–	$2.47\ 10^0$
70	156	0.125	0.536	0.669	–	$1.65\ 10^3$	–	$6.85\ 10^{-1}$
70	158	0.161	0.358	0.618	$3.70\ 10^3$	$2.31\ 10^3$	–	$5.25\ 10^{-1}$
72	156	0.035	0.858	0.606	–	$3.08\ 10^2$	–	$3.97\ 10^1$
72	158	0.107	0.476	0.600	–	$1.02\ 10^3$	–	$2.89\ 10^0$
72	160	0.152	0.390	0.624	–	$2.40\ 10^3$	–	$1.18\ 10^0$
72	162	0.180	0.285	0.570	$2.70\ 10^3$	$3.54\ 10^3$	–	$1.08\ 10^0$
74	162	0.134	0.450	0.542	–	$1.09\ 10^3$	–	$3.67\ 10^1$
74	164	0.161	0.332	0.564	–	$2.48\ 10^3$	–	$5.89\ 10^0$
74	166	0.181	0.252	0.532	–	$3.24\ 10^3$	–	$2.49\ 10^0$
76	166	0.134	0.431	0.511	–	$1.01\ 10^3$	–	$3.77\ 10^1$
76	168	0.162	0.341	0.477	–	$1.48\ 10^3$	–	$7.20\ 10^1$
76	170	0.171	0.287	0.487	–	$1.67\ 10^3$	–	$1.57\ 10^1$
76	172	0.190	0.228	0.490	$6.60\ 10^3$	$2.62\ 10^3$	$2.13\ 10^1$	$2.85\ 10^1$
78	172	0.126	0.457	0.472	–	$9.80\ 10^2$	–	$1.07\ 10^1$
78	174	0.153	0.394	0.499	–	$1.02\ 10^3$	–	$1.31\ 10^1$
78	176	0.171	0.264	0.514	$5.16\ 10^3$	$1.90\ 10^3$	$8.57\ 10^1$	$1.55\ 10^1$

We stress that $R_1 = 0, R_2 = 0$ corresponds to a pure isoscalar interaction with a common nucleon-nucleon interaction strength, i.e., $V_\pi = V_\nu = V_{\pi\nu}$. In Ref. [26] we investigated this case for transitions from the Rn isotopes. Now we have extended our analysis to the interval $-1 < R_1 < 1$. In particular, when $R_1 = -1$, $R_2 = 0$, one has $V_\pi = V_\nu = 0$ and only the effective interaction between proton and neutron systems $V_{\pi\nu}$ has a nonvanishing value. In the opposite extreme, i.e., for $R_1 = 1$, $R_2 = 0$, the effective interaction between proton and neutron systems vanishes, $V_{\pi\nu} = 0$. We also considered in our analysis a nonvanishing proton-neutron asymmetry parameter R_2, which was equal to zero in our previous reference.

First, we analyzed the behavior of the $B(E2)$ value as a function of the ratio R_1 and R_2 and excitation energy E_{2^+}. We used in Eq. (2.16) the bare charges $e_\pi = 1, e_\nu = 0$. As a typical example, in Fig. 4(a) we plot $B(E2)$ values as a function of R_1 and excitation energy for $R_2 = 0$ by considering the decay process $^{220}\rm Ra \rightarrow {}^{216}Rn$. In Fig. 4(b), we give a similar plot versus R_2 and excitation energy for $R_1 = 0$. One can see that the $B(E2)$ value decreases when R_1 and the excitation energy increase or when R_2 decreases. It is interesting that the dependence of the $B(E2)$ value on these variables is monotonic, except in the vicinity of $R_1 = 1$. This feature explains the universal behavior of experimental data, seen in Fig. 1. Therefore, we conclude that the QRPA is able to reproduce the experimental behavior of the $B(E2)$ value versus the excitation energy E_{2^+}.

Let us now consider the main quantity in our analysis, namely, the HF. In the three-dimensional Fig. 5(a), we plot this quantity as a function of the ratio R_1 (with $R_2 = 0$) and E_{2^+} for the decay process $^{220}\rm Ra \rightarrow {}^{216}Rn$ of region (C); while in Fig. 5(b), we plot the HF versus the ratio R_2 (with $R_1 = 0$) and E_{2^+}. One observes, first of all, that the HF has much stronger dependence upon R_1, R_2, and E_{2^+} than the $B(E2)$ value. This means that the HF is more sensitive to the Y_τ^2/X_τ^2 ratio than is the electromagnetic transition. On the other hand, as a general rule, the HF increases with the increase of the excitation energy, thus reproducing the main trend of experimental data in Fig. 2. In Fig. 6 we made the same plots as in Fig. 5 but for the transition $^{180}\rm Hg \rightarrow {}^{176}Pt$ from region (A). Comparing these two sets of figures one immediately notices a more complex behavior of the slopes of the HF vs E_{2^+} curves. Moreover, our numerical analysis for several decay processes showed that, as a general rule, the slope versus the excitation energy is larger in region (A) than in region (C). Thus, once again, the QRPA is able to reproduce the main experimental trends.

C. Systematic predictions

Finally, we computed the $B(E2)$ values and HF's for several vibrational and transitional nuclei, where α-decay half-lives were measured. We studied the dependence of the standard mean square deviation from experimental data both for the $B(E2)$ and HF's. It turned out that this quantity

TABLE III. Same as in Table II, but for α emitters above Pb. The interaction parameters are $R_1 = 0$, $R_2 = -0.75$, except for the first two nuclei, where $R_1 = 0.5$, $R_2 = -0.75$.

Z	A	β_2	E_{2^+}	V_+	$B(E2)_{\rm exp}$	$B(E2)$	$\mathrm{HF}_{\rm exp}$	HF
84	194	0.026	0.319	0.544	–	$4.55\ 10^{+2}$	$6.64\ 10^{+1}$	$9.80\ 10^{+1}$
84	196	0.136	0.463	0.519	–	$4.21\ 10^{+2}$	$1.74\ 10^{+2}$	$1.25\ 10^{+2}$
84	200	0.009	0.666	0.530	–	$5.34\ 10^{+2}$	–	$1.94\ 10^{+2}$
84	202	0.009	0.677	0.529	–	$4.80\ 10^{+2}$	–	$1.85\ 10^{+1}$
84	204	0.009	0.684	0.503	–	$3.03\ 10^{+2}$	$7.06\ 10^{-1}$	$3.25\ 10^{+0}$
84	206	−0.018	0.700	0.521	–	$2.39\ 10^{+2}$	$3.95\ 10^{+0}$	$1.32\ 10^{+0}$
84	212	0.045	0.727	0.745	–	$3.25\ 10^{+2}$	–	$1.19\ 10^{+1}$
84	214	−0.008	0.609	0.720	–	$6.41\ 10^{+2}$	$2.77\ 10^{+0}$	$3.92\ 10^{+0}$
84	216	0.020	0.550	0.691	–	$8.89\ 10^{+2}$	$1.77\ 10^{+0}$	$4.04\ 10^{+0}$
84	218	0.039	0.511	0.594	–	$5.81\ 10^{+2}$	$1.05\ 10^{+0}$	$3.37\ 10^{+1}$
86	202	−0.104	0.504	0.529	–	$9.17\ 10^{+2}$	–	$7.36\ 10^{+2}$
86	204	−0.087	0.543	0.544	–	$8.96\ 10^{+2}$	–	$4.09\ 10^{+1}$
86	206	−0.044	0.575	0.537	–	$6.47\ 10^{+2}$	–	$5.20\ 10^{+0}$
86	208	−0.026	0.636	0.494	–	$2.90\ 10^{+2}$	–	$3.84\ 10^{+0}$
86	214	0.008	0.694	0.750	–	$6.79\ 10^{+2}$	–	$4.63\ 10^{+0}$
86	216	0.008	0.465	0.730	–	$1.61\ 10^{+3}$	$1.56\ 10^{+0}$	$1.60\ 10^{+0}$
86	218	0.040	0.324	0.695	–	$2.57\ 10^{+3}$	$8.52\ 10^{-1}$	$9.43\ 10^{-1}$
86	220	0.111	0.241	0.663	$3.72\ 10^{+3}$	$3.28\ 10^{+3}$	$6.22\ 10^{-1}$	$8.05\ 10^{-1}$
88	208	−0.104	0.520	0.545	–	$9.15\ 10^{+2}$	–	$2.12\ 10^{+1}$
88	210	−0.053	0.603	0.527	–	$4.85\ 10^{+2}$	–	$5.02\ 10^{+0}$
88	216	0.008	0.688	0.747	–	$9.81\ 10^{+2}$	–	$5.20\ 10^{+0}$
88	218	0.020	0.389	0.720	$2.12\ 10^{+3}$	$2.38\ 10^{+3}$	$1.22\ 10^{+0}$	$1.17\ 10^{+0}$
90	218	0.008	0.689	0.747	–	$1.49\ 10^{+3}$	–	$9.70\ 10^{+0}$
90	220	0.030	0.373	0.719	–	$4.29\ 10^{+3}$	–	$2.63\ 10^{+0}$

has a pronounced minimum concerning the $B(E2)$ value for $R_1 = 0$, $R_2 = -0.75$ in region (C) and the right side of region (B). In region (A), this quantity is not sensitive to R_1 for the interval $R_1 \in [-1, 0]$. Concerning the HF, we found that the minimal standard square deviation is achieved close to the same values $R_1 = 0$, $R_2 = -0.75$.

Therefore, we chose these values to make predictions for both the $B(E2)$ values and the HF's for the other nuclei. In the last column of Table II, we give the HF's, as predictions by our model, for measured α decays connecting ground states of even-even nuclei with moderate deformations in the region $Z < 82$. We considered only those nuclei with $E_{2^+} \geqslant 0.2$ MeV. Here, we also give the corresponding $B(E2)$ values. One can see that the electromagnetic transitions are rather well reproduced, together with most of the measured HF's. In Table III we give similar predictions for even-even α emitters with $Z > 82$. We divided the table into the abovementioned (B) (upper part) and (C) (lower part) regions. Except for some values in the region (B) in beginning of the Table III, our results are in good agreement with experimental data, concerning both the $B(E2)$ values and the HF's. The value $R_1 = 0$ would correspond to an isoscalar symmetry for equal strengths.

Because $R_2 = -0.75$, the neutron strength dominates over the proton one ($V_\nu = 7V_\pi$), but at the same time it is comparable with the proton-neutron strength, $V_{\pi\nu} \approx 0.57V_\nu$. We stress that these strengths were obtained as the best fit result for $B(E2)$ values. Consequently, the neutron-proton asymmetry is at least partially explained by the use of a vanishing neutron charge in the transition operator. On the other hand, the HF's, obtained by using an independent approach, seem to confirm the validity of this result. Still, because of the relative small number of experimental data on α-decay intensities to excited states, a further investigation is necessary.

The phase transition in region (B) was reproduced by using different values of the ratio parameter R_1. Thus, the first two large HF's can be reproduced by using $R_1 = 0.5$, with the same R_2. For the moment, we do not have experimental data concerning $B(E2)$ values for these nuclei, and we can only point out this interesting feature.

We should also point out that several nuclei as ^{216,218}Po, ^{218,220}Rn, ^{218}Ra have important octupole deformations [34]. Concerning Po isotopes, our systematics indeed predicts HF's that are three times, larger, but for the remaining nuclei they are within the experimental errors. At the same time, let us mention that the excitation energies for Rn and Ra isotopes are two times less than in the case of Po isotopes. According to Eq. (3.3), the HF depends exponentially upon the excitation energy. Thus, the influence of octupole vibrations becomes indeed stronger in the former case.

Finally, we should point out that the spectroscopic factors for transitions connecting ground states, computed by using Eq. (2.15), have similar values for the decays below Pb, namely, $S_\alpha^{(0)} \approx 5 \times 10^{-3}$. For decays above Pb, we obtained $S_\alpha^{(0)} \approx 10^{-3}$. This gives the order of magnitude of the α-decay preformation probability, which agrees with the estimate of Ref. [37].

Thus we show once again that α-decay fine structure involving the first 2^+ state is a more sensitive tool for probing

the residual interaction than is the electromagnetic transition deexiting the first 2^+ state.

IV. CONCLUSIONS

In this article we presented a systematics of the α-decay HF and $B(E2)$ values of the first excited 2^+ states in even-even nuclei. We computed the α-decay HF within the spherical QRPA formalism. The single-particle spectrum is given by a diagonalization procedure of the Woods-Saxon mean field with the universal parametrization. We considered as a residual force a realistic two-body interaction, obtained from the G-matrix elements of the Bonn interaction. The only free parameters will the ratio of the isovector to the isoscalar strength R_1 and the proton-neutron asymmetry R_2.

We performed a systematic analysis of the HF and $B(E2)$ values versus these ratios and the energy E_{2^+} of the first collective state. This formalism was able to explain the main trends seen in the systematics of experimental data, namely, the universal decrease of the $B(E2)$ value and the increase of the HF with increasing energy E_{2^+} along any neutron chain. Moreover, the specific character of each isotope chain, concerning the slope of the HF versus E_{2^+}, could be explained by concrete nuclear structure details. We proposed an empirical linear dependence between the logarithm of the hindrance factor and the lowest energy E_{2^+}. This dependence was confirmed by our QRPA calculations.

We found out that most of the existing experimental data concerning the $B(E2)$ value and HF could be reproduced by using a single set of parameters, namely $R_1 = 0$, $R_2 = -0.75$, except for very neutron-deficient nuclei, where $R_1 = 0.5$.

ACKNOWLEDGMENTS

This work has been supported by the Academy of Finland under the Finnish Centre of Excellence Programme 2000–2005 (Project No. 44875, Nuclear and Condensed Matter Programme at JYFL). One of us (D.S.D.) is thankful for the hospitality extended to him by the Department of Physics of the University of Jyväskylä, where part of this work was performed. Discussions with R. Julin and M. Leino (Jyväskylä) are gratefully acknowledged.

[1] G. Gamow, Z. Phys. **51**, 204 (1928).
[2] R. G. Thomas, Prog. Theor. Phys. **12**, 253 (1954); A. M. Lane and R. G. Thomas, Rev. Mod. Phys. **30**, 257 (1958).
[3] H. J. Mang, Annu. Rev. Nucl. Sci. **14**, 1 (1964).
[4] J. K. Poggenburg, H. J. Mang, and J. O. Rasmussen, Phys. Rev. **181**, 1697 (1969).
[5] D. S. Delion, A. Sandulescu, and W. Greiner, Phys. Rev. C **69**, 044318 (2004).
[6] J. O. Rasmussen, Phys. Rev. **113**, 1593 (1959).
[7] J. O. Rasmussen and B. Segal, Phys. Rev. **103**, 1298 (1956).
[8] H. M. A. Radi, A. A. Shihab-Eldin, J. O. Rasmussen, and Luiz F. Oliveira, Phys. Rev. Lett. **41**, 1444 (1978).
[9] P. O. Fröman, Kgl. Dan. Vidensk. Selsk. Mat.-Fys. **1**, 3 (1957).
[10] A. Sandulescu and O. Dumitrescu, Phys. Lett. **19**, 404 (1965).
[11] A. Sandulescu and O. Dumitrescu, Phys. Lett. **B24**, 212 (1967).
[12] M. I. Cristu, O. Dumitrescu, N. I. Pyatov, and A. Sandulescu, Nucl. Phys. **A130**, 31 (1969).
[13] D. S. Delion, A. Florescu, M. Huyse, J. Wauters, and P. Van Duppen (ISOLDE Collaboration), Phys. Rev. Lett. **74**, 3939 (1995); Phys. Rev. C **54**, 1169 (1996).
[14] J. Wauters, P. Dendooven, P. Decrock, M. Huyse, R. Kirchner, O. Klepper, G. Reusen, E. Roeckl, and P. Van Duppen, Z. Phys. A **342**, 277 (1992).
[15] J. Wauters, P. Dendooven, M. Huyse, G. Reusen, P. Lievens, P. Van Duppen (ISOLDE Collaboration), Z. Phys. A **344**, 29 (1992).
[16] J. Wauters, P. Dendooven, M. Huyse, G. Reusen, P. Van Duppen, R. Kirchner, O. Klepper, and E. Roeckl, Z. Phys. A **345**, 21 (1993).
[17] J. Wauters, P. Dendooven, M. Huyse, G. Reusen, P. Van Duppen, and P. Lievens (ISOLDE Collaboration), Phys. Rev. C **47**, 1447 (1993).
[18] J. Wauters, N. Bijnens, H. Folger, M. Huyse, H. Y. Hwang, R. Kirchner, and J. von Schwarzenberg, Phys. Rev. C **50**, 2768 (1994).
[19] J. Wauters *et al*., Phys. Rev. Lett. **72**, 1329 (1994).
[20] N. Bijnens *et al*., Phys. Rev. Lett. **75**, 4571 (1995).
[21] R. G. Allatt *et al*., Phys. Lett. **B437**, 29 (1998).
[22] C. F. Liang, R. K. Sheline, P. Paris, M. Hussonnois, J. F. Ledu, and D. B. Isabelle, Phys. Rev. C **49**, 2230 (1994).
[23] C. N. Davids and H. Esbensen, Phys. Rev. C **64**, 034317 (2001).
[24] K. Hagino, Phys. Rev. C **64**, 041304(R) (2001).
[25] D. S. Delion and R. J. Liotta, Phys. Rev. C **56**, 1782 (1997).
[26] D. S. Delion and J. Suhonen, Phys. Rev. C **64**, 064302 (2001).
[27] D. S. Delion, A. Insolia, and R. J. Liotta, Phys. Rev. C **46**, 1346 (1992).
[28] T. Fliessbach and S. Okabe, Z. Phys. A **320**, 289 (1985).
[29] D. S. Delion, A. Insolia, and R. J. Liotta, Phys. Rev. C **54**, 292 (1996).
[30] D. S. Delion and J. Suhonen, Phys. Rev. C **61**, 024304 (2000).
[31] S. Raman, C. W. Nestor, Jr., and P. Tikkanen, At. Data Nucl. Data Tables **78**, 1 (2001).
[32] S. Raman, C. W. Nestor, S. Kahane, and K. H. Bhatt, Phys. Rev. C **43**, 556 (1991).
[33] Y. A. Akovali, Nucl. Data Sheets **84**, 1 (1998).
[34] P. Möller, J. R. Nix, W. D. Myers, and W. J. Swiatecki, At. Data Nucl. Data Tables **59**, 185 (1995).
[35] J. Dudek, Z. Szymanski, and T. Werner, Phys. Rev. C **23**, 920 (1981).
[36] K. Holinde, Phys. Rep. **68**, 121 (1981).
[37] R. Blendowske, T. Fliessbach, and H. Walliser, Nucl. Phys. **A464**, 75 (1987).

Paper II

Systematics of the α-decay to rotational states
D. S. Delion, S. Peltonen and J. Suhonen,
Phys. Rev. C **73**, 014315 (2006).

PHYSICAL REVIEW C **73**, 014315 (2006)

Systematics of the α-decay to rotational states

D. S. Delion,[1] S. Peltonen,[2] and J. Suhonen[2]
[1]*National Institute of Physics and Nuclear Engineering, Bucharest-Măgurele, POB MG-6, Romania*
[2]*Department of Physics, University of Jyväskylä, POB 35, FIN-40351, Jyväskylä, Finland*
(Received 28 November 2005; published 27 January 2006)

We analyze α decays to rotational states in even-even nuclei by using the stationary coupled channels approach. Collective excitations are described by the rigid rotator model. The α-nucleus interaction is given by a double folding procedure using M3Y plus Coulomb nucleon-nucleon forces. We use a harmonic oscillator repulsive potential with one independent parameter, to simulate the Pauli principle. The decaying state is identified with the first resonance inside the resulting pocketlike potential. The energy of the resonant state is adjusted to the experimental Q value by using the depth of the repulsion. We obtained a good agreement with existing experimental data concerning total half-lives and decay widths to $J = 2^+$ states by changing the factor multiplying the nucleon-nucleon interaction according to the rule $v_a = 0.668 - 0.004\,(A - 208)$. Concerning the decay widths to $J = 4^+$ states we obtained a good agreement for $Z = 90$ neutron chain and a satisfactory description for $Z = 92$, 96, and 98, chains. It is possible to improve the agreement concerning transitions to $J = 4^+$ states by considering a constant quenching strength $v_a = 0.6$ and by changing the width of the Gaussian describing the α-cluster density according to the rule $b = 1.744 - 0.032\,(A - 208)$. We found out that the computed widths to excited states are correlated with the corresponding deformation parameters. We conclude that the α-decay fine structure is a sensitive tool to probe fundamental aspects of the effective nuclear interaction and its dependence on the α clustering.

DOI: 10.1103/PhysRevC.73.014315 PACS number(s): 21.10.Tg, 23.60.+e, 24.10.Eq

I. INTRODUCTION

The importance of the Coulomb interaction for the α-decay width is well known [1]. It defines the probability for a preformed α particle to penetrate quantum-mechanically the electrostatic barrier. The relative values of half-lives can be satisfactorily described within this simple picture. To describe absolute half-lives it is also necessary to consider the α-particle spectroscopic factor, or preformation probability, multiplying the barrier penetrability. This factor was introduced within the R-matrix theory in Refs. [2–4]. It is defined by the square of the overlap between the internal wave function and the product of the daughter and α-particle wave functions.

The first systematic analysis of α-decay widths in even and odd-mass actinide nuclei was performed in Ref. [5], by using the pairing approach for the preformation probability and spherical penetration factors. Very recently we performed a systematic analysis of all measured decays between ground states by using a similar paring interaction but including single particle configurations in continuum and a deformed penetration factor. We evidenced the important role played by the preexisting α clustering [6] in addition to the shell-model preformation.

For transitions between ground states the preformation factor is a coherent superposition of many single-particle configurations, including states in continuum and therefore the decay width is not very sensitive to the nuclear structure details. The situation becomes quite different for transitions to excited states, because only those single-particle states that are around the Fermi surfaces are involved. Therefore decay widths to excited states are very sensitive to the structure of the wave function in the daughter nucleus. To separate the exponential dependence between the decay width and Q value one extracts the barrier penetration by introducing the so-called hindrance factors (HF) [7]. They define the ratio between preformation probabilities of two nuclear states.

The first attempts to compute HFs in vibrational nuclei within the quasiparticle random-phase approximation (QRPA) were performed in Refs. [8–10]. Later on, in Ref. [11] an explanation was given for the connection between the HF of the first excited 0^+ state and the neutron number for Pb isotopes. In the last decade the α-decay spectroscopy was used to investigate the 0^+ and 2^+ excited states in the Pb [12–19] and U region [20]. We analyzed some of the experimental results concerning the fine structure of 2^+ states by using the QRPA formalism in Refs. [21–23].

The first computations of the α-decay widths in rotational nuclei by using the coupled channels method were performed in Ref. [24]. In Ref. [25] HFs were estimated in rotational nuclei by using the Fröman approach [26] for the barrier penetration and a simple phenomenological ansatz for the preformation factor. The α-core potential was estimated by using the double folding procedure in Refs. [27,28] and more recently in Ref. [29]. In all these works it was concluded that the strength of the nucleon-nucleon force should be quenched (i.e., the Coulomb barrier should increase) to describe the right relation between the half-life and Q value. This kind of potential was used to estimate ground-state-to-ground-state half-lives within the spherical approach in Ref. [30]. In Ref. [31] the densities in the double-folded α-core potential were computed within the relativistic mean-field theory.

In several recent articles [32–34] we analyzed the double fine structure of emitted fragments in the cold fission of ^{252}Cf within the coupled channels formalism. The fissioning state was identified with a resonance in the interfragment potential, computed using the already-mentioned double

folding procedure. For the external part of the potential we used the two-body M3Y plus Coulomb interaction. The energy was adjusted to reproduce the experimental Q value by using an internal repulsive core. We found out that the yields to excited states in both fragments are very sensitive to nuclear structure details such as the mean-field deformation and density diffusivity. Unfortunately there are only few available experimental data to be analyzed in this field [35].

However, there are a lot of high-precision data on α-decay fine structure to rotational levels, see, e.g., Ref. [36]. The aim of this article is to apply the coupled channels technique, used to describe double fine structure in cold fission, in the simpler case of α decay. In this way we can test to what extent the microscopically computed interfragment potential is able to describe not only the total decay width but also the very complex picture of decay widths to rotational levels.

The article is organized according to the following plan: In Sec. II we shortly remind the main ingredients of the stationary coupled channels formalism describing α-decay fine structure to rotational states. In Sec. III we analyze the influence of the attractive and repulsive parts of the potential on the decay widths. In Sec. IV we give a systematics on measured α-decay widths. In the last section we draw conclusions.

II. THEORETICAL BACKGROUND

In this section we summarize the main theoretical details necessary to compute the decay width within the coupled channels formalism. The main ingredients were already introduced in Ref. [34] to investigate the double fine structure in cold fission. We supposed that both fragments were left in rotational states. In our case the theoretical description becomes simpler, because only the heavy fragment can be excited.

A. Coupled channels formalism

Let us consider an α-decay process

$$P \rightarrow D(J) + \alpha, \tag{1}$$

where J denotes the spin of the rotational state of an even-even nucleus, i.e., $J = 0, 2, 4, 6, \ldots$ We describe the α-core dynamics as in Ref. [34], by using the stationary Schrödinger equation

$$H\Psi(\mathbf{R}, \Omega_D) = E\Psi(\mathbf{R}, \Omega_D), \tag{2}$$

where $\mathbf{R} = (R, \Omega)$ denotes the distance between the centers of two fragments and $E = Q_\alpha$. The orientation of the daughter major axis in the laboratory system is given by Euler angles $\Omega_D = (\varphi_D, \theta_D, 0)$. Because of the fact that all measured decay widths are by many orders of magnitude smaller than the corresponding Q values the stationarity is a very good assumption and an α-decaying state is identified with a narrow resonant solution, containing only outgoing components.

The Hamiltonian describing the α decay in the laboratory system of coordinates is written as follows

$$H = -\frac{\hbar^2}{2\mu}\nabla_R^2 + H_D(\Omega_D) + V(\mathbf{R}, \Omega_D), \tag{3}$$

where μ is the reduced mass of the dinuclear system and H_D describes the rotation of the core. We estimate the interaction between nuclei in terms of the double folding between the nuclear densities [37,38], i.e.,

$$V(\mathbf{R}, \Omega_D) = \int d\mathbf{r}_D \int d\mathbf{r}_\alpha \rho_D(\mathbf{r}_D)\rho_\alpha(\mathbf{r}_\alpha)v(\mathbf{R} + \mathbf{r}_D - \mathbf{r}_\alpha), \tag{4}$$

where v denotes the nucleon-nucleon force. This procedure was widely used to compute the potential between heavy ions by using for their densities a Woods-Saxon shape. In our case the density of the daughter nucleus is given by such a distribution, whereas that of the α particle by a Gaussian with standard parameters [29].

The resulting potential can be divided into a spherical (V_0) and a deformed component (V_d) as follows:

$$V(\mathbf{R}, \Omega_D) = V_0(R) + V_d(\mathbf{R}, \Omega_D). \tag{5}$$

By expanding the nuclear densities in multipoles one obtains the deformed part of the interaction

$$V_d(\mathbf{R}, \Omega_D) = \sum_{\lambda>0} V_\lambda(R)\mathcal{Y}_\lambda(\Omega, \Omega_D). \tag{6}$$

Here the angular part of the wave function has the following ansatz:

$$\mathcal{Y}_\lambda(\Omega, \Omega_D) = [Y_\lambda(\Omega) \otimes Y_\lambda(\Omega_D)]_0. \tag{7}$$

Therefore the rotation of the core is compensated by the rotation of the α particle in the opposite direction. The relation in Eq. (6), with the angular part [Eq. (7)], is nothing else than a multipole-multipole expansion, where the multipole formfactors $V_\lambda(R)$ are given in terms of density distributions [38]. Some authors postulate the radial formfactors in a phenomenological way. In our computations we use the M3Y nucleon-nucleon [39] plus Coulomb force. For details see Ref. [38].

To this potential we also add a simple repulsive core, depending on one independent parameter. The role of this potential is similar to that in Refs. [32–34], where we investigated cold fission. Namely it simulates the Pauli principle and adjusts the energy of the system to the experimental Q value. We show that the total half-life and the partial decay widths do not depend on the shape of this repulsive potential.

If the rotational states of the core belong to the ground band (with the intrinsic angular momentum projection $K = 0$) the wave function is given by a similar superposition, i.e.,

$$\Psi(\mathbf{R}, \Omega_D) = \frac{1}{R}\sum_J f_J(R)\mathcal{Y}_J(\Omega, \Omega_D). \tag{8}$$

The wave functions describing the ground band rotations satisfy the following eigenvalue equations

$$H_D Y_{JM}(\Omega_D) = E_J Y_{JM}(\Omega_D), \tag{9}$$

i.e., they are the normalized Wigner functions with $K = 0$.

By using the orthonormality of angular functions entering the superposition in Eq. (8) one obtains in a standard way the coupled system of differential equations for radial components

$$\frac{d^2 f_J(R)}{d\rho_J^2} = \sum_{J'} A_{JJ'}(R) f_{J'}(R), \tag{10}$$

where the coupling matrix is given by the following:

$$A_{JJ'}(R) = \left[\frac{J(J+1)}{\rho_J^2} + \frac{V_0(R)}{E-E_J} - 1\right]\delta_{JJ'} + \frac{1}{E-E_J}\langle \mathcal{Y}_J | V_d(R) | \mathcal{Y}_{J'}\rangle. \tag{11}$$

Here we introduce the following short-hand notations:

$$\rho_J = \kappa_J R, \quad \kappa_J = \sqrt{\frac{2\mu(E-E_J)}{\hbar^2}}. \tag{12}$$

The matrix element $\langle \mathcal{Y}_J | V_d(R) | \mathcal{Y}_{J'}\rangle$ entering Eq. (11) is given by standard manipulations of angular-momentum algebra. The result is given in terms of the Clebsch-Gordan coefficient as follows:

$$\langle \mathcal{Y}_J | V_d(R) | \mathcal{Y}_{J'}\rangle = \sum_{\lambda>0} V_\lambda(R) \sqrt{\frac{2J+1}{4\pi(2J'+1)}} \times [\langle J, 0; \lambda, 0 | J', 0\rangle]^2. \tag{13}$$

Let us mention that at large distances, where the field becomes spherical and Coulombian the system of equations has a simple form

$$\left[-\frac{d^2}{d\rho_J^2} + \frac{J(J+1)}{\rho_J^2} + \frac{\chi_J}{\rho_J} - 1\right] f_J(\chi_J, \rho_J) = 0, \tag{14}$$

in terms of the so-called Coulomb parameter in the channel J, defined as twice the Sommerfeld parameter

$$\chi_J \equiv 2\frac{Z_\alpha Z_D e^2}{\hbar v_J}. \tag{15}$$

The system of Eq. (10) acquires this form practically beyond $R = R_c + 4\,\text{fm}$, where $R_c = 1.2(A_D^{1/3} + A_\alpha^{1/3})$, because the higher multipoles of the potential $\lambda \neq 0$ are centered around the nuclear surface $R_0 = 1.2A_D^{1/3} \pm 4\,\text{fm}$, as can be seen in Fig. 1.

B. Resonant states

We briefly review the procedure to integrate numerically this system of equations and to find resonant states. We first define N independent column-vector functions, satisfying inside the repulsive core at $R = R_0$, where $V_0(R_0) \gg Q_\alpha$, the following boundary conditions

$$\mathcal{R}_{JI}(R_0) = \delta_{JI}\varepsilon_J, \tag{16}$$

where ε_J are arbitrary small numbers. The index J labels the component, whereas I the solution. If the repulsion is soft then one considers $R_0 = \Delta R$, $\varepsilon_J = (\Delta R)^{J+1}$, where ΔR is the initial integration step.

We also determine N independent outgoing Coulomb column-vector functions satisfying at large distances the system (14), i.e.,

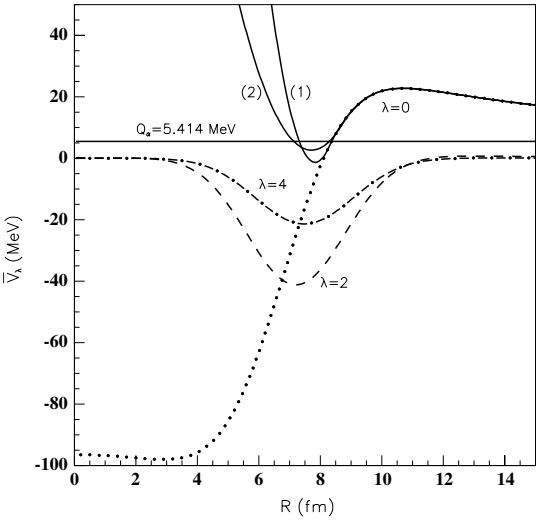

FIG. 1. The radial components of the renormalized α-nucleus potential (30) for $\lambda = 0$ (dots), $\lambda = 2$ (dashes), and $\lambda = 4$ (dot-dashes). The solid pocketlike curves (1) and (2) are the monopole parts of the interaction (31), giving the same Q value. Their parameters are (1) $c = 90.117\,(\text{MeV fm}^{-2})$, $Q_\alpha + v_0 = 10.272$ (MeV) and (2) $c = 30.296\,(\text{MeV fm}^{-2})$, $Q_\alpha + v_0 = -3.816$ (MeV). The horizontal line denotes the Q value. The decay process is $^{232}\text{Pu} \rightarrow {}^{228}\text{U} + \alpha$.

$$\mathcal{H}_{JI}^{(+)}(R) \equiv \mathcal{G}_{JI}(R) + i\mathcal{F}_{JI}(R) \overset{R\to\infty}{\longrightarrow} \delta_{JI} H_J^{(+)}(\chi_J, \rho_J) \equiv \delta_{JI}\left[G_J(\chi_J, \rho_J) + iF_J(\chi_J, \rho_J)\right], \tag{17}$$

where $G_J(\chi_J, \rho_J)$, $F_J(\chi_J, \rho_J)$ are the irregular and regular spherical Coulomb wave functions, respectively, depending on two independent variables in the channel J. These functions are found by a backward numerical integration.

Each component of the solution is built as a superposition of these N-independent fundamental solutions. We impose the matching boundary decay conditions at the radius R_1 inside the barrier, i.e., to have outgoing waves in all channels

$$f_J(R_1) = \sum_I \mathcal{R}_{JI}(R_1) M_I = \sum_I \mathcal{H}_{JI}^{(+)}(R_1) N_I, \tag{18}$$

and a similar condition for derivatives. The coefficients N_I are nothing else than the scattering amplitudes. These conditions give the following secular equation:

$$\det\begin{bmatrix} \mathcal{R}(R_1) & \mathcal{H}^{(+)}(R_1) \\ d\mathcal{R}(R_1)/dR & d\mathcal{H}^{(+)}(R_1)/dR \end{bmatrix} \approx \det\begin{bmatrix} \mathcal{R}(R_1) & \mathcal{G}(R_1) \\ d\mathcal{R}(R_1)/dR & d\mathcal{G}(R_1)/dR \end{bmatrix} = 0. \tag{19}$$

The first condition is exact and it is fulfilled for complex energies, determining the resonant (Gamow) states. In our case they practically coincide with the real scattering resonant states, because the imaginary parts of energies are much smaller than the corresponding real parts. This corresponds

to vanishing regular Coulomb functions F_J inside the barrier. Therefore the above approximation, given by the second equality, is very good. The roots of the system [Eq. (19)] do not depend on the matching radius R_1 because both internal and external solutions satisfy the same Schrödinger equation.

The coefficients M_I, N_I are fully determined from the normalization of the wave function in the internal region

$$\sum_J \int_{R_0}^{R_2} |f_J(R)|^2 dR = 1, \tag{20}$$

where R_2 is the external turning point. Beyond this radius the wave function has practically vanishing values. This is connected with the fact that all known half-lives in α emission are much larger that the characteristic nuclear time $T_{\min} \approx 10^{-6}\, s \gg T_N \approx 10^{-22}\, s$. Thus, any α-decaying state practically behaves like a bound state, having an exponential decrease versus radius inside the barrier.

One can derive a very useful relation for the scattering amplitude in terms of the wave-function components. By inverting Eq. (18) for some radius $R = R_1$ and then dividing and multiplying the result by $H_I^{(+)}(\rho_I)$ one obtains

$$N_I = \frac{1}{H_I^{(+)}(\rho_I)} \sum_J K_{IJ}(R) f_J(R), \tag{21}$$

where $\rho_I = \kappa_I R$. The propagator operator is defined in such a way that it becomes the unity matrix for a spherical Coulomb field, i.e.,

$$K_{IJ}(R) \equiv H_I^{(+)}(\rho_I)[\mathcal{H}^{(+)}(R)]^{-1}_{IJ} = \delta_{IJ} + \Delta K_{IJ}(R), \tag{22}$$

where $\Delta K_{IJ}(R) \to_{R\to\infty} 0$. Of course the scattering amplitude [Eq. (21)] does not depend on R.

The total decay width is a sum over partial channel widths. It can be derived from the continuity equation in a straightforward way and the result is the following:

$$\Gamma = \sum_J \Gamma_J = \sum_J \hbar v_J \lim_{R\to\infty} |f_J(R)|^2 = \sum_J \hbar v_J |N_J|^2, \tag{23}$$

where v_J is the center-of-mass velocity at infinity in the channel J, i.e.,

$$v_J = \frac{\hbar \kappa_J}{\mu}. \tag{24}$$

We stress on the fact that the wave-function components can be directly recovered by using the experimental information, namely the partial decay widths in Eq. (18)

$$f_J(R) = \sum_I \mathcal{H}^{(+)}_{JI}(R) \sqrt{\frac{\Gamma_I}{\hbar v_I}}, \tag{25}$$

because the matrix $\mathcal{H}^{(+)}$, defined by Eq. (17), is fully determined by the potential. Of course the wave function depends on the details of the used interaction. This is the main reason why we prefer to characterize the fine structure by the quantities

$$I_J \equiv \log_{10} \frac{\Gamma_0}{\Gamma_J}, \tag{26}$$

instead of the hindrance factors, defined as $HF(J) = |f_0/f_J|^2$, and that are model dependent.

III. INFLUENCE OF POTENTIAL PARAMETERS ON THE FINE STRUCTURE

First, let us analyze the sentivity of the α-decay fine structure on different parameters entering the potential [Eq. (4)]. We describe the density of the daughter nucleus by an axially deformed Woods-Saxon shape, i.e.,

$$\rho_{D,\tau}(\mathbf{r}_D) = \frac{\rho^{(0)}_{D,\tau}}{1 + e^{[r_D - R_{0,\tau}(\Omega_D)]/a}}, \tag{27}$$

where the radius of the nuclear surface is given by the following:

$$R_{0,\tau}(\Omega_D) = R_{0,\tau}\left[1 + \beta_2 Y_{20}(\Omega_D) + \beta_4 Y_{40}(\Omega_D)\right], \tag{28}$$

and the central densities are normalized by the total number of protons ($\tau = \pi$) and neutrons ($\tau = \nu$) separately. The α-particle density is given by a Gaussian distribution as follows:

$$\rho_\alpha(\mathbf{r}_\alpha) = \frac{4}{b^3\pi^{3/2}} e^{-(r_\alpha/b)^2}. \tag{29}$$

Concerning the α-nucleus interaction we multiplied the double folding integral [Eq. (6)] by a strength parameter v_a, to achieve the well-known relation between the half-life and Q value. This relation is mainly given by the ratio between the Q value and the height of the repulsive barrier and we show later that one should consider a quenching factor, i.e., $v_a < 1$. The necessity to use such a factor multiplying the double folded α-daughter potential was already stressed in Refs. [27,28]. It is connected with the fact that the parameters of the used M3Y interaction were fitted from scattering experiments involving heavy ions [37,39]. Thus, the renormalized multipoles of the interaction are given by the following:

$$\overline{V}_\lambda(R) = v_a V_\lambda(R). \tag{30}$$

They are plotted in Fig. 1. By dots we indicated the monopole component $\lambda = 0$, by dashes $\lambda = 2$ and by dot-dashes $\lambda = 4$ components, respectively. The horizontal solid line indicates the Q value of the process, which in our case is $^{232}\mathrm{Pu} \to {}^{228}\mathrm{U} + \alpha$. To obtain the experimental value of the half-life we used for the quenching factor $v_a = 0.62$. We also used the standard value of the diffusivity $a = 0.5$ fm, the α-particle size parameter $b = 1.19$ fm [29] and the deformations β_2, β_4 given by the systematics of Ref. [40].

This interaction is able to describe the α-daughter system for large distances $R > R_m$. To describe the internal two-body dynamics we used a repulsive core, taking care on the fact that an α-particle exists only on the nuclear surface. Indeed, microscopic computations, see, e.g., Fig. 2(a) of Ref. [6], suggest that the α-particle wave function is peaked in the region of the nuclear surface and it has a Gaussian-like shape. Moreover, the monopole component represents more than 90% of the total amount. Such a wave function corresponds to a shifted harmonic oscillator potential, which we have to consider in the internal region $R \leqslant R_m$, i.e.,

$$\begin{aligned} \overline{V}_0(R) &= v_a V_0(R),\ R > R_m \\ &= c(R - R_0)^2 - v_0,\ R \leqslant R_m. \end{aligned} \tag{31}$$

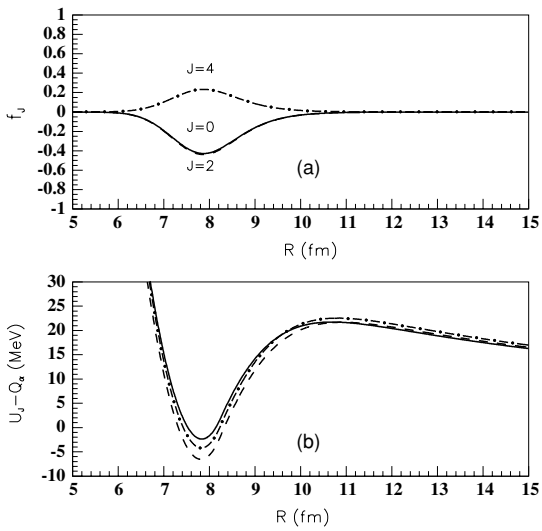

FIG. 2. (a) The radial components of the α-nucleus wave function inside the pocketlike potential for $J = 0$ (solid line), $J = 2$ (dashes), and $J = 4$ (dot-dashes). (b) The radial dependence of the diagonal α-nucleus matrix elements plus the centrifugal barrier [Eq. (33)] for $J = 0$ (solid line), $J = 2$ (dashes), and $J = 4$ (dot-dashes). In Fig. 1 the repulsive core is labeled (1). The decay process is $^{232}\mathrm{Pu} \rightarrow {}^{228}\mathrm{U} + \alpha$.

This interaction is given in Fig. 1 by two pocketlike curves. The curves labeled (1) and (2) give the same Q value. Their parameters are as follows: (a) $c = 90.117\,(\mathrm{MeV\,fm^{-2}})$, $Q_\alpha + v_0 = 10.272$ (MeV) and (b) $c = 30.296\,(\mathrm{MeV\,fm^{-2}})$, $Q_\alpha + v_0 = -3.816$ (MeV).

We considered the quantity $Q_\alpha + v_0$ because it is the excitation energy inside the pocketlike interaction. From this figure it is clear that if one considers a deformed part for repulsive multipoles with $\lambda \neq 0$ the effect can be renormalized by the monopole repulsion in the internal region $R < R_0 = 1.2A_D^{1/3}$.

We stress the fact that only three parameters, namely v_a, v_0, and c, are independent, because the radii R_0 and R_m are determined by using the matching conditions

$$\begin{aligned} v_a V_0(R_m) &= c(R_m - R_0)^2 - v_0 \\ v_a \frac{dV_0(R_m)}{dR} &= 2c(R_m - R_0). \end{aligned} \tag{32}$$

These conditions allows us to write down a single equation determining the matching radius for some given combination of v_a, v_0, c. The parameters of the repulsive cores (1) and (2) in Fig. 1 were chosen to give the best fit simultaneously for Q_α, Γ_J, $J = 0, 2, 4$.

This procedure to estimate the repulsive core is different from that of our previous references [22,33,34], where we used the same double folding procedure for a δ-like interaction. The advantage of the method used in this article is that we completely decouple the internal repulsion from the external

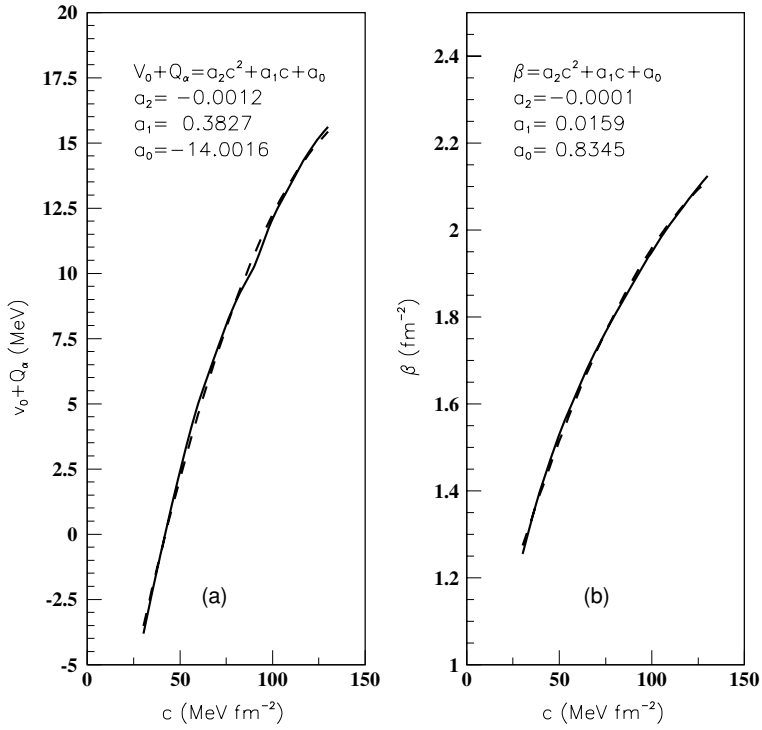

FIG. 3. (a) The dependence of the quantity $v_0 + Q_\alpha$ on the parameter c of the repulsive core defined by Eq. (31) (solid line). By dashes is given the quadratic fit. The fit parameters are given. (b) The dependence of the h.o. parameter for the monopole α-particle wave function defined by Eq. (34) versus the same parameter c (solid line). The parameters of the quadratic fit (dashes) are given. The decay process is $^{232}\mathrm{Pu} \rightarrow {}^{228}\mathrm{U} + \alpha$.

part and thus we are able to control the repulsive and atractive parameters independently, at variance with the δ-like force.

In Fig. 2(a) we plotted the radial components of the wave function for $J = 0$ (solid line), $J = 2$ (dashes), and $J = 4$ (dot-dashes), corresponding to the pocketlike repulsion (1) in Fig. 1. In Fig. 2(b) we give the radial dependencies of the diagonal terms [with the same symbols as in (a)], corresponding to the α-daughter potential plus the centrifugal barrier, i.e.,

$$U_J(R) = \langle \mathcal{Y}_J | \overline{V}(R) | \mathcal{Y}_J \rangle + \frac{\hbar^2 J(J+1)}{2\mu R^2} = \frac{1}{\sqrt{4\pi}} \sum_\lambda \overline{V}_\lambda(R) [\langle J, 0; \lambda, 0 | J, 0 \rangle]^2 + \frac{\hbar^2 J(J+1)}{2\mu R^2}. \quad (33)$$

Thus, in the spherical case, where the components with $\lambda > 0$ vanish, the decay widths to excited states are entirely determined by the corresponding centrifugal barriers.

An interesting observation is conected with the shape of the pocketlike potentials (1) and (2) in Fig. 1. The repulsive strength c and the quantity $Q_\alpha + v_0$ are strongly related and therefore the repulsive core is charactized by one independent parameter. Indeed, by increasing c one should simultaneously increase the excitation energy $Q_\alpha + v_0$, to obtain the same Q value and therefore the total half-life. This dependence is shown in Fig. 3(a). The parameters of the already mentioned curves (1) and (2) belong to this line.

In Fig. 3(b), we also plotted the width β of the monopole radial wave function component, shown in Fig. 2(a), as a function of the repulsive strength c. The width is obtained by fitting this component with a Gaussian, i.e.,

$$\frac{f_0(R)}{R} \approx A_0 e^{-\beta(R-R_0)^2/2}. \quad (34)$$

Moreover, our computations showed that the total half-life and the fine structure, defined by (26), is weakly affected by simultaneously changing the parameters of the repulsive potential for this decay process. This is shown in Fig. 4.

The importance of the quenching strength v_a is shown in Fig. 5. We plotted here with a solid line the Q value, with dots $\log_{10} T$, with a dashed line I_2, and with a dot-dashed line I_4, as a function of v_a, by considering fixed the parameters of the repulsive potential, i.e., $Q_\alpha + v_0 = 10.272$, $c = 90.117$. One sees a strong dependence of the first two quantities and a weaker variation for I_4, whereas I_2 is practically a constant. We stress that at the value $v_a \approx 0.62$ one obtains simultaneously the best fit with the experimental data (shown by short horizontal lines) for all considered quantities.

Once this parameter is fixed, we can adjust the Q values for different decays by using one parameter, namely the repulsive depth v_0, because for a given quenching strength v_a the repulsive strength c has a definite value. As mentioned above, we consider as an independent parameter the sum

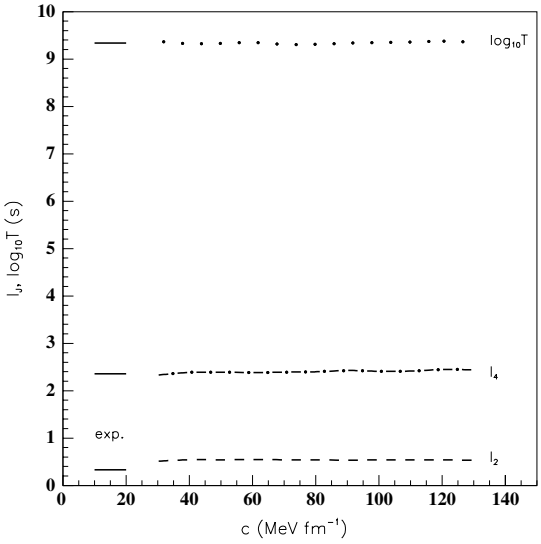

FIG. 4. The dependence of the ratios I_J, defined by Eq. (26) for $J = 2$ (dashed line) and $J = 4$ (dot-dashed line) upon the repulsive strength parameter c, when the parameter $v_0 + Q_\alpha$ simultaneously changes according to the curve in Fig. 3(a). The dependence between the logarithm of the total half-life versus c is plotted with dots. On the left side we give the corresponding experimental values. The decay process is $^{232}\mathrm{Pu} \rightarrow {}^{228}\mathrm{U} + \alpha$.

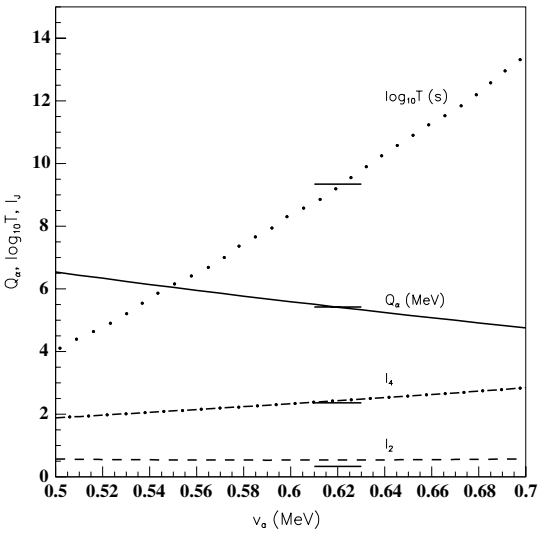

FIG. 5. The Q value (solid line), the logarithm of the total half-life (dots), I_2 (dashes) and I_4 (dot-dashes) versus the attraction strength v_a. The other potential parameters are $c = 90.117$ (MeV fm^{-2}), $Q_\alpha + v_0 = 10.272$ (MeV). The corresponding experimental values are shown by short horizontal lines. The decay process is $^{232}\mathrm{Pu} \rightarrow {}^{228}\mathrm{U} + \alpha$.

TABLE I. Experimental data for α decays from rotational nuclei: deformations, excitation energies, logarithm of the relative intensities, logarithm of the total half-life and Q value. The calculated data correspond to a variable quenching parameter v_a (labeled with a superscript a), or to a variable size parameter of the α-cluster density (labeled with a superscript b).

n	Z	A	β_2	β_4	E_2 (keV)	E_4 (keV)	I_2	I_2^a	I_2^b	I_4	I_4^a	I_4^b	$\log_{10} T$ (s)	$\log_{10} T_a$ (s)	$\log_{10} T_b$ (s)	Q_α (MeV)
1	90	226	0.173	0.111	72.200	226.430	0.324 *4*	0.602	0.594	2.25 *5*	2.415	2.426	6.26 *5*	6.323	6.281	5.993
2	90	228	0.182	0.112	57.759	186.823	0.335 *4*	0.556	0.538	2.36 *3*	2.364	2.419	9.336 *3*	9.321	9.423	5.414
3	90	230	0.198	0.115	53.200	174.100	0.400 *2*	0.565	0.536	2.55 *3*	2.519	2.610	12.889 *2*	12.871	12.815	4.859
4	90	232	0.207	0.108	49.369	162.120	0.46 *8*	0.572	0.534	2.45 *3*	2.530	2.663	14.869 *1*	14.870	14.935	4.572
5	90	234	0.215	0.102	49.550	163.000	0.58 *6*	0.622	0.572	3.01 *7*	2.673	2.835	17.149 *1*	17.299	17.354	4.270
6	92	230	0.199	0.115	51.720	169.500	0.3 *3*	0.429	0.399	2.2 *3*	2.072	2.157	5.723 *5*	5.645	5.566	6.310
7	92	232	0.207	0.117	47.572	156.570	0.355 *7*	0.429	0.388	2.6 *3*	2.125	2.247	7.955 *2*	7.912	7.782	5.867
8	92	234	0.215	0.110	43.498	143.351	0.389 *2*	0.427	0.378	2.83 *3*	2.099	2.259	9.442 *1*	9.274	9.298	5.593
9	92	236	0.215	0.102	45.242	149.476	0.429 *2*	0.480	0.418	2.932 *7*	2.182	2.373	11.329 *1*	11.357	11.304	5.256
10	92	238	0.215	0.093	44.910	148.410	0.513 *4*	0.519	0.446	3.40 *2*	2.215	2.435	13.073 *3*	13.020	13.101	4.984
11	94	236	0.215	0.110	44.630	147.450	0.391*13*	0.387	0.328	3.1 *3*	1.939	2.137	6.37 *2*	5.981	6.030	6.397
12	94	238	0.215	0.102	44.080	145.960	0.456 *2*	0.409	0.339	3.33 *3*	1.926	2.155	7.148 *1*	6.972	6.985	6.216
13	94	240	0.223	0.087	42.824	141.690	0.51 *3*	0.438	0.356	3.54 *3*	1.922	2.170	8.757 *3*	8.533	8.540	5.902
14	94	242	0.224	0.071	44.540	147.300	0.67 *3*	0.509	0.412	3.3 *5*	1.988	2.251	11.177 *4*	10.969	11.011	5.475
15	94	244	0.224	0.071	46.000	156.900	0.657 *6*	0.552	0.444	3.03 *7*	2.098	2.391	13.041 *8*	12.930	12.964	5.162
16	96	242	0.224	0.079	42.130	138.000	0.59 *3*	0.399	0.305	2.72 *6*	1.706	1.974	5.109 *7*	4.941	4.796	6.862
17	96	244	0.234	0.073	42.965	142.348	0.61 *3*	0.431	0.330	2.3 *3*	1.785	2.088	7.460 *4*	7.164	7.163	6.361
18	96	246	0.234	0.057	42.852	142.010	0.752 *7*	0.476	0.359	2.5 *3*	1.760	2.070	8.616 *3*	8.295	8.363	6.128
19	96	248	0.234	0.040	42.380	143.800	0.729 *9*	0.514	0.375	2.55 *8*	1.680	1.983	7.935 *2*	7.923	7.770	6.217
20	98	248	0.235	0.040	41.530	137.810	0.748 *7*	0.457	0.320	1.94 *2*	1.504	1.807	4.961 *1*	4.585	4.343	7.153
21	98	250	0.245	0.026	42.722	141.885	0.777*10*	0.475	0.327	2.02 *4*	1.454	1.768	4.067 *1*	3.842	3.698	7.307

$Q_\alpha + v_0$, because it gives the energy of the first excitation in the pocketlike potential.

IV. SYSTEMATICS OF THE FINE STRUCTURE

We analyzed α decays for 20 rotational nuclei with known ratios I_2 and I_4, and one where I_4 was only given as a limit. The experimental data, namely the excitation energies, total half-lives and Q values, are taken from the compilation [36]. We also compared fine structure intensities for $J = 2^+$, $J = 4^+$ states and total half-lives, with respective uncertainties, with the ENSDF database. Only one of the half-lives, namely ^{240}Pu, slightly differs from the value of Ref. [36]. The deformation parameters were taken from the systematics in Ref. [40]. These data for daughter nuclei are given in Table I.

Concerning the experimental errors, given by italic characters in Table I, we make the following observations. The errors for the 4^+ intensity were not given for the decays to ^{230}U, ^{232}U, ^{236}Pu, and ^{246}Cm. In these cases we considered relative uncertainty of 4^+ intensity to be 50%, as in ^{244}Cm measurement. For ^{242}Pu 4^+ the intensity was not given. We estimated the intensity limit and the uncertainty is taken to be 100%. The uncertainty of ^{230}U half-life was taken arbitrarily 10%, as in Ref. [36]. The uncertainty for α-decay intensity to 2^+ state in ^{230}U was not given, so that we considered the relative uncertainty to be 50%.

In Fig. 6(a) we plotted by squares the experimental Q values versus the number of the decay process, given in the first column of Table I. In the lower part [Fig. 6(b)] we give the logarithm of experimental half-lives by squares. In Fig. 7(a) shows the quadrupole (squares) and hexadecapole deformations (triangles), whereas in Fig. 7(b) the experimental values of the ratios I_2 and I_4 (squares).

The results of our computations are given in Figs. 6 and 7 by open circles and in Table I. It turns out that, to satisfy the relation between the half-life and Q value, the quenching strength should slowly decrease from $v_a \approx 0.6$ for $A = 226$ to $v_a \approx 0.5$ for $A = 250$. Thus, we introduced a linear decrease using the relation $v_a = 0.668 - 0.004\,(A - 208)$. In table the results are labeled with a. The value of the repulsive strength was taken $c = 100\,\mathrm{MeV\,fm^{-2}}$. As mentioned, we adjusted the energy of the first resonant state in the pocketlike potential by using the repulsive depth v_0, which is plotted in Fig. 6(a) with open circles.

The variation of this parameter can be correlated with the Q values in the same figure and it has an important consequence. It is known that the width of the Gaussian, fitting the microscopic preformation amplitude of the α particle, has practically no variation along any isotope chain [6]. However, according to Figs. 6(a) and 3(b) the width of the wave function within the present approach has a strong variation with the Q value. This feature is an evidence for the α-clustering phenomenon on the nuclear surface, in

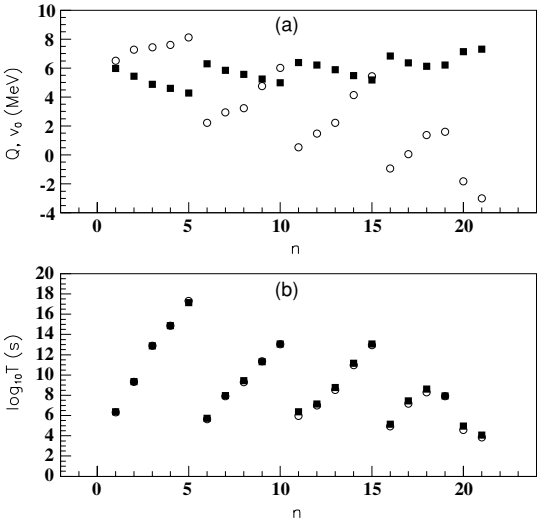

FIG. 6. (a) Q value (squares) and the depth of the repulsive potential v_0 (open circles) versus the decay number given by the first column in Table I. The attractive quenching parameter is given by the rule $v_a = 0.668 - 0.004\,(A - 208)$. (b) Logarithm of experimental half-lives (squares) and the corresponding computed values (open circles). In table the corresponding data are labeled with a superscript a.

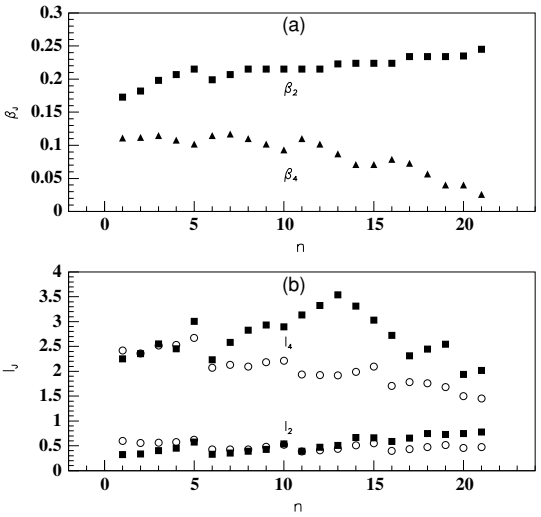

FIG. 7. (a) Deformation parameters β_2 (squares) and β_4 (triangles) versus the decay number given by the first column in Table I. (b) Experimental ratios I_2, I_4 defined by Eq. (26) (squares) and the corresponding computed values (open circles). The attractive quenching parameter is given by the rule $v_a = 0.668 - 0.004\,(A - 208)$. In Table I the corresponding data are labeled with a superscript a.

addition to the α preformation predicted by the standard shell model.

From Fig. 6(b) one sees that the computed half-lives (open circles) practically reproduce the experimental values. In Fig. 7(b) we show via open circles the results for I_2 and I_4. One sees that we obtained good agreement with experimental data for I_2. Concerning I_4, very good agreement was achieved only for the $Z = 90$ isotope chain. For the last $Z = 96$ and $Z = 98$ chains the agreement is within a half-order of magnitude, whereas the central peak, around the $Z = 94$ chain, is not reproduced. The difference between experiment and theory in this region is about 1.5 orders of magnitude.

The following observation is interesting. The main trend of the experimental and computed I_2 values in Fig. 7(b) is clearly correlated with the quadrupole deformation in Fig. 7(a). The same is true, but mainly for the computed I_4 values, which are correlated with β_4 in Fig. 7(a). This correlation between I_J and β_J can be understood from Eq. (33), expressing the barriers and therefore the penetrabilities for each partial wave, as a sum of all multipole terms. Thus, the existence of the central peak for experimental I_4 data corresponding to the neutron chain $Z = 94$ seems to be out of the correlation between the fine structure and deformation parameters. At this moment we have no explanation for this experimental feature.

The correlation between decay widths and deformation parameters seems to be an universal property of emission processes. This feature was already evidenced for α decays between ground states in Ref. [6]. However, the protons are emitted with given angular momenta from some proton-rich nuclei. Recently we found an almost 100% correlation between the quadrupole deformation and half-lives, corrected by the centrifugal barrier, in all measured proton emitters [41].

We have also checked higher resonances in the pocketlike potential, but, because the orthogonality with respect to the first state, they give a totally different picture of the fine structure, compared with experimental data.

The variation of the quenching parameter v_a by increasing the mass number corresponds to the change of the Coulomb barrier because of the nuclear part. Indeed the pure Coulomb barrier, according to Eq. (14) and $\chi \sim Z/\sqrt{Q_\alpha}$, would give the following dependence of the total half-life

$$\log_{10} T = c_1 \frac{Z}{\sqrt{Q_\alpha}} + c_2. \tag{35}$$

In reality the Viola-Seaborg empirical rule postulates a more complex dependence [42]

$$\log_{10} T = \frac{a_1 Z + a_2}{\sqrt{Q_\alpha}} + a_3 Z + a_4. \tag{36}$$

Thus, the influence of the internal nuclear part is expressed by the additional term $a_2/\sqrt{Q_\alpha} + a_3 Z$. In connection with this observation we have checked that a similar rule for the quenching factor depending on the charge number, i.e., $v_a = 0.7 - 0.125\,(Z - 82)$, gives very close results, which practically cannot be distinguished from theoretical results in Fig. 6(b), in comparison with the dependence on the mass number. Anyway, we should stress the fact that our description

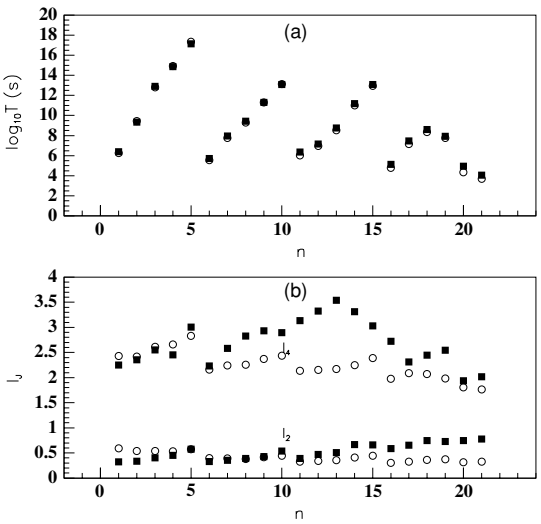

FIG. 8. (a) Logarithm of experimental half-lives (squares) and the corresponding computed values (open circles). The α-particle size parameter [Eq. (29)] is given by the rule $b = 1.744 - 0.032(A - 208)$ and the quenching parameter is $v_a = 0.6$. (b) Experimental ratios I_2, I_4 (squares) and the corresponding computed values (open circles). In Table I the corresponding data are labeled with a superscript b.

depends on only two parameters instead of four parameters in Eq. (36).

This effect can be also explained by considering an alternative picture, namely by changing the diffusivity parameter b of the α particle in Eq. (29) according to the rule $b = 1.744 - 0.032\,(A - 208)$, for a constant value $v_a = 0.6$. Microscopic estimates show that the change of the daughter nuclear difusivity should be very small. In this way the width of the α cluster in the surface region should decrease by increasing the mass number of the daughter nucleus to reproduce the total half-lives, as can be seen in Fig. 8(a) (open circles). The results are labeled in Table I by the index (b). In Fig. 8(b) the fine structure I_J is shown with open circles by considering the above change of the cluster size parameter. One sees that the values for I_4 are slightly improved with respect to those in Fig. 7(b).

As mentioned, one has a dependence of the cluster width on the Q value. Therefore there is a possible additional change of the cluster size in the region of the nuclear surface because of the dependence of the Coulomb barrier on the mass (or charge) number. A definite answer to the question: the effective nucleon-nucleon interaction or the size of the α-particle changes in the nuclear surface region, still remains open, because both approaches give qualitatively the same results. Anyway, this problem concerns fundamental aspects of the effective nuclear interaction and its dependence on the α clustering and thus gives the possibility to express the empirical parameters of the Viola-Seaborg rule in terms of microscopic parameters.

Our simple model is able to explain quantitatively the fine structure to $J = 2^+$ states, namely that the decay widths to $J = 2^+$ states are by 0.5 orders of magnitude smaller than the ones for transitions between ground states. At the same time it is able to explain the fact that most of the decay widths to $J = 4^+$ states are by 2.5 orders of magnitude smaller with respect to the widths between ground states.

V. CONCLUSIONS

We used in this article a simple model to explain the α-decay fine structure in rotational nuclei. We considered the coupled channels formalism to estimate decay widths and the double folding procedure to compute the interaction between the daughter plus α-particle. The daughter nucleus has as eigenstates the standard $K = 0$ Wigner functions. We considered as an effective particle-particle nuclear interaction the superposition of three Yukawa terms (M3Y), able to describe scattering data. The Q value of the system is reproduced by adjusting the depth of a parabolic repulsive core, simulating the Pauli principle. The decaying state was indentified with the first resonance in the resulting pocketlike potential.

It turned out that this simple rotational model is able to explain very well total half-lives and decay widths to the first 2^+ states, as soon as the basic M3Y interaction is quenched by a factor v_a whose value decreases with increasing mass number. Consequently the Coulomb barrier should increase. This effect can be also reproduced by keeping a constant value $v_a = 0.6$ and by changing the size of the α-cluster density as a function of the mass number. It is interesting to mention that the obtained results do not depend on the parameters of the repulsive potential. Does the effective nucleon-nucleon interaction or the size of the α-particle in the nuclear surface region change? This still remains an open question, because both approaches give qualitatively the same results. In any case, this analysis clearly shows that the effective nucleon-nucleon interaction is influenced by α clustering and this dependence changes with the mass number.

Concerning the decay widths to 4^+ rotational states we obtained a good agreement with experimental data for the lightest $Z = 90$ neutron chain and a satisfactory agreement for $Z = 92, 96$, and 98 chains. This simple model is able to qualitatively explain the gross feature of the fine structure, but still the computed values in the region around $Z = 94$ chain differ from experimental data by 1.5 orders of magnitude. It is an interesting observation that our theoretical results concerning I_J are proportional to the corresponding deformations β_J, whereas the experimental values of I_4 for the $Z = 94$ chain do not satisfy this rule. At this moment we have no explanation for this effect, which is not connected with the deformed neutron magic number $N = 152$.

We also stress on the fact that the parameters of the nucleon-nucleon interaction were fitted by using heavy ions scattering data. These experiments can probe potentials only in the region of the Coulomb barrier. However, the α decay is

a deep subbarrier process at low energies, where the scattering has a purely Rutherford pattern. Thus, α-decay fine structure is potentially a valuable tool to probe the nuclear interaction in the internal region. It is in principle able to improve our knowledge about how the effective nucleon-nucleon potential changes in the presence of α clustering.

[1] G. Gamow, Z. Phys. **51**, 204 (1928).
[2] R. G. Thomas, Prog. Theor. Phys. **12**, 253 (1954).
[3] A. M. Lane and R. G. Thomas, Rev. Mod. Phys. **30**, 257 (1958).
[4] H. J. Mang, Annu. Rev. Nucl. Sci. **14**, 1 (1964).
[5] J. K. Poggenburg, H. J. Mang, and J. O. Rasmussen, Phys. Rev. **181**, 1697 (1969).
[6] D. S. Delion, A. Săndulescu, and W. Greiner, Phys. Rev. C **69**, 044318 (2004).
[7] J. O. Rasmussen, Phys. Rev. **113**, 1593 (1959).
[8] A. Săndulescu and O. Dumitrescu, Phys. Lett. **19**, 404 (1965).
[9] A. Săndulescu and O. Dumitrescu, Phys. Lett. **B24**, 212 (1967).
[10] M. I. Cristu, O. Dumitrescu, N. I. Pyatov, and A. Săndulescu, Nucl. Phys. **A130**, 31 (1969).
[11] D. S. Delion, A. Florescu, M. Huyse, J. Wauters, P. Van Duppen, ISOLDE Collaboration, A. Insolia, and R. J. Liotta, Phys. Rev. Lett. **74**, 3939 (1995); Phys. Rev. C **54**, 1169 (1996).
[12] J. Wauters *et al*., Z. Phys. A **342**, 277 (1992).
[13] J. Wauters *et al*., Z. Phys. A **344**, 29 (1992).
[14] J. Wauters *et al*., Z. Phys. A **345**, 21 (1993).
[15] J. Wauters, P. Dendooven, M. Huyse, G. Reusen, P. Van Duppen, P. Lievens, and ISOLDE Collaboration, Phys. Rev. C **47**, 1447 (1993).
[16] J. Wauters, N. Bijnens, H. Folger, M. Huyse, H. Y. Hwang, R. Kirchner, J. von Schwarzenberg, and P. Van Duppen, Phys. Rev. C **50**, 2768 (1994).
[17] J. Wauters *et al*., Phys. Rev. Lett. **72**, 1329 (1994).
[18] N. Bijnens *et al*., Phys. Rev. Lett. **75**, 4571 (1995).
[19] R. G. Allatt *et al*., Phys. Lett. **B437**, 29 (1998).
[20] C. F. Liang, R. K. Sheline, P. Paris, M. Hussonnois, J. F. Ledu, and D. B. Isabelle, Phys. Rev. C **49**, 2230 (1994).
[21] D. S. Delion and R. J. Liotta, Phys. Rev. C **56**, 1782 (1997).
[22] D. S. Delion and J. Suhonen, Phys. Rev. C **64**, 064302 (2001).
[23] S. Peltonen, D. S. Delion, and J. Suhonen, Phys. Rev. C **71**, 044315 (2005).
[24] J. O. Rasmussen and B. Segal, Phys. Rev. **103**, 1298 (1956).
[25] H. M. A. Radi, A. A. Shihab-Eldin, J. O. Rasmussen, and Luiz F. Oliveira, Phys. Rev. Lett. **41**, 1444 (1978).
[26] P. O. Fröman, Mat. Fys. Skr. Dan. Vid. Selsk. **1**, 3 (1957).
[27] R. Neu and F. Hoyler, Phys. Rev. C **46**, 208 (1992).
[28] H. Abele and G. Staudt, Phys. Rev. C **47**, 742 (1993).
[29] Dao T. Khoa, Phys. Rev. C **63**, 034007 (2001).
[30] D. N. Basu, J. Phys. G **29**, 2079 (2003).
[31] Y. K. Gambhir, A. Bhagwat, M. Gupta, and Arun K. Jain, Phys. Rev. C **68**, 044316 (2003).
[32] D. S. Delion, A. Săndulescu, S. Mişicu, F. Cârstoiu, and W. Greiner, Phys. Rev. C **64**, 041303(R) (2001).
[33] D. S. Delion, A. Săndulescu, S. Mişicu, F. Cârstoiu, and W. Greiner, J. Phys. (London) G **28**, 289 (2002).
[34] D. S. Delion, A. Săndulescu, and W. Greiner, Phys. Rev. C **68**, 041303(R) (2003).
[35] A. Săndulescu, A. Florescu, F. Cârstoiu, W. Greiner, J. H. Hamilton, A. V. Ramayya, and B. R. S. Babu, Phys. Rev. C **54**, 258 (1996).
[36] Y. A. Akovali, Nucl. Data Sheets **84**, 1 (1998).
[37] G. R. Satchler and W. G. Love, Phys. Rep. **55**, 183 (1979).
[38] F. Cârstoiu and R. J. Lombard, Ann. Phys. (NY) **217**, 279 (1992).
[39] G. Bertsch, J. Borysowicz, H. McManus, and W. G. Love, Nucl. Phys. **A284**, 399 (1977).
[40] P. Möller, J. R. Nix, W. D. Myers, and W. J. Swiatecki, At. Data Nucl. Data Tables **59**, 185 (1995).
[41] D. S. Delion, R. J. Liotta, and R. Wyss, Phys. Rev. Lett. (in press).
[42] V. E. Viola and G. T. Seaborg, J. Inorg. Nucl. Chem. **28**, 741 (1966).

Paper III

Folding description of the fine structure of α decay to 2^+ vibrational and transitional states
S. Peltonen, D. S. Delion and J. Suhonen,
Phys. Rev. C **75**, 054301 (2007).

Folding description of the fine structure of α decay to 2^+ vibrational and transitional states

S. Peltonen,[1] D. S. Delion,[2] and J. Suhonen[1]
[1]*Department of Physics, University of Jyväskylä, POB 35, FIN-40351, Jyväskylä, Finland*
[2]*"Horia Hulubei" National Institute of Physics and Nuclear Engineering, 407 Atomistilor, Măgurele-Bucharest 077125, Romania*
(Received 16 November 2006; published 1 May 2007)

We analyze α-decays to ground and 2^+ vibrational states in even-even nuclei by using a coupled channels formalism. The α-nucleus interaction is simulated by a double folding procedure using M3Y plus Coulomb two-body forces. Collective excitations are described by vibrations of the nuclear surface. We use a repulsive potential, with one independent parameter, in order to simulate Pauli principle and to adjust the energy of the resonant state to the experimental Q-value. The decaying state is identified with the zero nodes resonance inside the resulting pocket-like potential. We have found that the fine structure is very sensitive to the strength of the repulsive core and the vibrational parameter of the α-nucleus potential. A satisfactory agreement with existing experimental data was obtained by using the vibrational strength as a free parameter. It turns out that the inverse of this parameter is proportional to the logarithm of the hindrance factor squared. Based on this fact we have made predictions for 15 vibrational α-emitters.

DOI: 10.1103/PhysRevC.75.054301 PACS number(s): 23.60.+e, 24.10.Eq, 25.70.Ef

I. INTRODUCTION

The α-decay width for transitions between ground states is a coherent superposition of many single-particle configurations and therefore it is sensitive only to mean field parameters, like the quadrupole deformation [1]. The situation becomes quite different for transitions to excited states, because only single-particle states around the Fermi surfaces are involved. Therefore α-decay widths to excited states are very sensitive to the structure of the wave function in the daughter nucleus. This feature explains why the α-decay to excited states is an important and sensitive tool to investigate nuclear structure details.

In order to extract the exponential dependence between the barrier penetration and Q-value one introduces the so-called hindrance factor (HF) [2]. It is the ratio of the preformation probabilities of two nuclear states. The first attempts to calculate HF's for 2^+ states in vibrational nuclei within the quasiparticle random-phase approximation (QRPA) framework were performed in Refs. [3–5]. Later on, in Ref. [6] an explanation in terms of proton-neutron pairing vibrations was given to the connection between the HF of the first excited 0^+ state and the neutron number in Pb isotopes. Recent calculations to estimate HF's to excited 0^+ states were performed in [7] within the Hartree-Fock-Bogoliubov approach. In the last decade the α-decay spectroscopy was used to investigate the 0^+ and 2^+ excited states in the Pb [8–15] and U region [16]. We analyzed some of the experimental results concerning the fine structure of 2^+ states by using the QRPA formalism in Refs. [17,18], and recently in [19].

The first calculations of the α-decay widths in rotational nuclei using the coupled channels method were performed in Ref. [20]. In Ref. [21] HF's in rotational nuclei were estimated by using the Fröman approach [22] for the barrier penetration and a simple phenomenological ansatz for the preformation factor. The α-core potential was estimated by using double folding procedure in Refs. [23,24], and more recently in [25]. This kind of potential was also used to estimate ground-state-to-ground-state half-lives within a spherical approach in Ref. [26]. In Ref. [27] branching ratios to the members of the ground-state rotational band were estimated by using a square α-core potential, together with the assumption that the formation probability in the excited state obeys the Boltzman distribution.

There are a lot of high precision data on α-decay fine structure, see, e.g., [28]. Recently we analyzed the α-decays to rotational states [29] within the coupled channels approach by using an α-nucleus potential, given by the double folding method. The aim of this paper is to apply a similar formalism to describe the fine structure in vibrational and transitional nuclei. The paper is organised according to the following plan. In Sec. II we shortly introduce the main ingredients of the stationary coupled channels formalism describing α-decay fine structure to vibrational states. In Sec. III we analyze the existing data on α-decay fine structure and the relevance of different parameters of the model. We also give a systematics of measured α-decay widths, together with predictions for 15 vibrational-transitional α emitters. In the last section we draw conclusions.

II. THEORETICAL BACKGROUND

In this section we give the main theoretical details, necessary to compute the decay widths for vibrational nuclei within the coupled channels formalism.

A. Coupled channels formalism

Let us consider an α-decay process

$$P \to D(J) + \alpha, \tag{2.1}$$

where J denotes the spin of the rotational state of an even-even nucleus, which in our case can be $J = 0, 2$. We describe the α-core dynamics by using the stationary Schrödinger

equation, i.e.,

$$H\Psi(\mathbf{R},\alpha_2) = E\Psi(\mathbf{R},\alpha_2), \tag{2.2}$$

where $\mathbf{R} \equiv (R,\Omega)$ denotes the distance between the centers of two fragments and α_2 is the quadrupole vibrational collective coordinate. Stationarity is a very good assumption due to the fact that all measured decay widths are by many orders of magnitude smaller than the corresponding Q-values. Therefore an α-decaying state is identified with a narrow resonant solution, containing only outgoing components.

The Hamiltonian describing α-decay is written as follows:

$$H = -\frac{\hbar^2}{2\mu}\nabla_R^2 + H_D(\alpha_2) + V(\mathbf{R},\alpha_2), \tag{2.3}$$

where μ is the reduced mass of the dinuclear system and H_D describes the vibration of the core. We assume that the interaction between the two nuclei can be written as

$$V(\mathbf{R},\alpha_2) = \sum_{\lambda=0,2} \overline{V}_\lambda(R)\mathcal{Y}_\lambda(\Omega,\alpha_2), \tag{2.4}$$

where the angular part is given by

$$\begin{aligned} \mathcal{Y}_2(\Omega,\alpha_2) &\equiv [Y_2(\Omega)\otimes\alpha_2]_0\,, \\ \mathcal{Y}_0(\Omega,\alpha_2) &\equiv \frac{1}{\sqrt{4\pi}}. \end{aligned} \tag{2.5}$$

The monopole part of the interaction is given by the same ansatz as in Ref. [29], i.e.,

$$\begin{aligned} \overline{V}_0(R) &= v_a V_0(R), \quad R > R_m \\ &= c(R-R_0)^2 - v_0, \quad R \leqslant R_m, \end{aligned} \tag{2.6}$$

where V_0 is the monopole part of the nuclear plus Coulomb interaction, estimated by using the double folding procedure with M3Y particle-particle interaction with Reid soft core parametrization [30–32]. Here $v_a = 1$ corresponds to a "pure" α-cluster model, i.e., that the α-particle is a real object on the nuclear surface. By taking $v_a < 1$ one assumes an α-cluster probability less than unity, necessary to reproduce the experimental half-life. The second line is the repulsive core mimicking the Pauli effect and by which we fix the energy of the first resonant state to the experimental Q-value, as done in Ref. [29].

We applied the same procedure as in our recent reference [29]. The matching radius R_m and the coordinate R_0, corresponding to the minimal value, were determined by using the equality between the external attractive potential (first line) and internal repulsion (second line), together with their derivatives [see Eqs. (32) of this reference]. Thus, the above interaction is continuous and it depends only upon two repulsive parameters: the repulsive strength c and its minimal value v_0.

The $\lambda = 2$ form factor is the linear term in the expansion of the nuclear surface, i.e.,

$$\overline{V}_2(R) = -v_2(R-R_0)\frac{d\overline{V}_0(R)}{dR}. \tag{2.7}$$

The wave function is given by a superposition similar to Eq. (2.4), i.e.,

$$\begin{aligned} \Psi(\mathbf{R},\alpha_2) &= \frac{1}{R}\sum_{J=0,2} f_J(R)\mathcal{Z}_J(\Omega,\alpha_2), \\ \mathcal{Z}_J(\Omega,\alpha_2) &\equiv [Y_J(\Omega)\otimes\Phi_J]_0\,, \end{aligned} \tag{2.8}$$

where Φ_J is the Jth eigenstate of the vibrational Hamiltonian $H_D(\alpha_2)$. In the above wave function we considered only one phonon excitations, because low-lying 2^+ states have large electromagnetic $E2$ rates to the ground state. In principle they can also couple with two-phonon components through the quadrupole operator α_2. An extensive analysis of this coupling was recently performed in several references within a microscopic approach (see [33] and the references therein). There an analysis of not only energy spectra, but also electromagnetic and beta decays has shown that in general this coupling is relatively weak. On the other hand, we are only interested in estimating the hindrance factor, i.e., the ratio between the ground state and $J = 2$ components and not the absolute decay widths. Our results in Table I of the next section clearly show that the experimental values can be reproduced by using only one free parameter, namely the coupling constant C_v, defined below by Eq. (2.12). Thus, the inclusion of two-phonon components may affect the absolute values of the ground state and one-phonon components, but should not affect their ratio. Moreover, the α-decay intensities to two-phonon states in vibrational and transitional nuclei are so small that they cannot be detected at the moment. This is supported by the available systematics [28]. Therefore, this is another argument that the coupling of these components should be relatively small. The above conclusion is also supported by our recent coupled channels analysis in rotational nuclei [29], where $J = 4$ intensities are very small but still measurable. They correspond to a relatively small wave function component, in spite of the fact that the $J = 0$ and 2 components are comparable, as can be seen in Fig. 2(a) of Ref. [29].

By using the orthonormality of angular functions entering the superposition (2.8) one obtains, in a standard way, the following coupled system of differential equations for radial components:

$$\frac{d^2 f_J(R)}{d\rho_J^2} = \sum_{J'=0,2} A_{JJ'}(R) f_{J'}(R), \quad J = 0, 2, \tag{2.9}$$

where the coupling matrix is given by

$$\begin{aligned} A_{JJ'}(R) = &\left[\frac{J(J+1)}{\rho_J^2} + \frac{\overline{V}_0(R)}{E-E_J} - 1\right]\delta_{JJ'} \\ &+ \frac{\overline{V}_2(R)}{E-E_J}\langle\mathcal{Z}_J|\mathcal{Y}_2|\mathcal{Z}_{J'}\rangle. \end{aligned} \tag{2.10}$$

Here we have introduced the following shorthand notations:

$$\rho_J = \kappa_J R, \quad \kappa_J = \sqrt{\frac{2\mu(E-E_J)}{\hbar^2}}. \tag{2.11}$$

The matrix element entering Eq. (2.10) has only off-diagonal nonvanishing values given by

$$\overline{V}_2(R)\langle\mathcal{Z}_2|\mathcal{Y}_2|\mathcal{Z}_0\rangle = \overline{V}_2(R)\frac{1}{\sqrt{4\pi}}\langle\Phi_2||\alpha_2||\Phi_0\rangle \equiv -C_v(R-R_0)\frac{d\overline{V}_0(R)}{dR}, \quad (2.12)$$

depending upon a new constant $C_v = v_2\langle\Phi_2||\alpha_2||\Phi_0\rangle/\sqrt{4\pi}$.

B. Resonant states

In order to integrate numerically the above system of equations and to find resonant states we first define N independent column-vector functions $\mathcal{R}_{JI}$. They satisfy inside the repulsive core, at $R = R_0$, the following boundary conditions:

$$\mathcal{R}_{JI}(R_0) = \delta_{JI}\varepsilon_J, \quad (2.13)$$

where ε_J are arbitrary small numbers. The index J labels the component and I numbers the solution.

We also determine N independent outgoing Coulomb column-vector functions, i.e.,

$$\mathcal{H}^{(+)}_{JI}(R) = \mathcal{G}_{JI}(R) + i\mathcal{F}_{JI}(R) \overset{R\to\infty}{\longrightarrow} \delta_{JI}H^{(+)}_J(\kappa_J R) \equiv \delta_{JI}\left[G_J(\kappa_J R) + iF_J(\kappa_J R)\right], \quad (2.14)$$

where $G_J(\kappa_J R)$, $F_J(\kappa_J R)$ are the irregular and regular spherical Coulomb wave functions, respectively, depending on the momentum κ_J in the channel J. These functions are found by a backward numerical integration.

Each component of the solution is built as a superposition of these N independent fundamental solutions. We impose the matching at the radius R_1 inside the barrier such that we have outgoing waves in all channels

$$f_J(R_1) = \sum_I \mathcal{R}_{JI}(R_1)M_I = \sum_I \mathcal{H}^{(+)}_{JI}(R_1)N_I, \quad (2.15)$$

and a similar condition for derivatives. The coefficients N_I are nothing else than the scattering amplitudes. These conditions give the following secular equation:

$$0 = \det\begin{bmatrix} \mathcal{R}(R_1) & \mathcal{H}^{(+)}(R_1) \\ d\mathcal{R}(R_1)/dR & d\mathcal{H}^{(+)}(R_1)/dR \end{bmatrix} \approx \det\begin{bmatrix} \mathcal{R}(R_1) & \mathcal{G}(R_1) \\ d\mathcal{R}(R_1)/dR & d\mathcal{G}(R_1)/dR \end{bmatrix}. \quad (2.16)$$

The first condition is exact and it is fulfilled for complex energies, determining the resonant states. In our case they practically coincide with the real scattering resonant states, because the imaginary parts of energies are much smaller than the corresponding real parts. This corresponds to vanishing regular Coulomb functions F_J inside the barrier. Therefore the above approximation, given by the second equality, is very good. The roots of the system (2.16) do not depend upon the matching radius R_1 because both internal and external solutions satisfy the same Schrödinger equation.

The coefficients M_I, N_I are fully determined from the normalisation of the wave function in the internal region

$$\sum_J \int_{R_0}^{R_2} |f_J(R)|^2 dR = 1, \quad (2.17)$$

where R_2 is the external turning point. Beyond this radius the wave function has practically vanishing values. This is connected with the fact that all known half-lives in α emission are much larger that the characteristic nuclear time $T_{\min} \approx 10^{-6}$ s $\gg T_N \approx 10^{-22}$ s. Thus, any α-decaying state practically behaves like a bound state, having an exponential radial decrease inside the barrier.

The total decay width is a sum over partial channel widths. It can be derived from the continuity equation in a straightforward way and the result is

$$\Gamma = \sum_J \Gamma_J = \sum_J \hbar v_J \lim_{R\to\infty} |f_J(R)|^2 = \sum_J \hbar v_J |N_J|^2, \quad (2.18)$$

where v_J is the center-of-mass velocity at infinity in the channel J, i.e.,

$$v_J = \frac{\hbar\kappa_J}{\mu}. \quad (2.19)$$

III. NUMERICAL RESULTS

A. Analysis of experimental data

We will investigate the so-called fine structure in α-decays to 2^+ states in even-even nuclei. It is defined as the logarithm of the ratio of Γ_0 to Γ_2, where Γ_0 (Γ_2) is the decay width (or intensity) to ground state (2^+ state), i.e.,

$$I \equiv \log_{10}\frac{\Gamma_0}{\Gamma_2}. \quad (3.1)$$

In order to remove the effect of the Coulomb barrier and to compare the corresponding formation probabilities one defines the hindrance factor (HF) as

$$\mathrm{HF} \equiv \frac{\Gamma_0}{\Gamma_2}\frac{P_2}{P_0}, \quad (3.2)$$

where P_J is the standard penetrability

$$P_J \equiv \frac{2\kappa_J R}{G_J^2(\kappa_J R)}, \quad (3.3)$$

in terms of the irregular Coulomb function $G_J(\kappa_J R)$. It is important to notice that HF practically does not depend on the radius R, because the ratio of penetrabilities in Eq. (3.2) has a weak dependence on this variable. For R we used in our calculations the touching radius, i.e., $R = 1.2(A_D^{1/3} + A_\alpha^{1/3})$. As it was shown in Ref. [29] the relation (3.2) gives results that are close to the standard Rasmussen definition [2].

We started by analyzing the energy spectra of all α emitters with known energies of the $J = 2$ and $J = 4$ levels. In Fig. 1(a) we plotted the ratio E_4/E_2 versus the quadrupole deformation β_2 for nuclei with $Z < 82$. One clearly sees that the vibrational region is given by $|\beta_2| \leqslant 0.1$, while the rotational region by

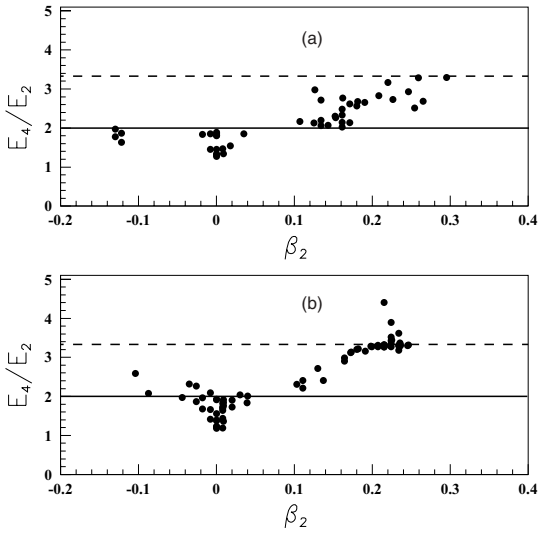

FIG. 1. (a) The ratio E_4/E_2 versus the quadrupole deformation for nuclei with $Z < 82$. The solid line denotes vibrational limit, while the dashed one rotational limit; (b) The same as 1 (a), but for nuclei with $Z \geqslant 82$.

$|\beta_2| > 0.2$. The solid line denotes vibrational limit, while the dashed one denotes the rotational limit. Thus, the transitional region is defined by the region of deformations $0.1 < |\beta_2| < 0.2$. We give similar dependencies in Fig. 1(b) for heavy nuclei with $Z \geqslant 82$. Our goal is to investigate vibrational and transitional regions, and therefore we exclude rotational nuclei with $E_2 \leqslant 100$ keV.

A clear difference between the vibrational-transitional and rotational regions is given in Fig. 2(a), where we plot the logarithm of the intensity ratio I (3.1) versus the energy E_2. All values of the rotational region with $E_2 \leqslant 0.1$ MeV are concentrated around $I \approx 0.5$, while for the other nuclei one notices an increasing trend, which is best fitted by the following linear ansatz:

$$I_{\text{fit}} = 4.361 E_2 + 0.924, \quad \sigma = 0.774, \tag{3.4}$$

shown by the solid line. Here σ denotes the mean error. In Fig. 2(b) we plot the same quantity against the neutron number. The smooth behavior of I in the rotational region with $N \geqslant 132$ can be clearly seen. The dependence of the experimental values $\log_{10}\text{HF}_{\text{exp}}$ Eq. (3.2) on E_2 is given in Fig. 3(a) and on neutron number in Fig. 3(b). Again the difference between the vibrational-transitional region and the rotational one is clear, characterized by small HF's.

Next we analyzed the dependence of the fine structure (3.1) and hindrance factors (3.2) on various parameters of our model. In computing the attractive part of the interaction we describe the density of the daughter nucleus by a Woods-Saxon shape, i.e.,

$$\rho_{D,\tau}(\mathbf{r}_D) = \frac{\rho^{(0)}_{D,\tau}}{1 + e^{[r_D - R_{D,\tau}]/a}}, \tag{3.5}$$

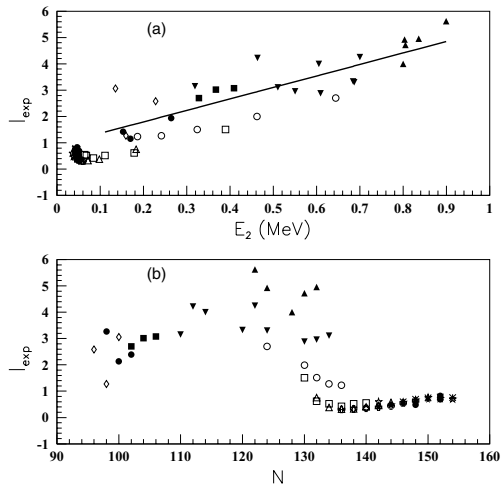

FIG. 2. (a) Experimental values of the logarithm of the intensity ratio (3.1) versus the 2^+ energy E_2. Different symbols denote different isotopic chains. The straight line fits the values of vibrational-transitional emitters in Table I. (b) Experimental values of the logarithm of the intensity ratio (3.1) versus the neutron number.

where the central densities are normalized by the total number of protons ($\tau = \pi$) and neutrons ($\tau = \nu$) separately. We use the standard value of the diffusivity, $a = 0.5$ fm, and nuclear radius, $R_{D,\tau} = r^{(0)}_{\tau} A_D^{1/3}$. The α-particle density is given by a

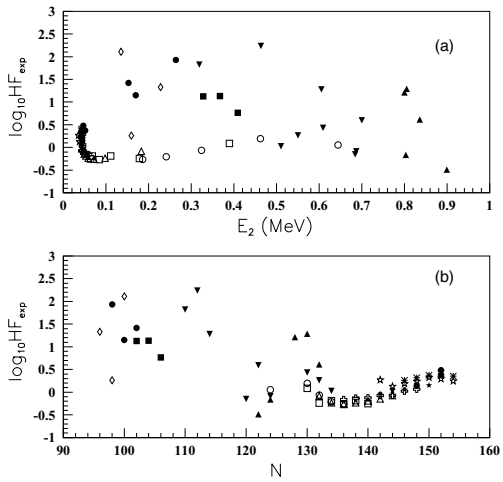

FIG. 3. (a) Experimental values of the logarithm of the hindrance factor (3.2) versus the 2^+ energy E_2. Different symbols denote different isotopic chains. (b) Experimental values of the logarithm of the hindrance factor (3.2) versus the neutron number.

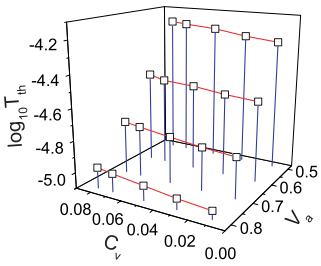

FIG. 4. (Color online) Logarithm of the half-life-(in seconds) as a function of the attraction parameters: double folding strength parameter v_a and vibrational coupling strength C_v.

Gaussian distribution, i.e.,

$$\rho_\alpha(\mathbf{r}_\alpha) = \frac{4}{b^3\pi^{3/2}} e^{-(r_\alpha/b)^2}, \tag{3.6}$$

where $b = 1.19$ fm is the α-particle size parameter [25].

In our previous reference [29] we multiplied the double folding integral by a strength parameter $v_a < 1$ in Eq. (2.6), in order to obtain the experimental half-life. The necessity to use such a factor, multiplying the double folded α-daughter potential, was already stressed in Refs. [23,24]. It is connected with the fact that the Reid parameters of the used M3Y interaction were fitted using scattering experiments involving free particles [31]. Therefore this potential with $v_a = 1$ describes the emission of an already existing α particle.

Our model has four essential parameters: v_a and C_v give the attractive part of the potential, and c and v_0 define the repulsive core. In Fig. 4 we plot the dependence of the logarithm of the half-life $T = \hbar \ln 2/\Gamma$ on the parameters v_a and C_v. One can see that it strongly depends on v_a while the dependence upon C_v is very weak. On the other hand one sees an opposite behavior in Fig. 5, where we plot the dependence between the logarithm of the intensity ratio I of Eq. (3.1) on

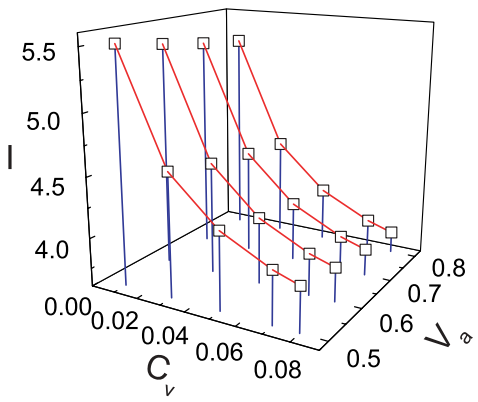

FIG. 5. (Color online) Logarithm (3.1) of the intensity ratio as a function of the attraction parameters: double folding strength parameter v_a and vibrational coupling strength C_v.

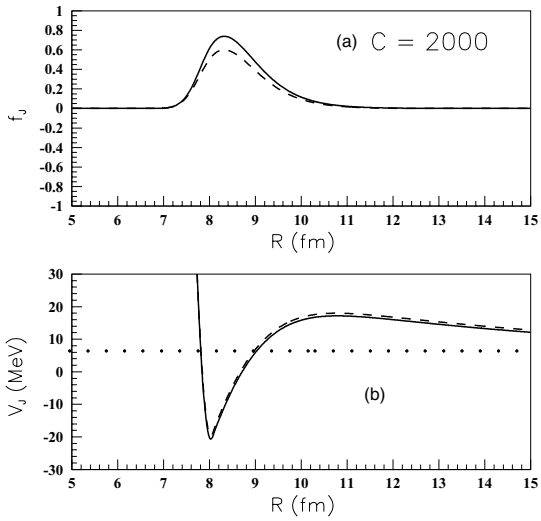

FIG. 6. (a) Wave function components for $J = 0$ (solid line) and $J = 2$ (dashed line) for the α-decay to ^{216}Po with the potential parameters $C_v = 0.15$ MeV^{-1}, $c = 2000$ MeV fm^{-2}, $v_0 = 65.6$ MeV. (b) Components of the diagonal matrix elements of the potential (3.8) for $J = 0$ (solid line) and $J = 2$ (dashed line).

the same parameters. This quantity practically does not depend on v_a and has a strong dependence on C_v.

Our goal is to investigate the fine structure given by Eq. (3.1). As stated above it mainly depends upon the vibrational parameter C_v, defining the coupling strength between the two considered channels with $J = 0, 2$. Since the dependence on v_a is only moderate we simplify the calculation by taking $v_a = 1$, corresponding to a "pure" α-cluster model. Therefore our calculations will provide the components $G_J(\kappa_J R)$ of the wave function giving the penetration factor P_J in Eq. (3.3). Actually the α-cluster exists on the nuclear surface with some probability $v_a < 1$ and therefore the ratio between theoretical and experimental half-lives,

$$S = \frac{T_{\text{th}}}{T_{\text{exp}}}, \tag{3.7}$$

will provide us this α-particle preformation probability, or the spectroscopic factor [34].

In Ref. [29] we have shown that the parameters c and v_0 of the repulsive core, used to determine the Q-value, are related to each other. This, and the above analysis means that our calculation will depend on only two parameters, namely the coupling parameter C_v and the repulsive strength c.

We have analyzed the α-decay fine structure I Eq. (3.1) for emitters with evaluated experimental data on both Γ_0 and Γ_2. Our calculations show that I can be reproduced for vibrational nuclei only with a strong repulsive core. That is at variance with rotational emitters where we used a soft repulsion [29]. We adopted a constant value $c = 2000$ MeV fm^{-2} of the repulsive strength. The components $J = 0$ (solid line) and

TABLE I. Compilation of the calculated and experimental α-decay quantities for vibrational nuclei used in the analysis. Given are the charge and mass numbers of the daughter nuclei, quadrupole deformations [36], Q-values and E_2 energies (MeV), experimental [28] and computed values of I of Eq. (3.1), HF's of Eq. (3.2), potential parameters C_v (MeV^{-1}) and c (MeV fm^{-2}), logarithm of experimental [28] and computed half-lives (s), and spectroscopic factors S of Eq. (3.7).

Z	A	β_2	Q	E_2	$I_{\rm exp}$	$I_{\rm fit}$	HF$_{\rm exp}$	HF$_{\rm th}$	C_v	c	$\log_{10}T_{\rm exp}$	$\log_{10}T_{\rm th}$	S
76	172	0.190	5.886	0.228	2.600	2.585	21.095	21.350	0.011	2×10^3	1.20	−0.26	0.348×10^{-1}
76	176	0.246	5.275	0.135	3.100	3.064	134.409	129.791	0.004	2×10^3	4.30	2.51	0.161×10^{-1}
78	176	0.171	6.258	0.264	3.300	3.268	87.916	85.766	0.005	2×10^3	0.79	−0.94	0.188×10^{-1}
78	178	0.254	5.997	0.170	2.100	2.136	14.462	14.128	0.013	2×10^3	1.90	0.08	0.150×10^{-1}
78	180	0.265	5.662	0.153	2.400	2.391	26.431	26.012	0.009	2×10^3	3.40	1.53	0.134×10^{-1}
80	182	−0.122	6.471	0.328	2.700	2.699	13.449	13.450	0.016	2×10^3	0.68	−0.98	0.216×10^{-1}
80	184	−0.130	6.111	0.367	3.000	3.018	13.003	13.553	0.016	2×10^3	2.00	0.43	0.268×10^{-1}
80	186	−0.130	5.698	0.409	3.100	3.076	5.852	5.809	0.030	2×10^3	3.90	2.30	0.252×10^{-1}
82	204	−0.008	5.216	0.899	5.600	6.555	0.328	2.807	0.150	2×10^3	8.00	5.56	0.365×10^{-2}
82	206	−0.008	5.407	0.803	4.900	5.514	0.683	2.688	0.150	2×10^3	7.10	4.52	0.264×10^{-2}
82	210	0.000	7.833	0.800	4.000	4.000	16.284	16.284	0.024	2×10^3	−3.80	−5.47	0.215×10^{-1}
82	212	0.000	6.907	0.805	4.700	4.721	19.605	19.458	0.022	2×10^3	−0.82	−2.41	0.256×10^{-1}
82	214	0.009	6.115	0.836	5.000	4.959	4.112	4.112	0.055	2×10^3	2.30	0.78	0.305×10^{-1}
84	194	0.026	7.354	0.319	3.200	3.155	65.193	66.539	0.006	2×10^3	−1.20	−2.77	0.266×10^{-1}
84	196	0.000	7.044	0.463	4.200	4.222	177.012	173.602	0.004	2×10^3	0.00	−1.75	0.179×10^{-1}
84	198	0.000	6.774	0.605	4.000	4.000	19.015	19.015	0.018	2×10^3	1.10	−0.66	0.173×10^{-1}
84	204	0.009	6.261	0.684	3.300	3.894	0.697	2.601	0.150	2×10^3	3.40	1.48	0.120×10^{-1}
84	206	−0.018	6.159	0.700	4.300	4.252	3.979	3.949	0.060	2×10^3	4.00	1.76	0.578×10^{-2}
84	208	−0.018	6.385	0.687	3.300	3.790	0.821	2.532	0.150	2×10^3	3.10	0.82	0.520×10^{-2}
84	214	−0.008	7.263	0.609	2.900	2.832	2.715	2.395	0.150	2×10^3	−1.50	−2.68	0.656×10^{-1}
84	216	0.020	6.405	0.550	3.000	3.031	1.844	2.176	0.150	2×10^3	1.70	0.59	0.783×10^{-1}
84	218	0.039	5.590	0.510	3.100	3.393	1.083	2.060	0.150	2×10^3	5.50	4.43	0.843×10^{-1}
86	210	−0.026	7.273	0.644	2.700	3.050	1.125	2.524	0.150	2×10^3	0.40	−1.76	0.692×10^{-2}
86	216	0.008	7.595	0.462	2.000	2.126	1.565	2.112	0.150	2×10^3	−1.60	−2.96	0.439×10^{-1}
86	218	0.040	6.681	0.324	1.500	1.523	0.858	0.894	0.420	5×10^1	1.60	0.57	0.933×10^{-1}
86	220	0.111	5.789	0.241	1.300	1.265	0.632	0.612	0.200	5×10^1	5.50	4.73	$0.170\times10^{+0}$
86	222	0.137	4.870	0.186	1.200	1.219	0.546	0.532	0.140	5×10^1	11.00	10.03	$0.108\times10^{+0}$
88	218	0.020	8.129	0.389	1.500	1.301	1.206	0.754	0.400	5×10^1	−2.60	−3.67	0.843×10^{-1}
88	220	0.103	7.304	0.178	0.620	0.623	0.578	0.578	0.150	5×10^1	0.11	−0.93	0.914×10^{-1}
88	222	0.130	6.451	0.111	0.520	0.514	0.648	0.641	0.170	5×10^1	3.40	2.37	0.923×10^{-1}
90	222	0.111	7.715	0.183	0.750	0.748	0.835	0.820	0.400	5×10^1	−0.30	−1.61	0.493×10^{-1}

$J=2$ (dashed line) of the first nodeless wave function are given in Fig. 6(a) for the α-decay to ^{216}Po. We considered this eigenstate as a decaying state based on results of the microscopic calculations. Indeed, the calculations performed within the QRPA [18] have shown that both the ground state and 2^+ formation probabilities have basically Gaussian shapes, as can be seen in Fig. 2 of this reference. Here the hindrance factor is estimated as a ratio between the integral of the corresponding preformation amplitudes squared, computed in the region beyond the last maximum. Small oscillations, present at larger distances [35], do not affect the value of this ratio. The corresponding values of the diagonal matrix elements

$$U_J(R)=\overline{V}_0(R)+\frac{\hbar^2J(J+1)}{2\mu R^2}, \tag{3.8}$$

are plotted in Fig. 6(b) by using the same symbols.

With the adopted value of the repulsive strength we plot in Fig. 7(a) the dependence of the computed I of Eq. (3.1) on the vibrational coupling strength C_v for the α-decay to ^{196}Po. One observes a decreasing behavior for $C_v\leqslant0.15$, as already seen in Fig. 5, followed by a plateau and slow increase. In Fig. 7(b) are given the corresponding values of the potential depth v_0, necessary to reproduce the experimental Q-value. Thus, by using only one parameter C_v and with $c=2000$ MeV fm^{-2} it was possible to reproduce the experimental values $I_{\rm exp}$ of most measured vibrational nuclei. The results of our calculations are given in Table I.

Concerning the last seven nuclei in Table I it turned out that their decay properties are closer to rotational nuclei investigated in our previous work [29], where we used a soft repulsive core. It turns out that only by using a rather small repulsive strength $c=50$ MeV fm^{-2} it is possible to reproduce their fine structure. The wave function components and the diagonal matrix elements of the potential (3.8) are plotted in Fig. 8(a) and 8(b), for the α-decay to ^{220}Rn.

It is interesting to witness the fact that the inverse of the vibrational coupling strength, $1/C_v$, is proportional to

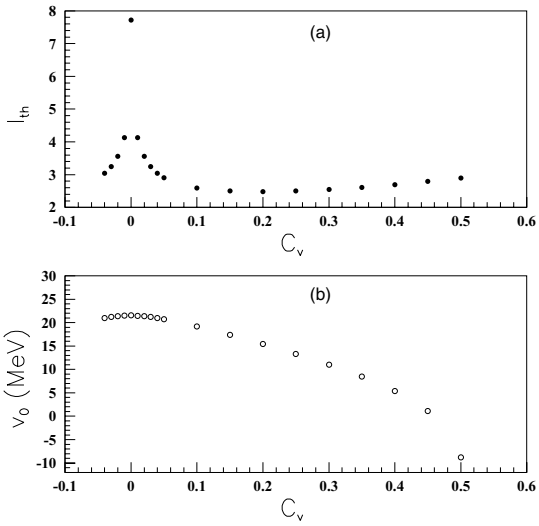

FIG. 7. (a) Logarithm (3.1) of the intensity ratio versus the vibrational potential parameter C_v for the α-decay to ^{196}Po. (b) Depth of the repulsive potential v_0 reproducing the experimental Q-value.

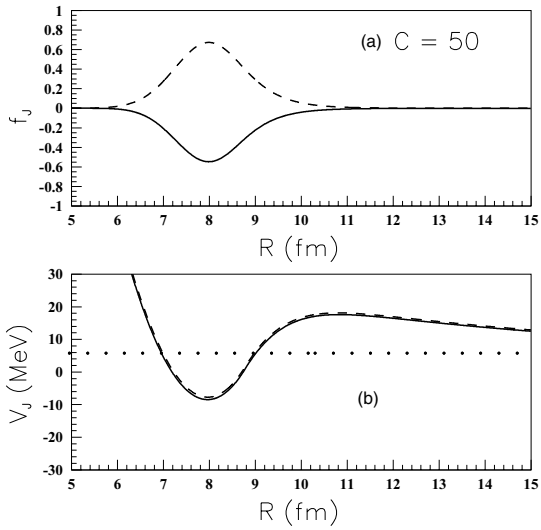

FIG. 8. (a) Wave function components for $J = 0$ (solid line) and $J = 2$ (dashed line) for the α-decay to ^{220}Rn with the potential parameters $C_v = 0.20$ MeV^{-1}, $c = 50$ MeV fm^{-2}, and $v_0 = 21.6$ MeV. (b) Components of the diagonal matrix elements of the potential (3.8) for $J = 0$ (solid line) and $J = 2$ (dashed line).

the square of the logarithm of the HF for all analyzed transitions, as shown in Fig. 9. Here the solid line represents the fit

$$\frac{1}{C_v} = 49.122\left(\log_{10}\mathrm{HF}\right)^2, \quad \sigma = 15.636. \tag{3.9}$$

B. Systematic predictions

The relation (3.4) is able to describe the logarithm of the intensity ratio (3.1) within a factor of five. At the same time from Fig. 9 one sees that the relation (3.9), connecting the vibrational strength and HF, is fulfilled with a much better accuracy for all emitters. By using the definitions (3.1) and (3.2) one derives from the quadratic fit of Eq. (3.9) the

TABLE II. Compilation of the predicted fine-structure and hindrance factors for vibrational nuclei. Given are the charge and mass numbers of the daughter nuclei, quadrupole deformations [36], Q-values and E_2 energies (MeV), the values of I estimated according to Eq. (3.4) and computed Eq. (3.10), computed HF's Eq. (3.2), potential parameters C_v (MeV^{-1}) and c (MeV fm^{-2}), logarithm of experimental [28] and computed half-lives (s), and spectroscopic factors S of (3.7).

Z	A	β_2	Q	E_2	I_q	I_{fit}	HF_{th}	C_v	c	$\log_{10}T_{exp}$	$\log_{10}T_{th}$	S
76	166	0.134	6.704	0.431	2.804	2.555	5.313	0.039	2×10^3	−2.20	−3.22	0.955×10^{-1}
76	168	0.162	6.465	0.341	2.411	2.499	8.678	0.023	2×10^3	−0.96	−2.52	0.274×10^{-1}
76	170	0.171	6.184	0.287	2.176	2.559	13.526	0.016	2×10^3	0.04	−1.42	0.348×10^{-1}
78	172	0.126	6.925	0.457	2.917	2.587	5.055	0.041	2×10^3	−1.50	−3.30	0.158×10^{-1}
78	174	0.153	6.578	0.394	2.642	2.629	7.207	0.028	2×10^3	−0.30	−2.15	0.141×10^{-1}
80	180	−0.122	6.775	0.434	2.817	2.694	6.293	0.032	2×10^3	−0.26	−2.10	0.145×10^{-1}
84	200	0.009	6.546	0.666	3.828	3.703	3.504	0.070	2×10^3	2.00	0.26	0.182×10^{-1}
84	202	0.009	6.384	0.677	3.876	3.871	3.401	0.071	2×10^3	2.70	0.85	0.143×10^{-1}
86	202	−0.104	7.416	0.504	3.122	2.819	6.144	0.033	2×10^3	−0.62	−2.22	0.251×10^{-1}
86	204	−0.087	7.273	0.543	3.292	2.976	5.390	0.038	2×10^3	0.15	−1.77	0.119×10^{-1}
86	206	−0.044	7.157	0.575	3.432	3.105	4.727	0.045	2×10^3	0.57	−1.31	0.133×10^{-1}
86	208	−0.026	7.032	0.636	3.698	3.340	3.828	0.060	2×10^3	1.10	−0.88	0.104×10^{-1}
88	208	−0.104	7.952	0.520	3.192	2.675	5.663	0.036	2×10^3	−1.50	−3.24	0.180×10^{-1}
88	210	−0.053	7.826	0.603	3.554	2.910	4.394	0.050	2×10^3	−1.10	−2.88	0.167×10^{-1}
90	220	0.030	8.620	0.373	2.551	2.416	13.489	0.016	2×10^3	−3.20	−4.79	0.257×10^{-1}

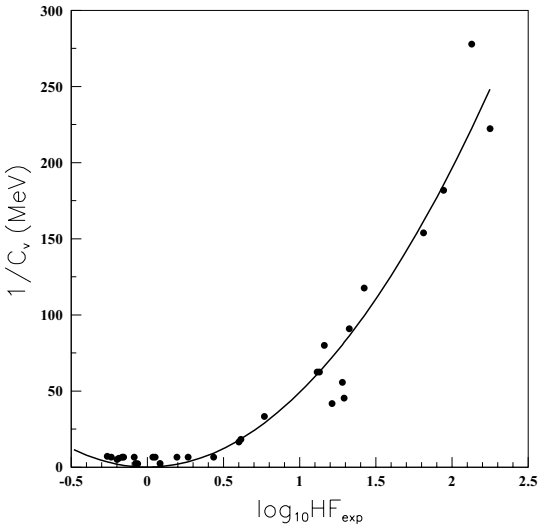

FIG. 9. Inverse of the vibrational coupling parameter as a function of the logarithm of the experimental HF. The parabola is the fit given by (3.9).

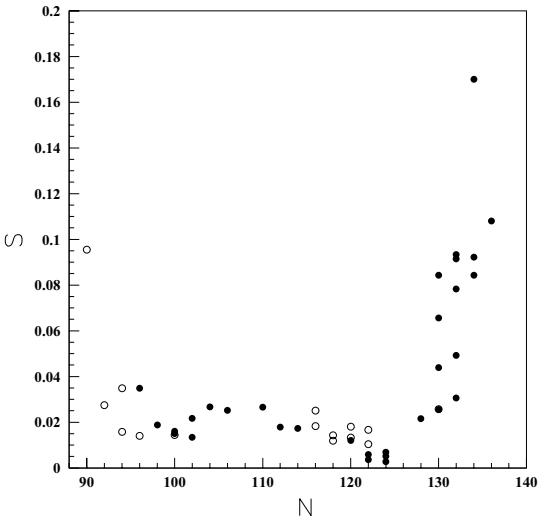

FIG. 10. The spectroscopic factor (3.7) versus the neutron number for transitions in Table I (dark circles) and Table II (open circles).

following relation:

$$I_q = \frac{1}{\sqrt{49.122 C_v}} - \log_{10}\frac{P_2}{P_0}. \tag{3.10}$$

On the other hand, the I_q provided by our calculation depends on the vibrational strength C_v as depicted in Fig. 7(a). In this way it becomes possible to simultaneously determine I_q and C_v, i.e., to obtain self-consistency between the above relation and the value obtained as a result of the coupled channels calculation. Based on this fact we can predict the fine structure I_q for several α-decays from vibrational nuclei. The results are given in Table II.

Finally, in Fig. 10, we give the values of the spectroscopic factor (3.7) versus the neutron number. One clearly sees the jump around the magic number $N = 126$, showing that in Rn isotopes α-clustering has the highest probability of around 20%. We emphasize once again that one can reproduce the experimental half lives by using a strength v_a in Eq. (2.6), that is inversely proportional to $\log_{10}S$, as can be seen from Fig. 4. On the other hand, as shown in Fig. 5, this parameter will practically not affect the value of the fine structure I.

IV. CONCLUSIONS

In this paper we have analyzed the α-decay fine structure (3.9) for decays to 2^+ states and the corresponding hindrance factors (3.2) in vibrational-transitional nuclei. We have used a stationary coupled channels formalism to describe 2^+ states in even-even nuclei in terms of a vibrational coupling between the daughter nucleus and the α-particle. This interaction was computed as a derivative of the initial potential, simulated by a double folding procedure that uses M3Y plus Coulomb forces for the attractive part. The internal part was given by a parabolic repulsion, simulating the fact that an α-particle exists only on the nuclear surface. We reproduce the experimental Q-value by adjusting the depth of the repulsive interaction. As a result a pocket-like potential was obtained.

The α-decaying state was identified as the zero-nodes eigenstate inside the pocket-like potential. This interpretation is based on results of microscopic calculations. The analysis of experimental data showed that the logarithm of the intensity ratio depends linearly on the 2^+ energy. Our calculations show that a strong repulsive core is able to reproduce experimental data. By using one parameter, namely the vibrational coupling strength C_v, it was possible to reproduce experimental fine structure. We discovered a remarkable dependence (3.9) between the inverse of this parameter and the hindrance factor squared. Based on this we made systematic predictions for several vibrational α emitters.

[1] D. S. Delion, A. Săndulescu, and W. Greiner, Phys. Rev. C **69**, 044318 (2004).
[2] J. O. Rasmussen, Phys. Rev. **113**, 1593 (1959).
[3] A. Săndulescu and O. Dumitrescu, Phys. Lett. **19**, 404 (1965).
[4] A. Săndulescu and O. Dumitrescu, Phys. Lett. **B24**, 212 (1967).
[5] M. I. Cristu, O. Dumitrescu, N. I. Pyatov, and A. Săndulescu, Nucl. Phys. **A130**, 31 (1969).
[6] D. S. Delion *et al.*, Phys. Rev. Lett. **74**, 3939 (1995); Phys. Rev. C **54**, 1169 (1996).
[7] D. Karlgren, R. J. Liotta, R. Wyss, M. Huyse, K. Van de Vel, and P. Van Duppen, Phys. Rev. C **73**, 064304 (2006).

[8] J. Wauters *et al.*, Z. Phys. A **342**, 277 (1992).
[9] J. Wauters *et al.*, Z. Phys. A **344**, 29 (1992).
[10] J. Wauters *et al.*, Z. Phys. A **345**, 21 (1993).
[11] J. Wauters, P. Dendooven, M. Huyse, G. Reusen, P. VanDuppen, P. Lievens (The ISOLDE Collaboration), Phys. Rev. C **47**, 1447 (1993).
[12] J. Wauters *et al.*, Phys. Rev. C **50**, 2768 (1994).
[13] J. Wauters *et al.*, Phys. Rev. Lett. **72**, 1329 (1994).
[14] N. Bijnens *et al.*, Phys. Rev. Lett. **75**, 4571 (1995).
[15] R. G. Allatt *et al.*, Phys. Lett. **B437**, 29 (1998).
[16] C. F. Liang, R. K. Sheline, P. Paris, M. Hussonnois, J. F. Ledu, and D. B. Isabelle, Phys. Rev. C **49**, 2230 (1994).
[17] D. S. Delion and R. J. Liotta, Phys. Rev. C **56**, 1782 (1997).
[18] D. S. Delion and J. Suhonen, Phys. Rev. C **64**, 064302 (2001).
[19] S. Peltonen, D. S. Delion, and J. Suhonen, Phys. Rev. C **71**, 044315 (2005).
[20] J. O. Rasmussen and B. Segal, Phys. Rev. **103**, 1298 (1956).
[21] H. M. A. Radi, A. A. Shihab-Eldin, J. O. Rasmussen, and Luiz F. Oliveira, Phys. Rev. Lett. **41**, 1444 (1978).
[22] P. O. Fröman, Kgl. Danske Videnskab. Selskab Mat. Fys. Skrifter **1**, No. 3 (1957).
[23] R. Neu and F. Hoyler, Phys. Rev. C **46**, 208 (1992).
[24] H. Abele and G. Staudt, Phys. Rev. C **47**, 742 (1993).
[25] Dao T. Khoa, Phys. Rev. C **63**, 034007 (2001).
[26] D. N. Basu, J. Phys. G **29**, 2079 (2003).
[27] C. Xu and Z. Ren, Nucl. Phys. **A778**, 1 (2006).
[28] Y. A. Akovali, Nucl. Data Sheets **84**, 1 (1998).
[29] D. S. Delion, S. Peltonen, and J. Suhonen, Phys. Rev. C **73**, 014315 (2006).
[30] G. Bertsch, J. Borysowicz, H. McManus, and W. G. Love, Nucl. Phys. **A284**, 399 (1977).
[31] G. R. Satchler and W. G. Love, Phys. Rep. **55**, 183 (1979).
[32] F. Cârstoiu and R. J. Lombard, Ann. Phys. (NY) **217**, 279 (1992).
[33] D. S. Delion and J. Suhonen, Nucl. Phys. **A781**, 88 (2007).
[34] P. Mohr, Phys. Rev. C **73**, 031301(R) (2006).
[35] P. Lotti, E. Maglione, F. Catara, and A. Insolia, Europhys. Lett. **6**, 125 (1988).
[36] P. Möller, J. R. Nix, W. D. Myers, and W. J. Swiatecki, At. Data Nucl. Data Tables **59**, 185 (1995).

Paper IV

α-decay spectroscopy of deformed nuclei reexamined
S. Peltonen, D. S. Delion and J. Suhonen,
Phys. Rev. C **78**, 034608 (2008).

PHYSICAL REVIEW C **78**, 034608 (2008)

α-decay spectroscopy of deformed nuclei reexamined

S. Peltonen,[1] D. S. Delion,[2,3] and J. Suhonen[1]
[1]*Department of Physics, University of Jyväskylä, POB 35, FIN-40351, Jyväskylä, Finland*
[2]*National Institute of Physics and Nuclear Engineering, Atomiştilor 407, Bucharest-Măgurele, 077125, Romania*
[3]*Academy of Romanian Scientists, 54 Splaiul Independenţei, Bucharest, 050085, Romania*
(Received 30 June 2008; published 23 September 2008)

We perform an extensive analysis of α-decays to 2^+ and 4^+ states in deformed even-even nuclei by using the stationary coupled channels approach. Collective excitations are described within the rigid rotor model. The α-nucleus interaction is given by a double folding procedure with M3Y plus Coulomb nucleon-nucleon forces. We use a repulsive potential with one independent parameter in order to localize the α-particle on the nuclear surface and to fit the experimental Q-value. The decaying state is identified with the first resonance inside the resulting pocket-like potential, as suggested by microscopic calculations. We obtain a good agreement with existing experimental data concerning decay widths to $J = 2^+, 4^+$ states. The total α-decay half-lives agrees very well with experimental values by fitting the spectroscopic factor in terms of charge and neutron numbers separately for $Z < 82$ and $Z > 82$. We give predictions for intensities and hindrance factors for 52 even-even α-emitters with $\beta_2 > 0.15$ and $E_{2^+} < 200$ kev. Comparison between the phenomenological and microscopic spectroscopic factors revealed large α-clustering components for nuclei close and above $N = 82$, $Z = 82$, $N = 126$ magic numbers.

DOI: 10.1103/PhysRevC.78.034608 PACS number(s): 21.10.Tg, 23.60.+e, 24.10.Eq

I. INTRODUCTION

In a phenomenological description of emission processes one supposes that the dynamics of emitted particles obeys the Schrödinger equation with a potential defined at any distance. The major role in decay processes is played by the interplay between the energy of the emitted particle (Q-value) and the Coulomb barrier [1]. In order to extract the effect of the barrier one defines the hindrance factor (HF) as the ratio between decay widths to the ground and excited state, divided by the corresponding Coulomb penetrabilities.

The most general approach to describe emission process from deformed nuclei is the coupled channels method. The first computations of the α-decay widths in deformed rotational nuclei within the coupled channels approach were performed in Ref. [2]. Later on, in Ref. [3], HF's were estimated in deformed nuclei by using an approximation of the coupled channel procedure, given by the Fröman approach [4], and adopting a simple phenomenological ansatz for the preformation factor.

The most important ingredient of such calculations is the interfragment interaction. Several calculations estimated the α-core potential by using the double folding procedure in Refs. [5,6] and more recently in [7,8]. This kind of potential was used to estimate ground-state-to-ground-state half-lives within the spherical approach in Ref. [9]. In Ref. [10] the densities in the double folded α-core potential were computed within the relativistic mean-field theory. Very recently a global calculation of α-decay widths by using a density dependent folding approach was performed in Ref. [11].

In the above-mentioned works it was concluded that the strength of the nucleon-nucleon force should be quenched (i.e., the Coulomb barrier should increase) in order to describe the correct relation between the half-life and Q-value. This is explained by the fact that the nucleon-nucleon interaction is derived from scattering data. Thus, one implicitly supposes that the fragments are already born. This is in contradiction with the fact that at small distances only the parent nucleus exists. One way to simulate such a situation is to introduce a repulsive core, giving vanishing values of the interfragment wave function for these distances. It turns out that this procedure is not enough to reproduce the absolute values of experimental data [12,13], and the ratio between the theoretical and experimental half-lives, defining the phenomenological spectroscopic factor [14], is less than unity. This means that the used α-daughter potential is too low and the nuclear part of the interaction is too strong (too negative). By quenching the effective nucleon-nucleon interaction with a factor around 0.6 [12] it is possible to increase the Coulomb barrier in the region of the touching configuration, in order to reproduce experimental half-lives.

In several papers [15–17] we analyzed the double fine structure of emitted fragments in the cold fission of ^{252}Cf within the coupled channels formalism. We found that the yields to excited states in both fragments are very sensitive to nuclear structure details such as the mean field deformation and diffusivity. Unfortunately there are only few available experimental data to be analyzed in this field [18]. On the other hand, there are a lot of high precision data on α-decay fine structure to rotational levels, see, e.g., [19].

The aim of this paper is to extend the coupled channels technique used in Ref. [12] in order to analyze the α-decay fine structure of more than 50 deformed even-even α-emitters. On the other hand, we will compare the phenomenological spectroscopic factor with a similar quantity derived within a microscopic approach. The paper is organized according to the following plan. In Sec. II we shortly review the main ingredients of the stationary coupled channels formalism that describes α-decay fine structure to rotational states. We also give a short description of the used α-core potential. In Sec. III

we give a systematics of α-decay widths to ground as well as to excited states in even-even emitters. We also give predictions for those nuclei where the intensities to low-lying states are still not measured. In the last Section we draw conclusions.

II. THEORETICAL BACKGROUND

In this section we summarize the main theoretical details necessary to compute the decay width within the coupled channels formalism. The main ingredients were already introduced in Refs. [12,17]. We describe the α-core dynamics by using the stationary Schrödinger equation

$$H\Psi(\mathbf{R},\Omega_D)=E\Psi(\mathbf{R},\Omega_D), \tag{2.1}$$

where $\mathbf{R}=(R,\Omega)$ denotes the distance between the centers of emitted fragments, $E=Q_\alpha$ and $\Omega_D=(\varphi_D,\theta_D,0)$ are the Euler angles defining the daughter major axis in the laboratory system of coordinates. An α-decaying state is identified with a narrow resonant solution, containing only outgoing components (Gamow state).

The Hamiltonian describing the α-decay in the laboratory system of coordinates

$$H=-\frac{\hbar^2}{2\mu}\nabla_R^2+H_D(\Omega_D)+V(\mathbf{R},\Omega_D), \tag{2.2}$$

depends upon the reduced mass of the dinuclear system μ. Here H_D describes the rotation of the even-even core with eigenvalues E_J, $J=0,2,4,\ldots$. The interaction between nuclei is estimated by the double folding procedure [21,22]. The resulting potential can be divided into a spherical (V_0) and a deformed component (V_d) as follows:

$$\begin{aligned}V(\mathbf{R},\Omega_D)&=V_0(R)+V_d(\mathbf{R},\Omega_D)\\&=V_0(R)+\sum_{\lambda>0}V_\lambda(R)\mathcal{Y}_\lambda(\Omega,\Omega_D).\end{aligned} \tag{2.3}$$

Here the angular part of the wave function has the following ansatz:

$$\mathcal{Y}_\lambda(\Omega,\Omega_D)=[Y_\lambda(\Omega)\otimes Y_\lambda(\Omega_D)]_0\,. \tag{2.4}$$

Therefore the rotation of the core is compensated by the rotation of the α-particle in the opposite direction. The relation (2.3), with the angular part (2.4), is nothing more than a multipole-multipole expansion, where the multipole form factors $V_\lambda(R)$ are given in terms of density distributions [22]. In our computations we will use the standard M3Y nucleon-nucleon [23] plus Coulomb force. For details see [22].

To Eq. (2.3) we add a simple repulsive core, depending on one independent parameter. The role of this potential is similar to that in Refs. [15–17] where we investigated cold fission and in Ref. [12] devoted to the α-decay. It simulates the Pauli principle by locating the cluster on the nuclear surface and adjusts the energy of the system to the experimental Q-value. In Ref. [12] it was shown that the total half-life and the partial decay widths do not depend on the shape of this repulsive potential.

We will describe transitions from the ground state of the parent nucleus. If the rotational states of the core belong to the ground band (with the intrinsic angular momentum projection $K=0$) the wave function contains an angular part similar to Eq. (2.4), i.e.,

$$\Psi(\mathbf{R},\Omega_D)=\frac{1}{R}\sum_J f_J(R)\mathcal{Y}_J(\Omega,\Omega_D). \tag{2.5}$$

By using the orthonormality of angular functions, entering the above superposition, one obtains in a standard way the coupled system of differential equations for the radial components

$$\frac{d^2f_J(R)}{d\rho_J^2}=\sum_{J'}A_{JJ'}(R)f_{J'}(R), \tag{2.6}$$

where the coupling matrix

$$\begin{aligned}A_{JJ'}(R)=&\left[\frac{J(J+1)}{\rho_J^2}+\frac{V_0(R)}{E-E_J}-1\right]\delta_{JJ'}\\&+\frac{1}{E-E_J}\langle\mathcal{Y}_J|V_d(R)|\mathcal{Y}_{J'}\rangle,\end{aligned} \tag{2.7}$$

depends on the reduced radius $\rho_J=\kappa_J R$ and channel momentum $\kappa_J=\sqrt{2\mu(E-E_J)}/\hbar$. The matrix element entering Eq. (2.7) is given by standard manipulations of angular-momentum algebra [12]. The result is a superposition of terms containing the multipole form factor of the potential, $V_\lambda(R)$. At large distances, where the field becomes spherical, the system of equations becomes decoupled and contains only Coulomb parameters in each channel J

$$\chi_J\equiv 2\frac{Z_\alpha Z_D e^2}{\hbar v_J}. \tag{2.8}$$

In order to find resonant solutions of Eq. (2.6) we first define N independent column-vector functions, that satisfy inside the repulsive core, at $R=R_0$, where $V_0(R_0)\gg Q_\alpha$, the following boundary conditions:

$$\mathcal{R}_{JI}(R_0)=\delta_{JI}\varepsilon_J, \tag{9}$$

where ε_J are arbitrary small numbers. The index J labels the component, while I labels the solution.

We also determine N independent outgoing Coulomb column-vector functions, satisfying at large distances the condition

$$\begin{aligned}\mathcal{H}^{(+)}_{JI}(R)&\equiv\mathcal{G}_{JI}(R)+i\mathcal{F}_{JI}(R)\overset{R\to\infty}{\longrightarrow}\delta_{JI}H^{(+)}_J(\chi_J,\rho_J)\\&\equiv\delta_{JI}\left[G_J(\chi_J,\rho_J)+iF_J(\chi_J,\rho_J)\right],\end{aligned} \tag{2.10}$$

where $G_J(\chi_J,\rho_J)$ and $F_J(\chi_J,\rho_J)$ are the irregular and regular spherical Coulomb wave functions, respectively. These functions are found by a backward numerical integration.

Each component of the solution is built as a superposition of these N independent fundamental solutions. We impose the matching boundary decay conditions

$$f_J(R)=\sum_I\mathcal{R}_{JI}(R)M_I=\sum_I\mathcal{H}^{(+)}_{JI}(R)N_I, \tag{2.11}$$

at the radius R inside the barrier, to have outgoing waves in all channels. Similar conditions are assumed for derivatives. The coefficients N_I are nothing else than the scattering amplitudes.

These conditions give the following secular equation:

$$0 = \det\begin{bmatrix} \mathcal{R}(R) & \mathcal{H}^{(+)}(R) \\ d\mathcal{R}(R)/dR & d\mathcal{H}^{(+)}(R)/dR \end{bmatrix} \approx \det\begin{bmatrix} \mathcal{R}(R) & \mathcal{G}(R) \\ d\mathcal{R}(R)/dR & d\mathcal{G}(R)/dR \end{bmatrix}. \quad (2.12)$$

The first condition is exact and it is fulfilled for complex energies, determining the resonant (Gamow) states. In our case they practically coincide with the real scattering resonant states, because the imaginary parts of energies are much smaller than the corresponding real parts. This corresponds to a vanishing regular Coulomb functions F_J inside the barrier. Therefore the above approximation, given by the second equality, is very good.

The coefficients M_I and N_I are fully determined from the normalization of the wave function in the internal region

$$\sum_J \int_0^{R_2} |f_J(R)|^2 dR = 1, \quad (2.13)$$

where R_2 is the external turning point. Beyond this radius the wave function has practically vanishing values. Thus, any α-decaying state practically behaves like a bound state, having an exponential decrease versus radius inside the barrier.

By inverting Eq. (2.11) for some radius R, then dividing and multiplying the result by $H_I^{(+)}(\rho_I)$ one obtains

$$N_I = \frac{1}{H_I^{(+)}(\rho_I)} \sum_J K_{IJ}(R) f_J(R), \quad (2.14)$$

where $\rho_I = \kappa_I R$. The propagator operator is defined in such a way that it becomes the unity matrix for a spherical Coulomb field, i.e.,

$$K_{IJ}(R) \equiv H_I^{(+)}(\rho_I)[\mathcal{H}^{(+)}(R)]^{-1}_{IJ} = \delta_{IJ} + \Delta K_{IJ}(R), \quad (2.15)$$

where $\Delta K_{IJ}(R) \to_{R\to\infty} 0$. The semiclassical limit of K_{IJ} is symmetric and is called the Fröman matrix [4]. Of course the scattering amplitude (2.14) does not depend on R.

The total decay width is a sum over partial channel widths. It can be derived from the continuity equation in a straightforward way and the result is the following:

$$\Gamma = \sum_J \Gamma_J = \sum_J \hbar v_J \lim_{R\to\infty} |f_J(R)|^2 = \sum_J \hbar v_J |N_J|^2, \quad (2.16)$$

where v_J is the center of mass velocity at infinity in the channel J, i.e.,

$$v_J = \frac{\hbar \kappa_J}{\mu}. \quad (2.17)$$

The wave function components can be directly recovered by using the experimental partial decay widths

$$f_J(R) = \sum_I \mathcal{H}_{JI}^{(+)}(R) \sqrt{\frac{\Gamma_I}{\hbar v_I}}, \quad (2.18)$$

because the matrix $\mathcal{H}^{(+)}$, defined by Eq. (2.10), is fully determined by the potential. Of course, the wave function depends on the details of the used interaction. This is the main reason why we prefer to characterize the fine structure by the quantities

$$I_J \equiv \log_{10} \frac{\Gamma_0}{\Gamma_J}, \quad (2.19)$$

instead of the hindrance factors, defined as

$$HF_J = \left| \frac{f_0(R)}{f_J(R)} \right|^2, \quad (2.20)$$

and which are model dependent.

In Ref. [12] we multiplied the double folding integral (2.3) by a strength parameter $v_a < 1$ in order to describe the experimental relation between the half-lives and the corresponding Q-values. Here we will consider the true potential derived from scattering experiments, i.e., $v_a = 1$. This interaction describes the α-daughter dynamics for large distances $R > R_m$. In order to describe the internal two-body motion we use a repulsive core for the monopole component, taking care on the fact that an α-particle is localized at the nuclear surface [26]

$$\begin{aligned} \overline{V}_0(R) &= V_0(R), \quad R > R_m \\ &= c(R - R_0)^2 - v_0, \quad R \leqslant R_m. \end{aligned} \quad (2.21)$$

We stress the fact that only two parameters, namely v_0, c, are independent, because the radii R_0 and R_m are determined by the matching conditions

$$V_0(R_m) = c(R_m - R_0)^2 - v_0, \quad \frac{dV_0(R_m)}{dR} = 2c(R_m - R_0). \quad (2.22)$$

These conditions allow us to write down a single equation determining the matching radius for a given combination of v_0, c. Our analysis in Ref. [12] showed that the total half-life and the fine structure, defined by Eq. (2.19), is only weakly affected by simultaneously changing the parameters c and v_0.

Once the parameter c is fixed, we can adjust the Q-values for different decays by using one parameter, namely the repulsive depth v_0.

III. α-DECAY FINE STRUCTURE

The most important ingredient of our calculations is the α-daughter potential, given by the double folding between fragment densities. We describe the density of the daughter nucleus by an axially deformed Woods-Saxon shape, i.e.,

$$\begin{aligned} \rho_{D,\tau}(\mathbf{r}_D) &= \frac{\rho_{D,\tau}^{(0)}}{1 + \exp\{[r_D - R_{0,\tau}(\Omega_D)]/a\}}, \\ R_{0,\tau}(\Omega_D) &= R_{0,\tau}[1 + \beta_2 Y_{20}(\Omega_D) + \beta_4 Y_{40}(\Omega_D)], \end{aligned} \quad (3.1)$$

where the central densities are normalized by the total number of protons ($\tau = \pi$) and neutrons ($\tau = \nu$) separately. The α-particle density is given by a Gaussian distribution

$$\rho_\alpha(\mathbf{r}_\alpha) = \frac{4}{b^3 \pi^{3/2}} e^{-(r_\alpha/b)^2}. \quad (3.2)$$

We use the standard value of the diffusivity $a = 0.5$ fm and the α-particle size parameter is $b = 1.19$ fm [8].

TABLE I. Compilation of the experimental and computed α-decay quantities. The energies are given in keV and total α-decay half lives in seconds.

n	Z	A	β_2	β_4	Q_α	E_2	E_4	$I_2^{\rm exp}$	$I_2^{\rm th}$	$HF_2^{\rm exp}$	$HF_2^{\rm th}$	$I_4^{\rm exp}$	$I_4^{\rm th}$	$HF_4^{\rm exp}$	$HF_4^{\rm th}$	$lgT^{\rm exp}$	$lgT^{\rm th}$	S
1	74	168	0.208	0.000	5254	199.300	562.300	–	1.510	–	1.703	–	4.638	–	5.250	3.283	3.365	0.101
2	74	170	0.226	−0.006	4900	156.720	462.330	–	1.267	–	1.310	–	4.250	–	4.112	5.342	5.254	0.056
3	74	182	0.259	−0.084	2846	100.106	329.427	–	1.479	–	0.772	–	6.528	–	9.482	22.800	22.806	0.016
4	76	176	0.246	−0.011	5285	135.100	395.500	–	0.982	–	1.079	–	3.632	–	4.603	4.271	4.120	0.041
5	76	178	0.247	−0.027	4977	131.600	397.700	–	0.990	–	0.976	–	3.921	–	5.164	5.764	5.820	0.052
6	76	180	0.238	−0.045	4618	132.110	408.620	–	1.063	–	0.918	–	4.362	–	5.763	7.786	8.023	0.062
7	76	182	0.239	−0.062	4352	127.000	400.400	–	1.075	–	0.846	–	4.654	–	6.832	9.899	9.849	0.025
8	76	184	0.229	−0.071	4033	119.800	383.770	–	1.124	–	0.830	–	4.903	–	6.875	12.483	12.324	0.015
9	76	186	0.220	−0.082	3272	137.159	434.087	–	1.687	–	0.815	–	7.090	–	11.018	19.312	19.379	0.018
10	78	182	0.255	−0.026	5236	154.900	419.080	–	1.070	–	0.963	–	4.259	–	11.629	5.663	5.696	0.023
11	78	184	0.247	−0.044	4740	162.970	435.960	–	1.245	–	0.910	–	5.080	–	21.743	8.688	8.655	0.016
12	88	224	0.164	0.000	5520	84.373	250.783	0.424	0.811	0.533	1.301	2.503	2.570	2.060	2.404	7.781	7.791	0.207
13	88	226	0.172	0.112	4770	67.670	211.540	0.513	0.545	0.645	0.695	2.803	3.492	3.304	16.146	12.376	12.304	0.161
14	88	228	0.180	0.113	4083	63.823	204.680	0.557	0.632	0.568	0.676	3.054	3.900	2.503	17.560	17.647	17.675	0.196
15	90	226	0.173	0.111	5993	72.200	226.430	0.324	0.426	0.552	0.698	2.249	3.058	2.256	14.536	6.255	6.152	0.087
16	90	228	0.182	0.112	5414	57.762	186.828	0.334	0.392	0.592	0.676	2.356	3.081	3.116	16.543	9.337	9.425	0.127
17	90	230	0.198	0.115	4859	53.200	174.100	0.400	0.408	0.638	0.650	2.553	3.326	3.680	21.817	12.889	12.889	0.101
18	90	232	0.207	0.108	4573	49.460	162.250	0.455	0.415	0.710	0.647	2.692	3.351	4.702	21.441	14.869	14.846	0.097
19	90	234	0.215	0.102	4270	49.550	163.000	0.577	0.460	0.848	0.647	3.006	3.505	6.770	21.361	17.149	17.300	0.151
20	92	228	0.191	0.114	6716	59.000	196.666[a]	0.308	0.289	0.695	0.665	–	2.810	–	17.369	3.949	3.919	0.060
21	92	230	0.199	0.115	6310	51.720	169.500	0.327	0.272	0.737	0.650	2.230	2.867	4.994	21.649	5.723	5.695	0.056
22	92	232	0.207	0.117	5867	47.580	156.540	0.351	0.272	0.762	0.635	2.478	2.990	8.160	26.526	7.955	7.886	0.050
23	92	234	0.215	0.110	5593	43.498	143.352	0.389	0.269	0.837	0.635	2.830	2.974	18.722	26.083	9.442	9.341	0.046
24	92	236	0.215	0.102	5256	45.244	149.478	0.429	0.313	0.841	0.644	2.938	3.032	17.762	22.054	11.316	11.347	0.066
25	92	238	0.215	0.093	4984	44.915	148.390	0.513	0.343	0.967	0.654	3.396	3.039	42.456	18.661	13.071	13.113	0.073
26	92	240	0.224	0.079	4666	45.000	151.000	0.619	0.385	1.138	0.664	–	3.086	–	15.122	15.403	15.337	0.064
27	94	234	0.216	0.109	6620	46.000	153.333[a]	0.358	0.221	0.873	0.637	–	2.796	–	24.851	5.352	5.297	0.031
28	94	236	0.215	0.110	6398	44.630	147.450	0.391	0.225	0.930	0.634	3.136	2.841	52.813	26.776	6.369	6.298	0.030
29	94	238	0.215	0.102	6216	44.080	146.000	0.456	0.238	1.061	0.642	3.326	2.798	76.744	22.753	7.149	7.131	0.035
30	94	240	0.223	0.087	5902	42.824	141.690	0.510	0.258	1.166	0.653	3.541	2.750	114.055	18.455	8.757	8.690	0.034
31	94	242	0.224	0.071	5475	44.540	147.300[a]	0.664	0.313	1.512	0.674	–	2.757	–	13.622	11.177	11.083	0.036
32	94	244	0.224	0.071	5162	44.200	155.000	0.657	0.337	1.405	0.672	3.032	2.856	18.344	12.232	13.079	12.996	0.044
33	94	246	0.235	0.040	5208	46.000	155.000	–	0.370	–	0.713	–	2.674	–	8.353	12.163	12.560	0.160
34	96	236	0.215	0.102	7719	45.000	150.000[a]	0.327	0.175	0.916	0.646	–	2.558	–	21.557	1.821	1.886	0.026
35	96	238	0.215	0.093	7516	35.000	116.666[a]	0.602	0.149	1.849	0.652	–	2.401	–	19.026	2.321	2.590	0.041
36	96	240	0.224	0.087	7329	38.000	126.666[a]	0.477	0.167	1.331	0.652	–	2.457	–	18.841	3.221	3.247	0.025
37	96	242	0.224	0.079	6862	42.130	137.000	0.585	0.210	1.570	0.662	2.723	2.509	27.100	16.557	5.109	5.122	0.026
38	96	244	0.234	0.073	6361	42.965	142.348	0.611	0.238	1.558	0.660	2.301	2.614	7.939	16.322	7.460	7.383	0.024
39	96	246	0.234	0.057	6128	42.852	142.010	0.752	0.266	2.092	0.683	2.451	2.527	10.136	12.074	8.616	8.482	0.024
40	96	248	0.234	0.040	6217	43.400	143.600	0.729	0.281	1.997	0.712	2.545	2.384	12.908	8.910	7.935	7.937	0.041
41	96	250	0.225	0.030	5926	43.000	143.333[a]	0.689	0.315	1.755	0.742	–	2.327	–	6.799	9.227	9.354	0.068
42	98	242	0.224	0.079	8374	45.000	150.000[a]	0.602	0.166	1.816	0.665	–	2.344	–	15.639	0.078	0.477	0.039
43	98	244	0.234	0.073	8002	41.000	136.666[a]	0.602	0.161	1.822	0.660	–	2.353	–	16.171	1.588	1.621	0.018
44	98	246	0.234	0.057	7557	44.000	146.666[a]	0.689	0.204	2.092	0.685	–	2.307	–	11.786	3.342	3.215	0.014
45	98	248	0.235	0.040	7153	41.530	137.810	0.748	0.227	2.361	0.711	1.938	2.207	4.820	8.955	4.961	4.777	0.014
46	98	250	0.245	0.026	7307	42.721	141.875	0.777	0.234	2.535	0.726	2.016	2.136	5.849	7.711	4.067	4.007	0.023
47	98	252	0.236	0.015	7027	45.720	151.740	0.753	0.281	2.265	0.764	–	2.098	–	5.821	5.067	5.084	0.035
48	100	248	0.235	0.049	8549	44.000	146.666[a]	0.477	0.178	1.386	0.696	–	2.138	–	10.344	0.593	0.642	0.015
49	100	250	0.235	0.033	8226	44.000	145.000[a]	–	0.206	–	0.726	–	2.050	–	7.909	1.753	1.643	0.012
50	100	252	0.245	0.018	8581	46.600	155.333[a]	0.826	0.214	3.049	0.745	–	1.962	–	6.545	0.466	0.328	0.014
51	102	252	0.236	0.024	8995	46.400	153.800	–	0.202	–	0.744	–	1.934	–	6.749	0.301	0.051	0.006
52	104	256	0.247	−0.007	9923	51.000	170.000[a]	0.689	0.205	2.346	0.770	–	1.810	–	5.518	−2.143	−1.933	0.017

[a]These energies are not measured, but a simple perfect rotor approximation we used in our calculations.

We have analyzed α-decays from 52 deformed emitters [24], described in Table I. Here are given deformation parameters [25], Q_α-values, excitation energies, experimental intensities defined by Eq. (2.19) and half-lives [19,20]. The corresponding computed values were estimated using the decay widths given by Eq. (2.16) for the first resonant state in the pocket-like interfragment potential. We considered a fixed strength of the repulsive potential (2.21), $c = 50$ MeV fm^{-2}.

The HF's (2.20) were estimated by approximating Eq. (2.18) by the diagonal elements, i.e.,

$$HF_J \approx \frac{\Gamma_0}{\Gamma_J}\frac{P_J(R)}{P_0(R)}, \tag{3.3}$$

where $P_J = \rho_J/G_J^2(\chi_J, \rho_J)$ is the standard penetrability, computed at the reduced geometrical touching radius

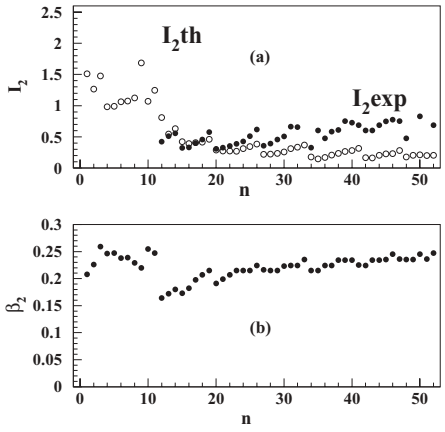

FIG. 1. (a) The experimental quadrupole intensities I_2, given by Eq. (2.19), (dark circles) versus "n" and the calculated values (open circles). (b) Quadrupole deformation parameters β_2 versus "n."

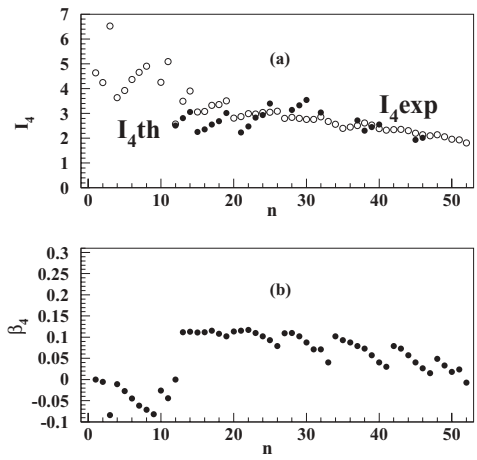

FIG. 2. The same as in Figure 1, but for the hexadecapole quantities.

$\rho_J = \kappa_J 1.2(A_D^{1/3} + 4^{1/3})$. It turns out that HF's are very well approximated at this distance, due to the fact that the off-diagonal elements of the propagator matrix ΔK_{IJ} in Eq. (2.15) are less than 10% of the diagonal elements that are unity. They weakly depend on the considered radius in the region of the nuclear surface.

The experimental values, together with the theoretical results are given in Table I. We have also plotted various quantities versus the number "n," labeling isotope chains with fixed charge number Z of the daughter nucleus, given in the second column of this table. The α-decay fine structure is given by the intensities I_J, defined in Eq. (2.19).

In Fig. 1(a) we give the experimental quadrupole intensities I_2 (dark circles) versus "n" and the results of our calculations (open circles), including predictions for some light emitters.

In Fig. 1(b) are plotted the corresponding quadrupole deformation parameters β_2 versus "n." One sees a clear correlation between calculated intensities and deformations, already mentioned in Ref. [12]. At the same time we notice an abrupt change at $n = 12$ for both quantities, corresponding to the magic numbers $Z_0 = 82$, $N_0 = 126$.

Similar plots are given in Fig. 2(a) and 2(b) for the hexadecapole intensities I_4 and deformation parameters β_4, respectively, versus "n." A similar connection between intensities and deformations is observed by crossing the above magic numbers, but in the right region the correlation is less pronounced than in the quadrupole case. In any case, the abrupt change for both the intensity and the deformation parameter is also present for hexadecapole quantities.

The nuclear structure effects are better shown by the so-called spectroscopic factor. In emission processes this quantity can by estimated in two ways. In Fig. 3 we plotted the so-called phenomenological spectroscopic factor, defined by

$$S = \frac{T_{\rm comp}}{T_{\rm exp}}, \tag{3.4}$$

versus the label "n" (dark circles). The computed values $T_{\rm comp}$ are provided by the coupled channels procedure.

It turns out that this function can be well fitted by the following ansatz:

$$\begin{aligned} \log_{10} S_{\rm fit} &= c_0^{(m)} + \sum_{k=1}^{2} \left[a_k^{(m)} (Z - Z_0)^k + b_k^{(m)} (N - N_0)^k \right], \\ c_0^{(1)} &= -27.6011, \quad a_1^{(1)} = +2.10550, \\ a_2^{(1)} &= -0.0409892, \\ b_1^{(1)} &= -0.0248138, \quad b_2^{(1)} = -0.000687941; \\ Z > Z_0 &= 50, N > N_0 = 82 \\ c_0^{(2)} &= 0.594206, \quad a_1^{(2)} = -0.165954, \end{aligned} \tag{3.5}$$

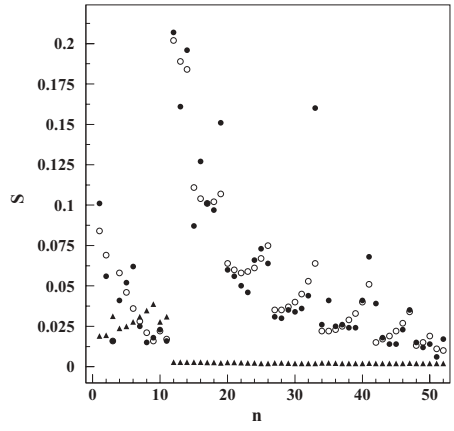

FIG. 3. Phenomenological spectroscopic factor (3.4) (dark circles), fitted values given by Eq. (3.6) (open circles) and microscopic spectroscopic factor (3.7) (triangles) versus "n."

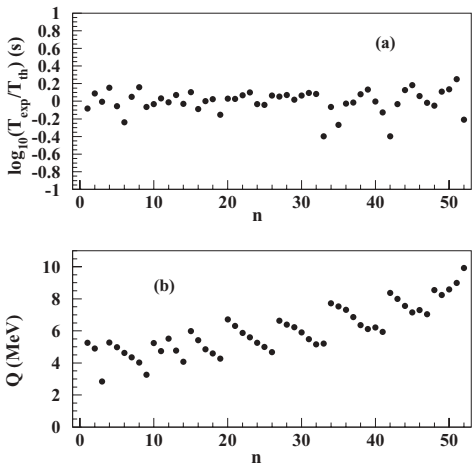

FIG. 4. (a) The difference of the logarithms of experimental half lives and theoretical half lives given by Eq. (3.6) versus the running number "n" in the first column of the Table I. (b) Q_α-values versus the label "n."

$$a_2^{(2)} = 0.00254353,$$
$$b_1^{(2)} = -0.0584801, \quad b_2^{(2)} = 0.0020089;$$
$$Z > Z_0 = 82, \quad N > N_0 = 126,$$

and it is plotted in Fig. 3 by open circles. The standard deviations for the two regions are $\sigma_1 = 0.012$ and $\sigma_2 = 0.02$.

The theoretical half-lives given in Table I are estimated according to the following relation:

$$T_{\rm th} = T_{\rm comp}/S_{\rm fit}. \tag{3.6}$$

In Fig. 4(a) we compare theoretical half-lives, given by Eq. (3.6), with experimental ones by plotting the difference of their logarithms, in other words the logarithm of their ratio, versus the label "n," given in the first column of Table I. The agreement is very good for most of the considered decays. In Fig. 4(b) the Q_α-values versus the same label "n" are plotted.

The ratio given by Eq. (3.4) represents the probability of the α-daughter configuration inside the parent wave function. One sees that this probability is much less than unity and the magic numbers $Z_0 = 82$, $N_0 = 126$ divide the plot into two regions. We notice that by crossing these magic numbers one has a jump of one order of magnitude. The meaning is simple: in the region above Pb isotopes the probability that an α-particle exists at the nuclear surface is much higher. Thus, the α-clustering structure of nuclei above ^{208}Pb is much more pronounced.

This statement is nicely confirmed by microscopic calculations. One defines the microscopic spectroscopic factor by the following integral:

$$S_{\rm micr} = \int_0^\infty |\mathcal{F}(\mathbf{R})|^2 d\mathbf{R}, \tag{3.7}$$

in terms of the so-called preformation amplitude $\mathcal{F}$. It is expressed as an overlap integral between the parent wave function and the product between daughter and α-particle wave functions, i.e.,

$$\mathcal{F}(\mathbf{R}) = \int \Psi_P^*(\mathbf{x}_P)\Psi_D(\mathbf{x}_D)\Psi_\alpha(\mathbf{x}_\alpha) d\mathbf{x}_D d\mathbf{x}_\alpha, \tag{3.8}$$

taken over the internal coordinates $\mathbf{x}_D, \mathbf{x}_\alpha$. The preformation amplitude depends on the distance between the centers of emitted fragments $\mathbf{R}$ and it defines the amount of the α-clustering inside the initial wave function. In Ref. [26] we estimated the microscopic preformation amplitude by considering the pairing approach for the parent and daughter wave functions in Eq. (3.8) for axially deformed nuclei. The resulting integral is given as a superposition of the spherical harmonic oscillator (ho) wave functions, depending on the single particle ho parameter $\beta = M\omega/\hbar$ multiplied by four:

$$\mathcal{F}(\mathbf{R}) = \sum_{LN} W_{NL} \mathcal{R}_{NL}^{(4\beta)}(R) Y_{L0}(\hat{R}). \tag{3.9}$$

The W-coefficients contain the spectroscopic information given by the single-particle Nilsson wave functions and the products of BCS amplitudes uv. Our calculations have shown that the leading monopole component with $L = 0$ gives more that 90% in the above summation for the most deformed emitters.

The numerical results are given in Fig. 3 versus the label "n" by triangles. One can see that a very important conclusion concerning the structure of α-emitters emerges, namely the α-particle can be described as a component of the parent pairing wave function only in regions well beyond magic numbers. When the emitters are just above magic numbers $N_0 = 82 (n = 1)$ and $Z_0 = 82$, $N_0 = 126 (n = 12)$ an additional α-clustering component is necessary in order to explain the experimental half lives, because the microscopic spectroscopic factor $S_{\rm micr}$ is much less than the phenomenological value S.

IV. CONCLUSIONS

We used in this paper the rotor model to describe the α-decay fine structure in deformed nuclei. We considered the coupled channels formalism to estimate decay widths and the double folding procedure to compute the interaction between the daughter and α-particle. We adopted an effective particle-particle nuclear interaction given by the M3Y potential, which is able to describe scattering data. The Q-value of the system is reproduced by adjusting the depth of a parabolic repulsive core, simulating the Pauli principle. The decaying state was identified with the first resonance in the resulting pocket-like potential.

It turned out that this simple rotational model is able to explain very well the decay widths to the first 2^+ states. The obtained results practically do not depend on the parameters of the repulsive potential.

Concerning the decay widths to 4^+ rotational states we obtained a good agreement with experimental data for the lightest $Z < 90$ neutron chains and a satisfactory agreement for the other chains. The rotational model is able to qualitatively explain the gross features of the fine structure, but still the computed values in the region around the $Z = 94$ chain

differ from experimental data by 1.5 orders of magnitude. The theoretical intensities I_J are proportional to the corresponding deformations β_J, including sharp changes around $Z = 82$. We made predictions concerning the fine structure of those α-emitters where the intensities to excited levels were still not measured.

We also estimated the phenomenological spectroscopic factor as the ratio between the computed and measured half-lives. The comparison with the corresponding microscopic values leads to comparable values for regions well beyond magic numbers and much smaller for nuclei just above $N_0 = 82$ and $Z_0 = 82$, $N_0 = 126$. Thus, in these last regions the microscopic procedure to compute the shell model preformation amplitude is not able to reproduce experimental data. The difference can be explained by supposing an additional α-clustering component. On the other hand the fitted values of the phenomenological factor describe very well the experimental values of the total α-decay half-lives.

[1] G. Gamow, Z. Phys. **51**, 204 (1928).
[2] J. O. Rasmussen and B. Segal, Phys. Rev. **103**, 1298 (1956).
[3] H. M. A. Radi, A. A. Shihab-Eldin, J. O. Rasmussen, and Luiz F. Oliveira, Phys. Rev. Lett. **41**, 1444 (1978).
[4] P. O. Fröman, Mat. Fys. Skr. Dan. Vid. Selsk. **1**, No. 3n (1957).
[5] R. Neu and F. Hoyler, Phys. Rev. C **46**, 208 (1992).
[6] H. Abele and G. Staudt, Phys. Rev. C **47**, 742 (1993).
[7] U. Atzrott, P. Mohr, H. Abele, C. Hillenmayer, and G. Staudt, Phys. Rev. C **53**, 1336 (1996).
[8] Dao T. Khoa, Phys. Rev. C **63**, 034007 (2001).
[9] D. N. Basu, J. Phys. G **29**, 2079 (2003).
[10] Y. K. Gambhir, A. Bhagwat, M. Gupta, and Arun K. Jain, Phys. Rev. C **68**, 044316 (2003).
[11] C. Xu and Z. Ren, Phys. Rev. C **74**, 014304 (2006).
[12] D. S. Delion, S. Peltonen, and J. Suhonen, Phys. Rev. C **73**, 014315 (2006).
[13] S. Peltonen, D. S. Delion, and J. Suhonen, Phys. Rev. C **75**, 054301 (2007).
[14] P. Mohr, Phys. Rev. C **73**, 031301(R) (2006).
[15] D. S. Delion, A. Săndulescu, S Mişicu, F. Cârstoiu, and W. Greiner, Phys. Rev. C **64**, 041303(R) (2001).
[16] D. S. Delion, A. Săndulescu, S. Mişicu, F. Cârstoiu, and W. Greiner, J. Phys. G **28**, 289 (2002).
[17] D. S. Delion, A. Săndulescu, and W. Greiner, Phys. Rev. C **68**, 041303 (2003).
[18] A. Săndulescu, A. Florescu, F. Cârstoiu, W. Greiner, J. H. Hamilton, A. V. Ramayya, and B. R. S. Babu, Phys. Rev. C **54**, 258 (1996).
[19] Y. A. Akovali, Nucl. Data Sheets **84**, 1 (1998). Data retrieved from ENSDF data files, NNDS web page Feb. 2, 2008.
[20] Y. A. Akovali, Nucl. Data Sheets **87**, 249 (1999); **87**, 287 (1999); **77**, 433 (1996); **94**, 131 (2001); **96**, 177 (2002); **99**, 197 (2003); Agda Artna-Cohen, *ibid.* **80**, 227 (1997); **80**, 723 (1997); **84**, 901 (1998); F. E. Chukreev, V. E. Makarenko, and M. J. Martin, *ibid.* **97**, 129 (2002); F. E. Chukreev and Balraj Singh, *ibid.* **103**, 325 (2004); Coral M. Baglin, *ibid.* **96**, 611 (2002); S.-C. Wu and H. Niu, *ibid.* **100**, 483 (2003); M. S. Basunia, *ibid.* **107**, 791 (2006); Coral M. Baglin, *ibid.* **99**, 1 (2003); N. Nica, *ibid.* **106**, 813 (2005); E. Browne, *ibid.* **107**, 2579 (2006); E. Browne and J. K. Tuli, *ibid.* **107**, 2649 (2006); **108**, 681 (2007); ENSDF (2000); B. Singh and R. B. Firestone, Nucl. Data Sheets **74**, 383 (1995); R. B. Firestone, *ibid.* **58**, 243 (1989); V. S. Shirley, *ibid.* **71**, 261 (1994); E. Browne, *ibid.* **72**, 221 (1994); data retrieved from ENSDF data files, NNDS web page Feb. 2, 2008.
[21] G. R. Satchler and W. G. Love, Phys. Rep. **55**, 183 (1979).
[22] F. Cârstoiu and R. J. Lombard, Ann. Phys. (NY) **217**, 279 (1992).
[23] G. Bertsch, J. Borysowicz, H. McManus, and W. G. Love, Nucl. Phys. **A284**, 399 (1977).
[24] B. Buck, A. C. Merchand, and S. M. Perez, At. Data Nucl. Data Tables **54**, 53 (1993).
[25] P. Möller, J. R. Nix, W. D. Myers, and W. J. Swiatecki, At. Data Nucl. Data Tables **59**, 185 (1995).
[26] D. S. Delion, A. Săndulescu, and W. Greiner, Phys. Rev. C **69**, 044318 (2004).

ISBN 978-951-39-3603-7
ISSN 0075-465X